INTEGRATED ACTIVE AND REACTIVE POWER MANAGEMENT OF POWER DISTRIBUTION SYSTEM CONSIDERING DISTRIBUTED ENERGY STORAGE AND PV FARMS

by

Muhammad Ahmed

A dissertation submitted to the faculty of
The University of North Carolina at Charlotte
in partial fulfillment of the requirements
for the degree of Doctor of Philosophy in
Electrical Engineering

Charlotte

2018

Approved by:

Dr. Sukumar Kamalasadan

Dr. Valentina Cecchi

Dr. Yogendra Kakad

Dr. Mohamed Ali-Hasan

Dr. Maciej Noras

©2018
Muhammad Ahmed
ALL RIGHTS RESERVED

ABSTRACT

MUHAMMAD AHMED. Integrated Active and Reactive Power Management of Power Distribution System Considering Distributed Energy Storage and PV Farms. (Under the direction of DR. SUKUMAR KAMALASADAN)

Modern electric distribution system with distributed Photo-Voltaic (PV) farms and energy storage units have been facing technical challenges due to the difficulty in managing them collectively. This dissertation presents new solutions for energy management of PV farms integrated power distribution systems using energy storage. First, a new local net active power management methodology for PV point of common coupling (PCC) is discussed. Further, this approach is extended as an integrated net active power management architecture based on an optimal ramp rate algorithm. The approach considers the ramp rate and state-of-charge of the energy storage device that can be used for resource allocation. Second, an integrated feeder level peak load management methodology with a load prediction approach is illustrated with the methodology applied to separated and decomposed load types. Third, a coordinated volt-var control approach considering a fast and slow change in the active power is illustrated. Fourth, a dynamic volt-var control approach with sensitivity based algorithm is illustrated. The novelty in the volt-var control approach is that the methodology coordinate with legacy devices and voltage source converters. Also, a dynamically changing framework is designed based on active and reactive power sensitivity. Finally, an integrated volt-var-watt control approach is illustrated. This approach coordinates with active and reactive power in the feeder considering the reactive and active power capability of the device.

ACKNOWLEDGMENTS

I would like to express my appreciation to my supervisor Professor Sukumar Kamalasadan for his consistent support throughout this study. Without his guidance and patience, this dissertation could not have been possible. I am also thankful to my Ph.D. program committee members; Dr. Yogendra Kakad, Dr. Valentina Cecchi, Dr. Mohamed-Ali Hasan, and Dr. Maciej Noras. Their guidance and supportive comments throughout the previous proposal was a great help to this accomplishment.

Also, I am so grateful for all the financial support provided by the Energy Production and Infrastructure Center (EPIC) and the department of electrical and computer engineering. I am also honored to be part of Duke Energy research team, thanks to Dr. Sukumar Kamalasadan and Dr. Sherif Abdelrazek for introducing me to the team. I gained most of my substantial knowledge in my program throughout Duke Energy Projects.

I would also like to thank everyone in our research team for their help and being there for each other. I am greatly appreciative to the inspirational environment created by our friend Dr. Rojan Bhattarai.

Finally, I would like to express my sincere appreciation to my parents for their patience and unconditional support.

TABLE OF CONTENTS

LIST OF FIGURES

LIST OF TABLES

CHAPTER 1: INTRODUCTION

PV photovoltaic solar energy resource is one of the common distributed energy resources (DER) that has been lately developed in modern power distribution networks [37]. It also has become more economical and clean for PV solar energy to be utilized in higher penetration level throughout distribution networks. Nevertheless, technical issues remain rising with harmful effects on distribution feeders due to DERs operation without any energy management (active and reactive power management) [94]. Moreover, as solar energy usage expanded in many electricity grids, the phenomenon of "Duck Curve" emerged with multiple generation and grid operation risks to be tackled [32]. Whereas energy storage systems (ESS) is substantial mean of active power management in RER integrated distribution grids, feeder load prediction plays a crucial role in generation management and operations in general and energy storage ancillary services in particular. Solar energy high penetration level and long-term feeder load prediction are the main motives for the research work presented in this dissertation. This chapter discusses all technical related introductory literature about methodologies developed in this dissertation.

This dissertation presents an integrated active and reactive power management solution with the aid of distribution level day ahead active load prediction. The active power management part incorporates three main ancillary services of energy storage systems; PV output power smoothing, active power ramp rate control for distribu-

tion system's net-load locations, and energy time shift (ETS) application. Also, the reactive power management part incorporates utilization of reactive power capability of voltage source converters (VSC) of energy storage systems. The contribution of reactive power management is the development of online voltage sensitivity analysis so that all VSCs at their given locations are able to regulate the voltage level at any chosen location of interest. Finally, integrated active and reactive power management (VVWC) solution is developed so that the active and reactive power capability (PQ curves) of the converter is taken into consideration. The weather forecasts based day ahead active load prediction aids the ETS application. It is also discussed in the future work to be used to aid net-load active power management.

1.1 PV Output Power Smoothing

Due to randomness in clouds patterns, sun irradiation profile tends to have some severe fluctuations. These fluctuations, in turn, cause an intermittent output power at the interface point with the grid (point of common coupling (PCC)). Fast changes greatly affect voltage profile throughout the big part of the network and subsequently cause unwanted actions by voltage regulation legacy equipment such as online load tap changer (OLTC), line regulators and switched capacitor banks. PV output smoothing is also called "PV capacity firming," and it is defined as the action of using an intermittent power source as almost constant. Due to fast response, Battery energy storage systems are commonly used, nowadays, to mitigate these output power fluctuations. In this dissertation, the proposed algorithms provide an optimized energy storage output that allows smoothing the PV output at various conditions. The

key features of this algorithm are that the PV output changes are tracked, so that reference curves get adjusted accordingly. The system under study is 1 MW solar PV station tied with (250 kW/750 kWh) battery energy storage system BESS. Both systems are connected to a distribution network of practical 720 nodes on medium voltage level 12.475 kV. The system is already deploying real-time control architecture for many energy storage applications such that PV smoothing, energy arbitrage, and voltage support. The work proposed is simulation results on some historical data of the PV station.

1.2 Power Distribution Network Net-Load Active Power Management

As presented by California Independent System Operator (CAISO) [32], grid's conventional generation units are expected to have a significant decrease during noon time with a subsequent steep ramp rate due to increase in demand. A net-load profile could be defined as all the generated power injected by all the conventional power generation resources. It also has the name of Duck Curve. The so-called (Duck Curve) is the result of subtracting all the renewable generated power connected to a given system from the total load connected to this system. Fig. **??** shows net-load profiles at given distribution network in North Carolina, it is also developed assuming different penetration level of photo-voltaic solar farms. This phenomenon increases the risk of over-generation during the day when the system's supply outweighs the demand. As in [37], the duck curve starts to get fatter which leads to an immediate active power management solution. However energy storage technology costs are still crucial, it is still one of the means to be considered to approach net-load active power

management. Addressing the generation curve "Duck Curve" as well as addressing RER's intermittent changes became two different types of active power management; fast changes and ramp rate changes. Therefore, energy storage units are sought to be placed differently than where it is usually placed for RER active power smoothing. For medium scale power distribution network, a net-load profile is represented by substation location. However, in larger systems, there shall be multiple locations to be considered as system's local net-load location.

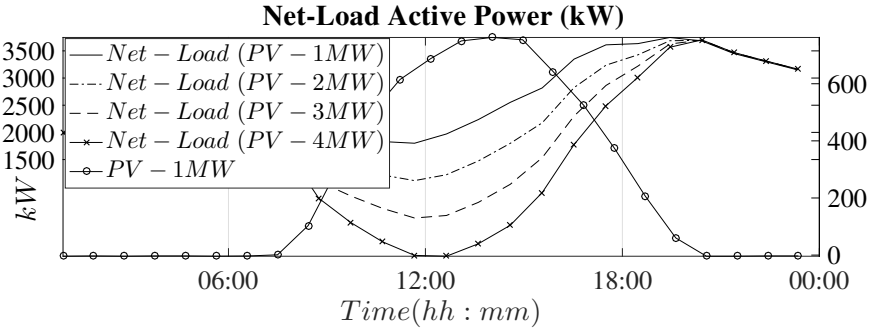

Fig. 1.1. Distribution Feeder Net-Load profile at of PV penetration

Few work in the literature [43, 50, 74, 83, 86] discussed net-load management using energy storage systems. Energy storage systems locations are not studied in details. Also, due to steep ramp rates of duck curve, approached techniques are considered as energy management more than active power management because energy storage systems are expected to dispatch consistently for significant time duration. Besides, managing PV active power smoothing and BESS state of charge (SoC) control is not taken into full consideration. This dissertation addresses energy storage allocation for RER active power management as well as an optimal approach to control large power distribution networks' local net-load locations. The proposed methodology provides a significant decrease in active power ramp rate on the net-load side as well as voltage

regulation benefit as it reduces power losses in the system as well as reducing taps operations at all voltage regulators.

1.3 Long Term Feeder Load Prediction

Load prediction is the action of forecasting active power demand at a certain time in the future [81]. Load prediction could be short term, medium term, and long term. In the literature [41], load prediction methodologies are categorized based on techniques; multiple regression, exponential smoothing, adaptive load forecasting, iteratively reweighted least-squares, ARMAX models based on genetic algorithms, fuzzy logic, and neural networks [89]. However, detailed load prediction methodologies based on load types decomposition. Increased penetration of renewable energy based generators throughout modern distribution networks makes it crucial to seek elevated levels of accuracy in forecasting methods. First, energy time shift (ETS) application relies on knowing the peak load time few hours beforehand so that state of charge (SoC) could be controlled and adjusted to be at the maximum value possible at this time. Second, having a complete pattern of anticipated feeder load gives quite an accurate estimate of the expected net-load rate of change. This dissertation presents an intelligent load forecasting method for residential distribution feeders. It uses, load time series decomposition to distinguish between all types of loads and events on a feeder. Then, back-propagation artificial neural network (BP-ANN) technique is used to utilize the day ahead weather variables forecasting to predict weather dependent load component. The proposed algorithm is evaluated on a residential feeder. Results show the very accurate prediction for active power as well as the lighting load peak

time.

1.4 Co-ordinated Voltage Control Utilizing Voltage Source Converters In PV/BESS Hybrid Distribution Systems

Modern-day distribution systems (DS) is now hosting an increasing number of both small and large-scale distributed energy resources (DERs). Even though these DERs can support reactive power along with the active power they provide, practitioners are still hesitant in utilizing the reactive power potential from these DERs. One of the major concerns for the distribution system operator is the coordination between the existing voltage regulators and the inverter based reactive power sources in the DS. The utility-scale photovoltaic (PV) farm and battery energy storage are growing in numbers with the continued growth and focus on the integration of large-scale renewable energy resources (RERs) in the power grid as mandated by the Renewable Portfolio Standards (RPS) [57] in many states in the United States. However, these RERs impose challenges in the control and operation of the distribution system, mainly on feeder level voltage regulation. One source that can provide additional reactive power support is the voltage source converters (VSCs). VSCs are primarily connected to the distribution system to convert active power from the RERs and feed generated power into the network. Recently, grid codes in many countries have been modified such that the reactive power capability of the these grid-connected VSCs can be utilized [78]. Even though using VSCs as additional voltage control devices is promising, coordinating the existing legacy controllers in the feeder (such as on-load tap changing transformers (OLTCs), voltage regulators, capacitor banks,

etc.) with the VSCs is very challenging. Without proper coordination, the interaction between these devices can lead to unwanted operations and switching of these legacy controllers [60], which is undesirable for the utility regarding quality and economic reasons. For example, a sudden shift of tap position of the OLTCs and line regulators causes voltage transient in the feeder and also mechanical wear and tear of the devices [53]. Also, unwanted reactive power support from the VSCs based RERs is undesirable because of unwanted switching losses in the converters. Thus, there is a need to intelligently provide reactive power support from the VSCs without affecting the operation of legacy controllers. This dissertation presents a control strategy for coordinating the operation of OLTC, line voltage regulators and VSCs of battery energy storage. This technique aims to maintain the load end voltage of the feeder within the allowed band while minimizing the operation of the line regulators. The realization of the control depends on the broadcast of the voltage out of band warning signal from the line regulators. Based on this, VSCs inject/absorb the reactive power to/from the feeder, such that the feeder load end voltage is at the allowable voltage band.

1.5 Voltage Sensitivity Based Volt-Var Control

One of the major concerns for the distribution system operator is the coordination between the existing voltage regulators and the inverter based reactive power sources in the DS. Besides, connected renewable energy resources (RERs) impose challenges in the control and operation of the distribution system, mainly on feeder level voltage regulation. One source that can provide additional reactive power support is the

voltage source converters (VSCs). VSCs are primarily connected to the distribution system to convert active power from the RERs and feed generated power into the network. Recently, grid codes in many countries have been modified such that the reactive power capability of these grid-connected VSCs can be utilized [79]. Even though utilizing VSCs as additional voltage control devices is promising, coordinating the existing legacy controllers in the feeder (such as on-load tap changing transformers (OLTCs), voltage regulators, capacitor banks, etc.) with the VSCs is very challenging. Without proper coordination, the interaction between these devices can lead to unwanted operations and switching of these legacy controllers [61], which is undesirable for the utility concerning quality and economic reasons. For example, a sudden shift of tap position of the OLTCs and line regulators causes voltage transient in the feeder and also mechanical wear and tear of the devices [54]. Also, unwanted reactive power support from the VSCs based RERs is undesirable because of unwanted switching losses in the converters.

Fig. 1.2 presents an illustrative schematic that shows the connectivity between the proposed methodology in this dissertation.

1.6 Research Contributions

This section presents the research contribution to the research as mentioned earlier topics.

- A new error minimization based PV capacity firming methodology. The methodology is based off an optimization formulation that can follow the fast weather changes in the level of clouds states such that battery energy storage units stay

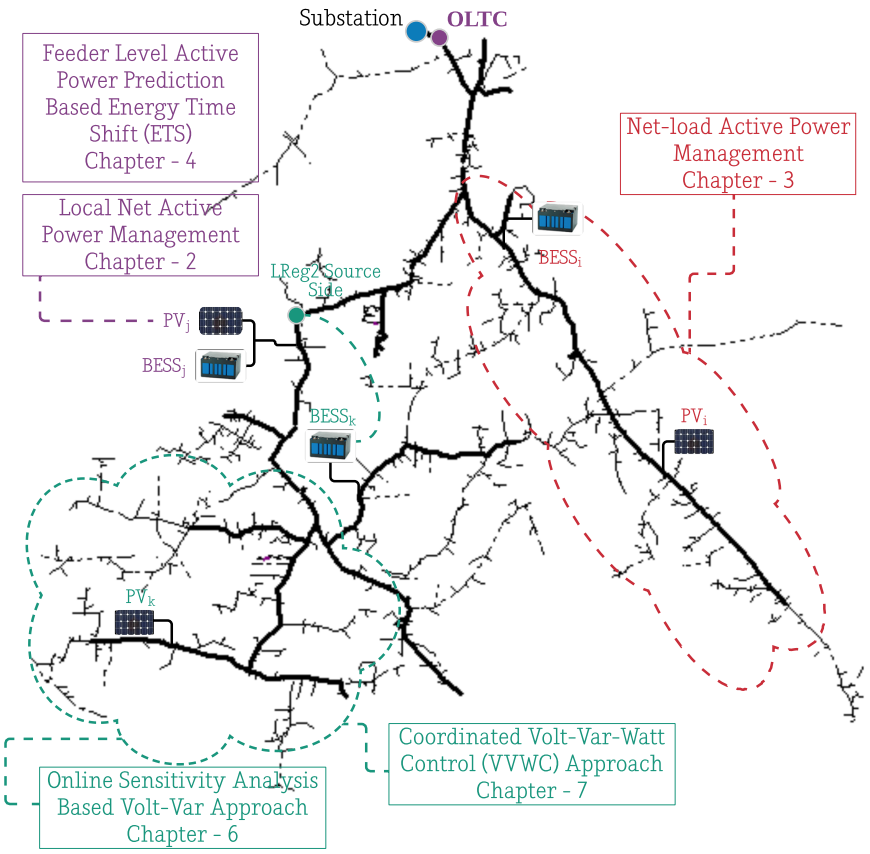

Fig. 1.2. Connectivity schematic diagram to show the connectivity between the proposed methodologies.

functioning with operable state of charge (SoC). Also, the methodology problem is formulated as an objective function with error minimization which allows the control of the point of common coupling shape accurately.

- A new optimal active power management for local net-load locations in power distribution networks. First, the approach incorporates Fast Fourier Transform (FFT) / Inverse Fast Fourier Transform (IFFT) to historical local net-load locations to generate local net-load reference curves. The methodology uses SoC feedback based PI controller to calculates all threshold values for inequality and

equality constraints for the optimization problem. Based on assumed PV/BESS sizing, the proposed simulation contributed to the significant control of duck curve ramp rate as well as avoiding the risk of over-generation.

- An intelligent approach in day ahead feeder load prediction is developed. The feeder load curve is decomposed into all types and different behaviors. Then, an artificial neural network (ANN) to predict the weather-dependent component of feeder load based on the day ahead weather forecasting. Also, the novelty of the proposed methodology is it is accurately predicting peak time to aid energy time shift (ETS) energy storage application. The proposed presents a significant sample of implementation results as well as simulation results.

- An integrated volt-var control (IVVC) methodology which aims to maintain the load end voltage of the feeder within the allowed band, while minimizing the operation of the line regulators. The realization of the control depends on the knowledge of the regulator voltage out of band warning signal from the line regulators. Based on this, VSCs inject/absorb the reactive power to/from the feeder, such that the feeder load end voltage is at the allowable voltage band. The architecture is implemented using a communication network already available at the utility.

- A novel online sensitivity analysis based coordinated volt-var control is developed. The algorithm is dynamically estimating the sensitivity indexes between reactive power changes at the location of the utilized voltage source converters (VSCs) and voltage changes at other locations of interests. The modernity of

this methodology is not only splitting reactive power capability between two locations regulation but also ability to set a target value for each location which leads to almost avoiding a high number of taps actions at some of the feeder line regulators.

- An integrated Volt-Var-Watt control (VVWC) is developed where optimal active power management net-load control and sensitivity analysis based volt-var control (VVC) are combined.

1.7 Dissertation Organization

This dissertation is organized as follows:

- Chapter 1: This chapter discusses an overview and introduction to energy storage system active and reactive power applications and feeder load prediction. It also summarizes the research contribution.

- Chapter 2: This chapter presents an error minimization based PV capacity firming algorithm.

- Chapter 3: This chapter presents optimal net-load active power management methodology to solve duck curve due to high PV penetration. It discusses different PV penetration levels.

- Chapter 4: This chapter present weather forecasting based day ahead feeder load prediction. The methodology is developed in Java, and it presents both simulation and implementation results for a real feeder in North Carolina, USA.

- Chapter 5: This chapter presents a coordinated voltage control strategy for voltage regulators and voltage source converters for the distribution network.

- Chapter 6: This chapter presents a novel online sensitivity analysis based coordinated volt-var control for power distribution networks. The methodology is developed in Python and applied to IEEE 8500-Node large system.

- Chapter 7: This chapter presents a multi-objective optimization approach for Volt-Var-Watt control (VVWC). The methodology combines both optimal approaches presented in chapter 3 and sensitivity analysis based volt-var control methodology.

CHAPTER 2: LOCAL NET ACTIVE POWER MANAGEMENT BASED ON PCC ERROR MINIMIZATION

This is chapter presents an error minimization based local active power management for the intermittent out power of photovoltaic solar PV farms.

2.1 Introduction

Electrical grids tied with energy storage systems are gaining quantitative as well as qualitative benefits for maintaining an economical and reliable system. As categorized in [2], energy storage systems can serve in bulk energy supply using energy time shift (arbitrage) application. Also, the energy storage system can support several ancillary services such as output power smoothing (capacity firming) for renewable energy resources (PV/wind), regulation, load following, and voltage support. Furthermore, energy storage can be used for infrastructure deferral at both the transmission and distributions levels. One important application for energy storage is the PV capacity firming. Renewable capacity output firming is a method for utilizing the intermittent renewable energy resources as almost constant and smoothed power source [35]. Generally, intermittency and unwanted fluctuations in the output power of a PV farm must be compensated by the other dispatchable generation units in the grid which is not quite achievable due to rapid changes. Energy storage can be used to mitigate this intermittency by efficient charge/discharge cycles if these storage system work in conjunction with the PV farms. The energy management system is the main controller

which observes all the system states and generates the reference set point to be drawn from the battery energy storage system (BESS) for smoothing the output power at the point of common coupling. Thus a robust control system for energy storage is necessary and significantly crucial for this application. Several works have focused on developing control architecture for PV output smoothing. In [34, 49], control architecture is presented to smooth out the high-frequency component of PV output power based on a low pass filter (LPF), and the output of the LPF is subtracted from the original PV data as a smoothing error. Then, based on the state of charge the BESS reference power is calculated. A comparison between the moving average filter and a filter based on optimal control formulation has been proposed in [82]. Results show that the optimal control based filter had the lowest max ramp (MW/min) using moderate BESS capacity compared with the moving average models. Reference [6, 7] presented a novel real-time controller BESS/PV applications such that PV capacity firming (PVCF), energy time-shift (ETS) and voltage support. The intuition in the proposed battery energy management system is that maximizing the state of charge by the end of the day was a critical concern to let the battery do ETS at the peak demand period. Real-time BESS-based smoothing control architectures for the hybrid PV/wind hybrid power system were proposed in [65, 66, 91]. As in [65], the control used SoC of the BESS as feedback as well as the power fluctuations rate. Recently, ref. [58] presents an adaptive control based PV ramp control which utilizes the PV power ramp rate as control feedback to the smoothing algorithm to prove a better performance over the moving average based algorithms. Also, PV power smoothing method was proposed in [48,98] using hybrid energy storage system (HESS) using su-

per capacitor bank (SCB) and vanadium redox battery (VRB). The primary goal was to smooth the PV power as well as minimizing the power from the SCB to one fifth the power from the VRB rating to increase its operational efficiency. This chapter uses an error minimization based optimization technique to develop PCC smoothing methodology to smooth the active power output of PV solar farm due to continuous intermittent irradiation.

2.2 Proposed Methodology I

Least squares minimization (LSM) has been applied in many applications and different research fields. As introduced in [14], LSM is an approach to solving the overdetermined set of equations as long as curve fitting applications. In the proposed methodology, LSM will be used to minimize the sum of squared residuals (errors) between the PCC power and another smooth reference value to mitigate all PV power fluctuations by the help of the battery energy storage system which is commonly connected to the point of common coupling. This section will present some terms definitions and the first proposed least squares minimization methodology (LSM-I). The first proposed LSM methodology uses the smoothed current PV power as reference profile.

2.2.1 PV Characteristics Reference Power Curve

As proposed in [15], this curve represents the maximum PV output power for the last few weeks. It provides the normal trend and shape of the maximum PV power at this specific time in the year as shown in Fig. 2.1. The PVCF algorithm uses short term historical PV station output to develop a characteristic maximum PV curve for

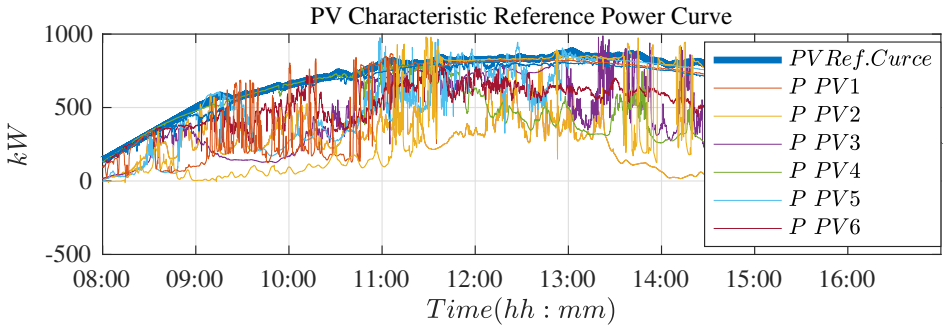

Fig. 2.1. PV Characteristics Reference Power Curve

the PV station location at that time of year. For a daily output power of PV station $P_k(t)$ where k signifies the day; k = 1,2,3,4, ...n, the characteristic maximum and minimum PV curve is given by equations 2.1,2.2.

$$P_{max}(t) = max(P_{PV1}(t), P_{PV2}(t), ..., P_{PVn}(t)) \tag{2.1}$$

$$P_{PVRef.}(t) = \begin{cases} P_{max}(t) & for \ -0.1 < R_{PV} < 0.1 \\ P_{PVRef.}(t - \Delta t) - 0.1 * \Delta * t & for \ R_{PV} > 0.1 \\ P_{PVRef.}(t - \Delta t) + 0.1 * \Delta * t & for \ R_{PV} < -0.1 \end{cases} \tag{2.2}$$

2.2.2 Point of Common Coupling (PCC) Reference set-point

It is assumed that the PCC reference set-point will be close to PV characteristic reference curve during sunny days and a fraction of it during cloudy and overcast days. On that basis, point of common coupling reference power PCC Ref. could be derived as in 2.3. Since the PPCC Ref. is calculated, the battery energy storage

reference power PBatt. Ref. will be calculated as in 2.4.

$$P_{PCCRef.}(t) = m * P_{PVRef.} \tag{2.3}$$

$$P_{Batt.Ref.}(t) = P_{PCCRef.}(t) - P_{PV}(t) \tag{2.4}$$

such that $P_{PCCRef.}$ is the targeted point of common coupling power, P_{PV} is the instantaneous PV power and finally $P_{Batt.Ref.}$ is the () reference power should be drawn from the BESS.

2.2.3 Least Squares Minimization Method I

This proposed method will aim to minimize the error between the last minute average PV power curve and the PCC generation power in such way of trying to minimize the BESS output power for smoothing the output power. It is desired to minimize the BESS output power to make it always capable of smoothing as its power capacity is 250 kW and the intermittency level most of the time exceeds those limits. Hence, the problem objective function will be as follows:

$$min\ U = \sum_{i=t}^{t-10} (1/2) * (P_{PVi} - P_{PCCRef.})^2 \tag{2.5}$$

$$min\ U = \sum_{i=t}^{t-10} (1/2) * (P_{PVi} - m * P_{PVRef.})^2 \tag{2.6}$$

As in 2.6, this is a linear least squares minimization method which chooses the optimal value of the multiplication factor m to reduce this squared error as much as possible. Explicitly, objective constraints are the 250 kW charging/discharging limits of the

BESS which will be translated as upper and lower bounds of the multiplication factor (m) as stated in 2.7.

$$\frac{P_{PVi} + 250}{P_{PVRef.}} \leq m \geq \frac{P_{PVi} - 250}{P_{PVRef.}} \tag{2.7}$$

2.3 Proposed Methodology II

Including the PV power in the objective function in LSM I has some drawbacks because of the high stochastic nature of the PV power behavior. This section presents next developed method which is based on assumed reference set-point to replace the PV power term in last methodology.

2.3.1 Sinusoidal P_{set} Generation

To attain perfect firming level, the point of common coupling generation will be compared with a smoothed set- point waveform which is assumed to be a half-cycle sinusoidal waveform as in Fig. 2.2 It is clear that this selection is based on the similarity between normal shape of PV power and sinusoidal waveform. Generation of the P_{Set} waveform is based on a developed algorithm that utilizes the PV characteristic reference curve to detect the sunrise and sunset instants as well as using the weather (cloud states) forecasting to determine its peak at the beginning of the day.

2.3.2 Last Minute PV Averaging

As the PV power level varies significantly across the day period, the peak of the sinusoidal reference curve PSet should be controlled to be always following the PV power level. To fulfill this target, the last minute PV power average is utilized to get the appropriate positioning of the PSet waveform. As in 2.8, the average power is

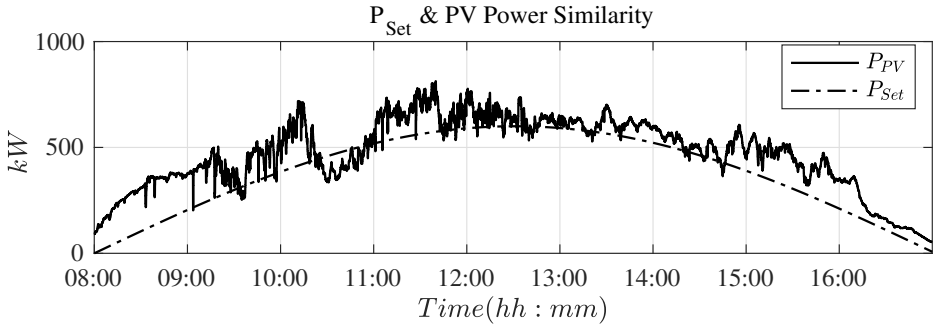

Fig. 2.2. P_{Set} and P_{PV} similarity

calculated based on the last 12 instantaneous PV power as the time step is 5 seconds. Then, this value will be subtracted from the instantaneous value of PSet to get and error as in 2.9. Based on 200 kW threshold values for this error, the sinusoidal reference is being controlled.

$$P_{PVAvg.}(i) = (\sum_{i=t}^{t-12} *(P_{PVi}(i))/12 \tag{2.8}$$

$$error(i) = P_{PVAvg.}(i) - P_{PSet}(i) \tag{2.9}$$

As a case study for this control algorithm, Fig. 2.11 shows firming results for a partially cloudy day. By picking a constant P_{Set} peak as 600 kW, it was not quite suitable for getting a smooth PCC power because the BESS will get fully charged before noon and will not operate properly for the rest of the day. By adaptively controlling PSet position, the PCC profile will be smoothed throughout the whole day as it can change to 700 kW peak.

2.3.3 Least Squares Minimization Method II

This method will aim to optimally choose the value of the multiplication factor (m) that reduces the error between the P_{Set} and $P_{PCCRef.}$ as much as possible taking into consideration last 10 time steps which represent last 50 seconds. Objective function is as follows:

$$min\ U = \sum_{i=t}^{t-10} (1/2) * (P_{Seti} - P_{PCCRef.})^2 \tag{2.10}$$

$$min\ U = \sum_{i=t}^{t-10} (1/2) * (P_{Seti} - m * P_{PVRef.})^2 \tag{2.11}$$

where the system constraints are the same as previous method constraints in 2.7. In this case, PV power does not exist in the objective function, but its effect is taken care of by both the objective function constraints and the last minute PV averaging control algorithm. Fig. 2.3 Shows simple description of method II from how the PV power is memorized and processed till getting the battery reference power.

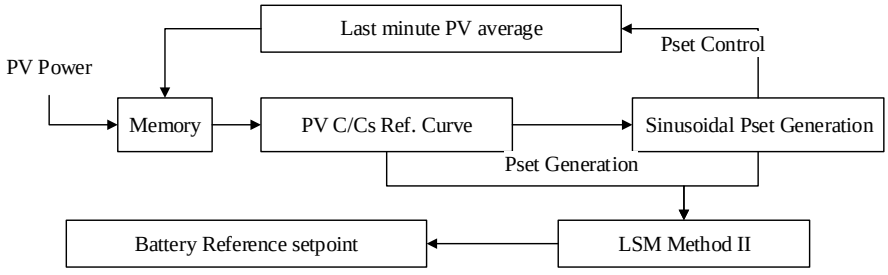

Fig. 2.3. LSM II function block diagram

2.4 Simulation Results

This section shows the simulation results for both proposed PCC smoothing methodologies; LSM-I, and LSM-II. There are two metrics for performance evaluation for both methods. The first metric is comparing the rate of change of the PV power and the smoothed point of common coupling (PCC) power for the last time step which is 5 seconds as in 2.12,2.13. An initial state of charge (SoC) of the battery is adjusted to 0.6 in both algorithms to possibly let the BESS equally charge and discharge from the beginning of the day. The second power smoothing index is the 5 minutes PV and PCC power differential (peak to peak) which measures how much the PV intermittency is attenuated as shown in Fig. 2.4(d), Fig. 2.5 (d), and Fig. 2.6 (d). This can be represented as follows:

$$R_{PV} = (P_{PV}(t) - P_{PV}(t-1))/\Delta t \tag{2.12}$$

$$R_{PCC} = (P_{PCC}(t) - P_{PCC}(t-1))/\Delta t \tag{2.13}$$

such that R_{PV} and R_{PCC} are the rate of change of PV and point of common coupling power respectively in kW/5sec unit.

2.4.1 Methodology I Simulation Results Case-I

This subsection shows simulation results for methodology I for partly cloudy day (Day-I). This case presents moderate level of intermittency that is almost equal to active power capacity of energy storage unit. Fig. 2.4 (a) shows the optimal reference curve for the point of common coupling as well as the firming limitations based on charging and discharging limits of the energy storage unit. Also, Fig. 2.4 (b) shows

the active power for the three active power profile; PV, PCC, and BESS. It is noticed that the algorithm terminated around 12:00 PM due to reaching maximum allowable state of charge (SoC), however, the methodology was able to attain high level of firming as it is shown in Fig. 2.4 (d) where 5 minutes power differential for the PV was reduced from 450 kW/5minutes to 250 kW/5minutes. Finally, the state of charge is quite maintained at the average of the starting SoC at the beginning of the day as shown in Fig. 2.4 (c).

2.4.2 Methodology I Simulation Results Case-II

This subsection shows simulation results for methodology I for half cloudy/half clear day (Day-II). Day-II starts with cloudy condition and ends with clear condition. Fig. 2.5 (b) shows the active power smoothing results. Also, the active power 5 minutes power differential is reduced from 500 kW/5minutes to 300 kW/5minutes as shown in Fig. 2.5 (d).

2.4.3 Methodology I Simulation Results Case-III

This subsection shows simulation results for methodology I for mostly cloudy day (Day-III). The results showed better performance due to balance in the PV intermittency fluctuations as per Fig. 2.6 (a), and Fig. 2.6 (b). Moreover, state of charge is also maintained in an average of 0.4 throughout all day as shown in Fig. 2.6 (c). Finally, the 5 minutes power differential for PV was at the optimal level of reduction as it is reduced from 600 kW/5minutes to 200 kW/5minutes.

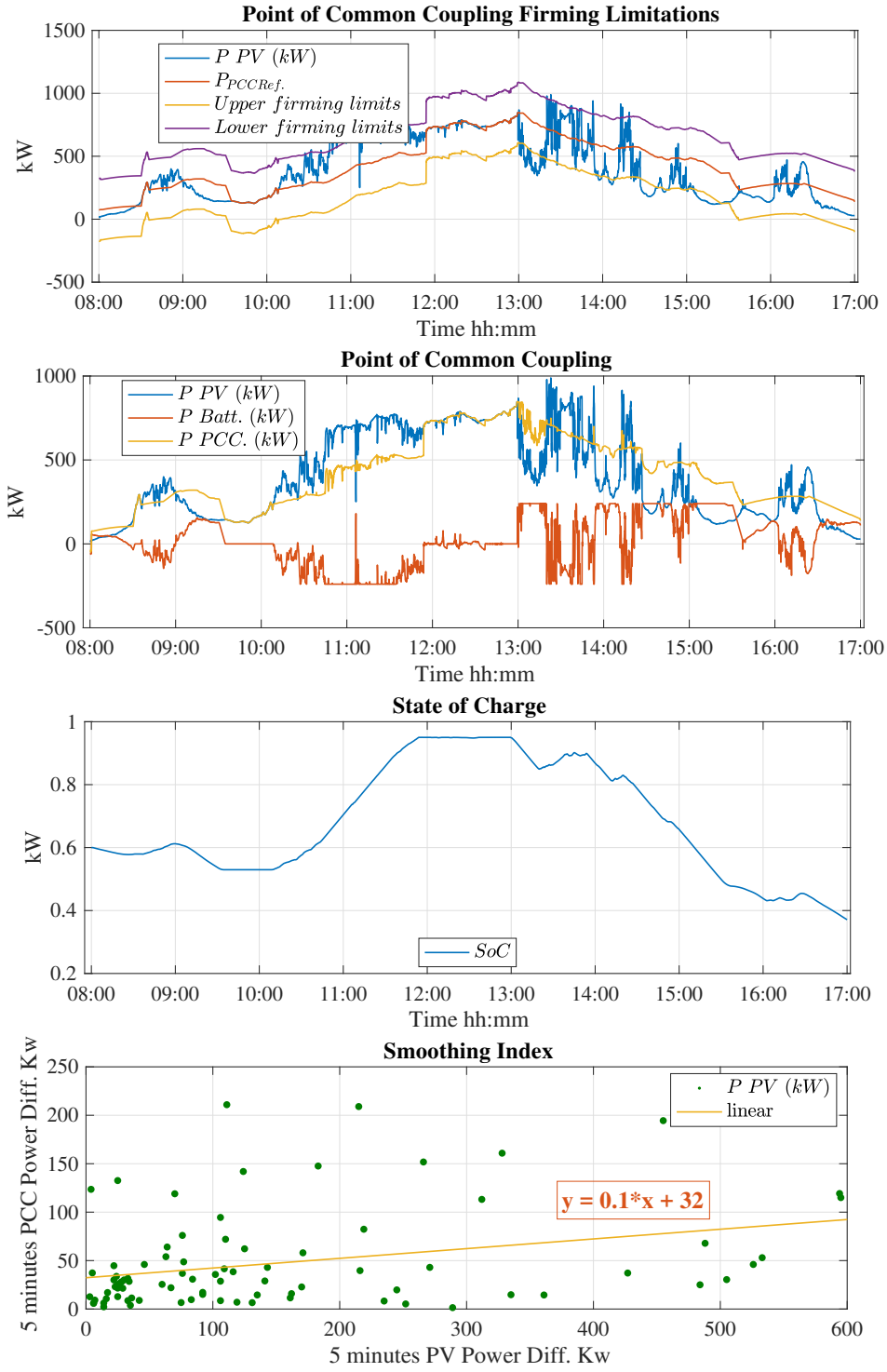

Fig. 2.4. P_{PV} based LSM I results for case-I. (a) Upper and lower firming limits and $P_{PCCRef.}$ curves.; (b) Smoothed PCC and Battery reference power.; (c) State of Charge (Soc).; (d) Smoothing index.

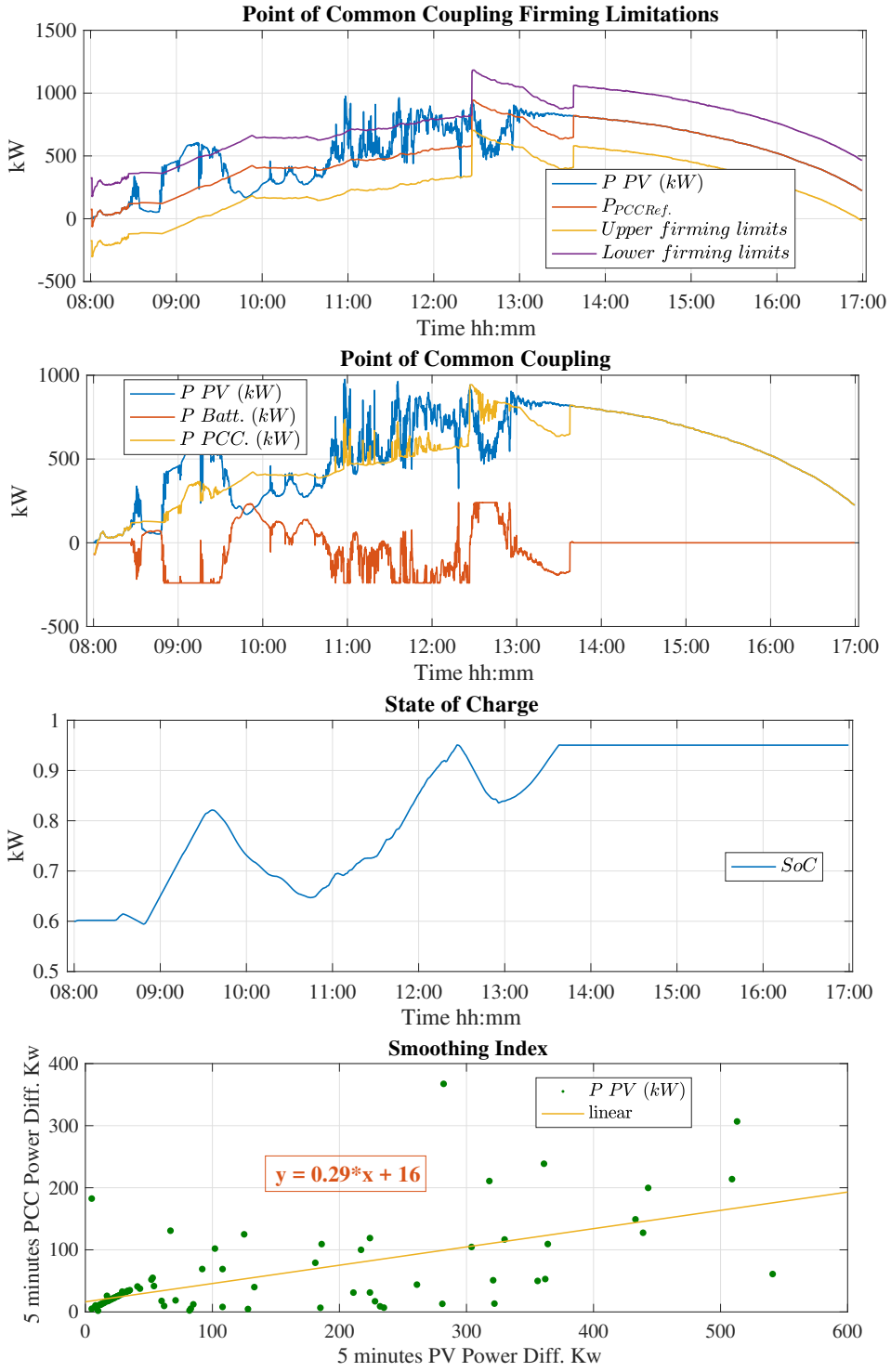

Fig. 2.5. P_{PV} based LSM I results for case-II. (a) Upper and lower firming limits and $P_{PCCRef.}$ curves.; (b) Smoothed PCC and Battery reference power.; (c) State of Charge (Soc).; (d) Smoothing index.

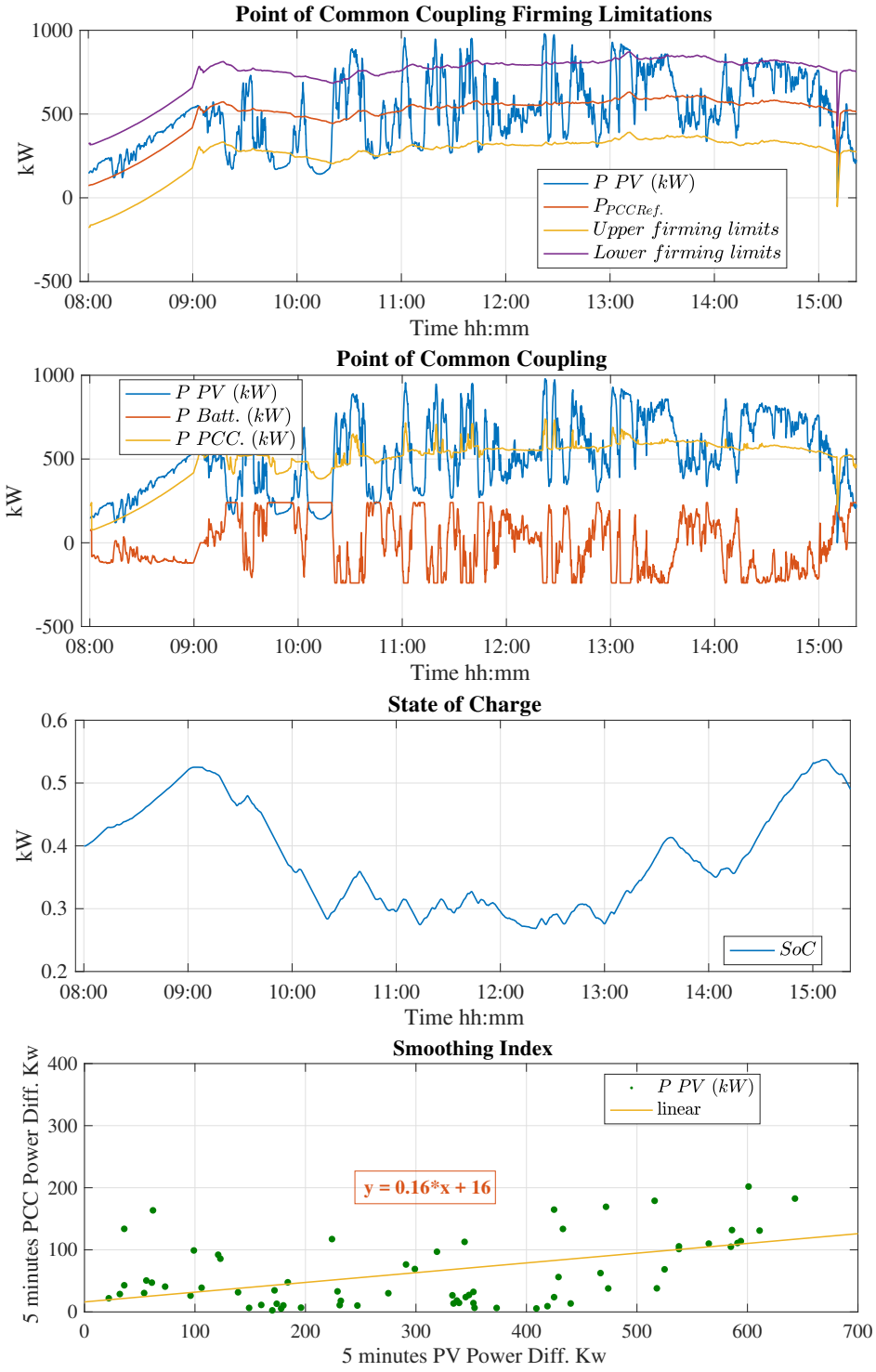

Fig. 2.6. P_{PV} based LSM I results for case-III. (a) Upper and lower firming limits and $P_{PCCRef.}$ curves.; (b) Smoothed PCC and Battery reference power.; (c) State of Charge (Soc).; (d) Smoothing index.

2.4.4 Methodology II Simulation Results Case-I

This subsection shows simulation results for methodology II for partly cloudy day (Day-I). Fig. 2.7 (a) shows P_{Set} control depends upon change in PV active power level. Then, the smoothed PCC output power is shown in Fig. 2.7 (c), and finally state of charge is depicted in Fig. 2.7 (d). Greatly, the 5 minutes power differential metric is reduced significantly from 400 kW/5minutes to 60 kW/5minutes as shown in Fig. 2.10 (a).

2.4.5 Methodology II Simulation Results Case-II

This subsection shows simulation results for methodology II for half cloudy/half clear day (Day-II). Fig. 2.8 (a) shows P_{Set} control depends upon change in PV active power level. Then, the smoothed PCC output power is shown in Fig. 2.8 (c), and finally state of charge is depicted in Fig. 2.8 (d). Greatly, the 5 minutes power differential metric is reduced significantly from 500 kW/5minutes to 150 kW/5minutes as shown in Fig. 2.10 (a).

2.4.6 Methodology II Simulation Results Case-III

2.4.7 Comparative Simulation Results

It is depicted in Fig. 2.5 (b) that the PCC power output is quite smooth except for some point of time such as 12:00 PM when PCC power experienced around 300 kW increase within almost one minute. However, it is noticed that the aforementioned problem with LSM I at 12:00 PM has completely vanished and $P_{PCCRef.}$ is as smooth as the corresponding P_{Set} curve at this time. As overall improvement, all the indices

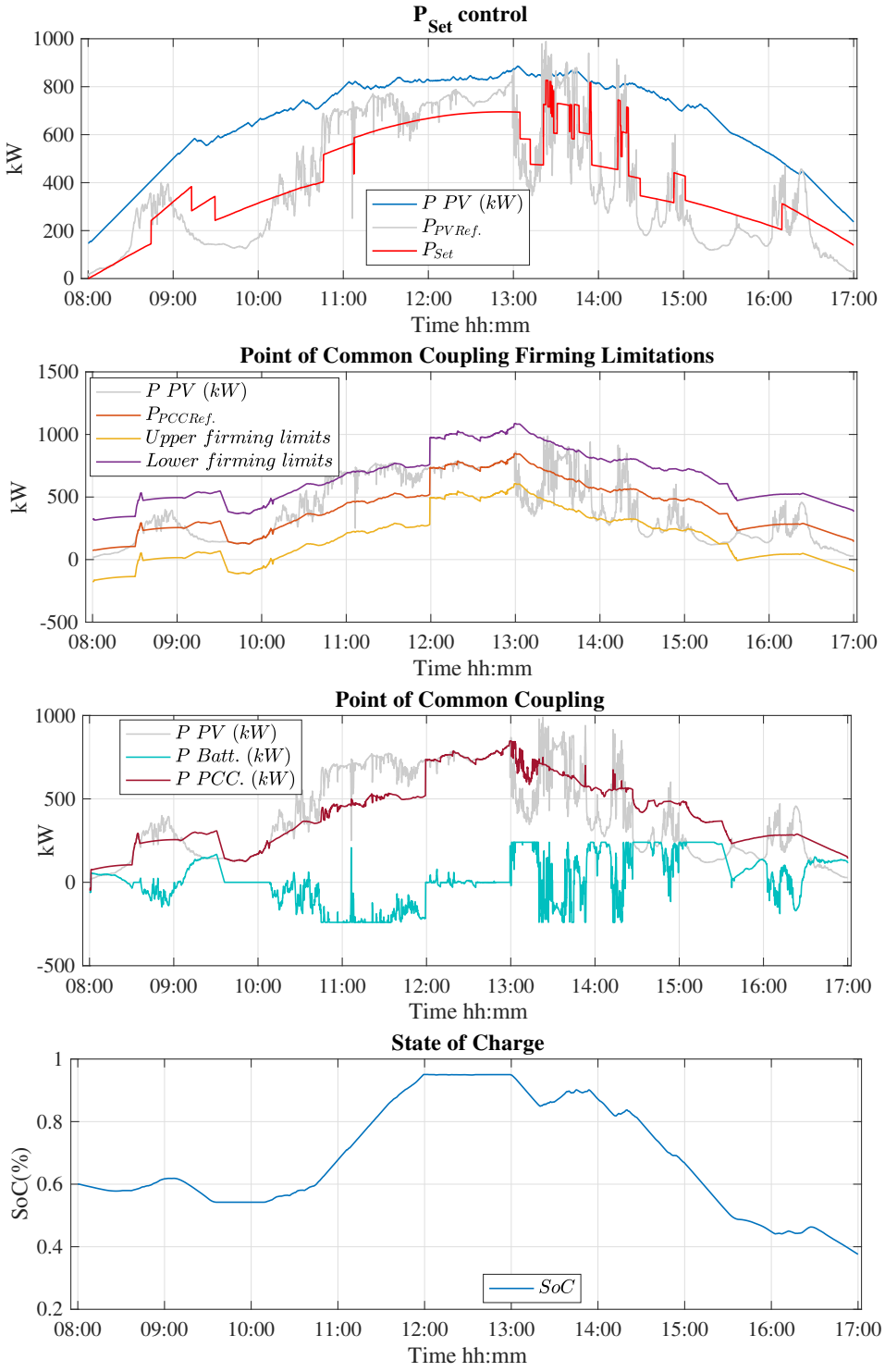

Fig. 2.7. P_{Set} based LSM II results for Day-1.(a) P_{Set} curve generation; (b) Upper and lower firming limits and $P_{PCCRef.}$ curves.; (c) Smoothed PCC and Battery reference power.; (d) State of Charge (SoC)

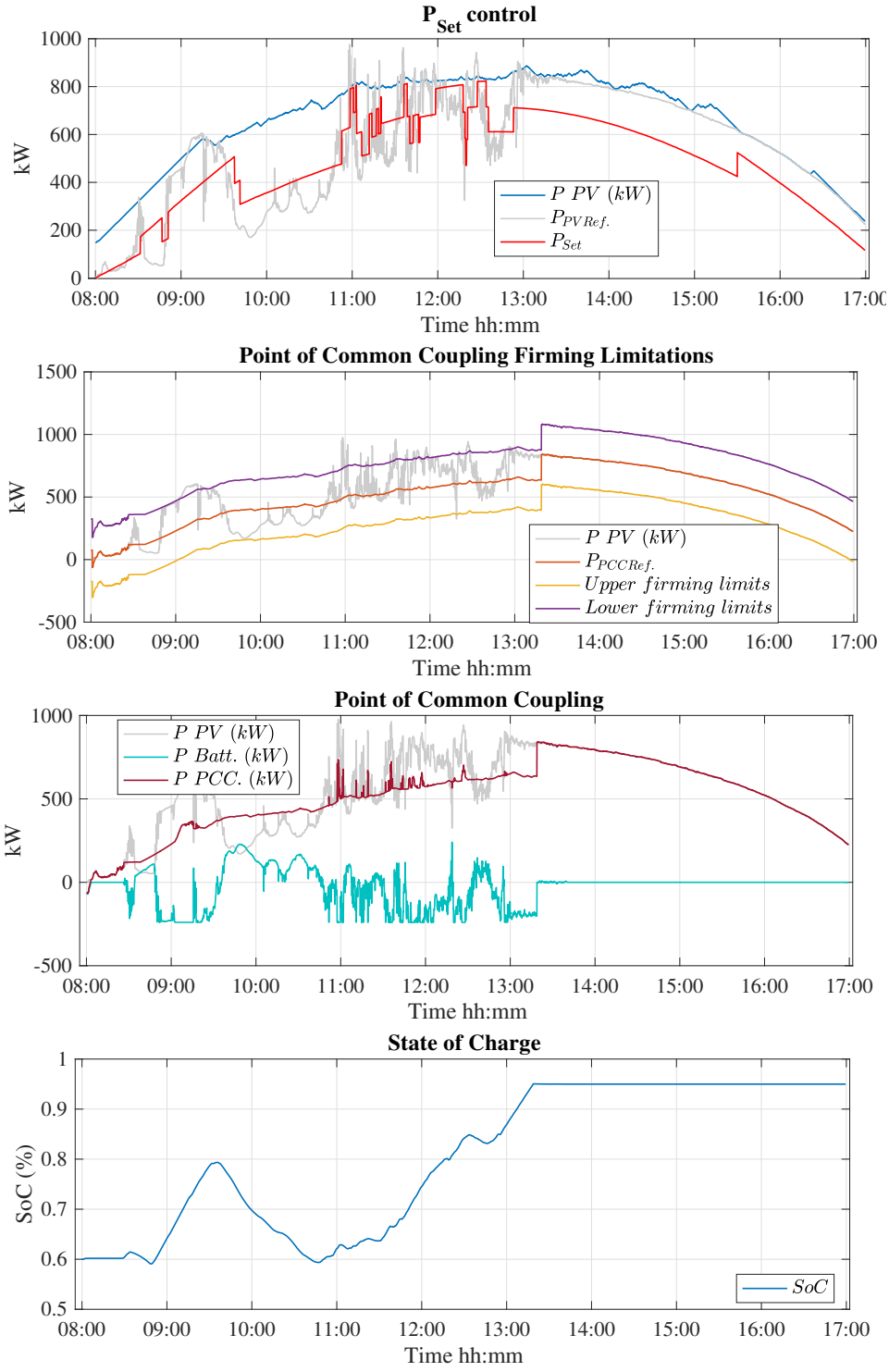

Fig. 2.8. P_{Set} based LSM II results for Day-2.(a) P_{Set} curve generation; (b) Upper and lower firming limits and $P_{PCCRef.}$ curves.; (c) Smoothed PCC and Battery reference power.; (d) State of Charge (SoC)

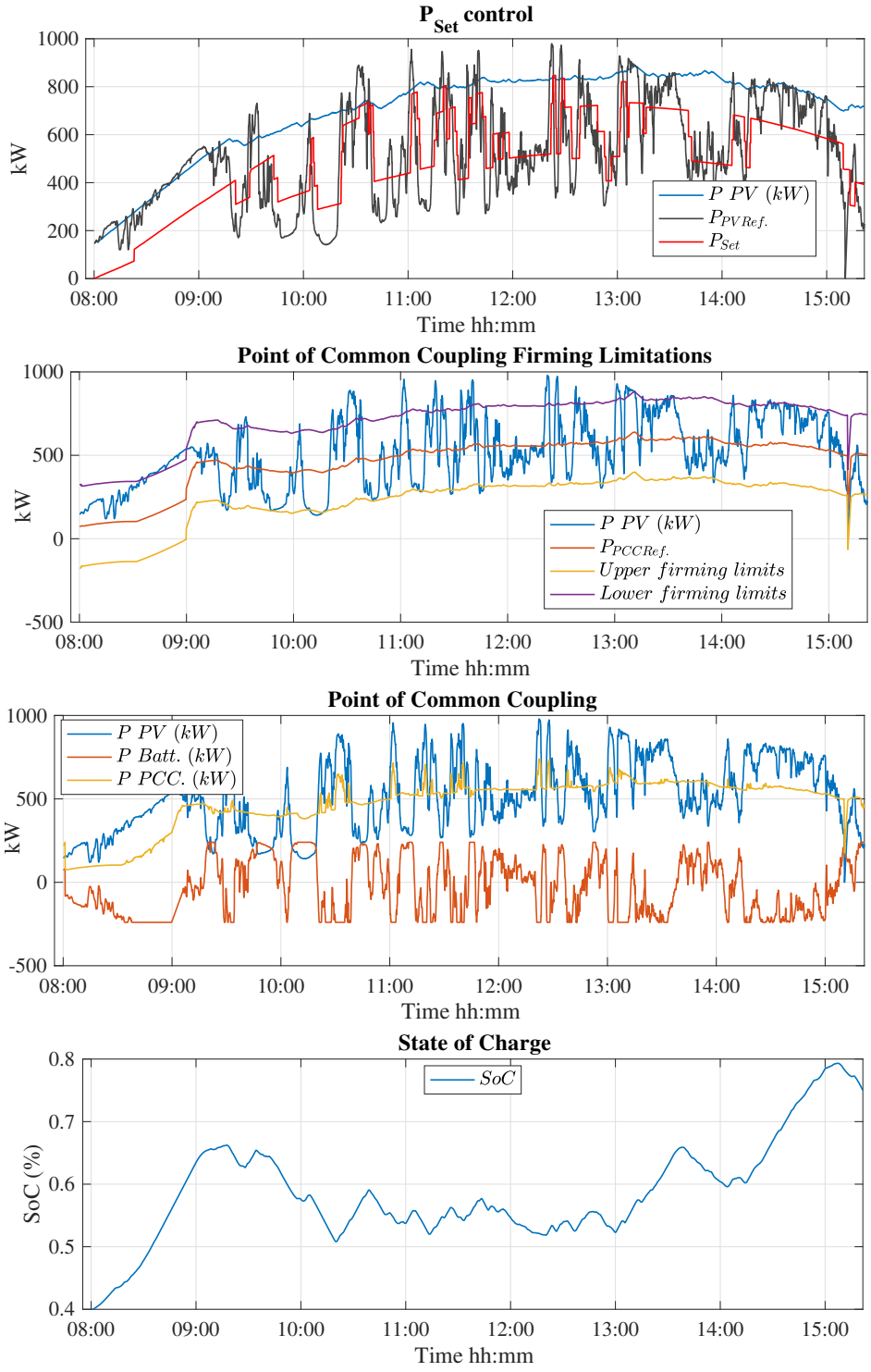

Fig. 2.9. P_{Set} based LSM II results for Day-3.(a) P_{Set} curve generation; (b) Upper and lower firming limits and $P_{PCCRef.}$ curves.; (c) Smoothed PCC and Battery reference power.; (d) State of Charge (SoC)

above 100 kW/5mints in LSM I are driven down significantly below 50 kW/5mints in LSM II results.

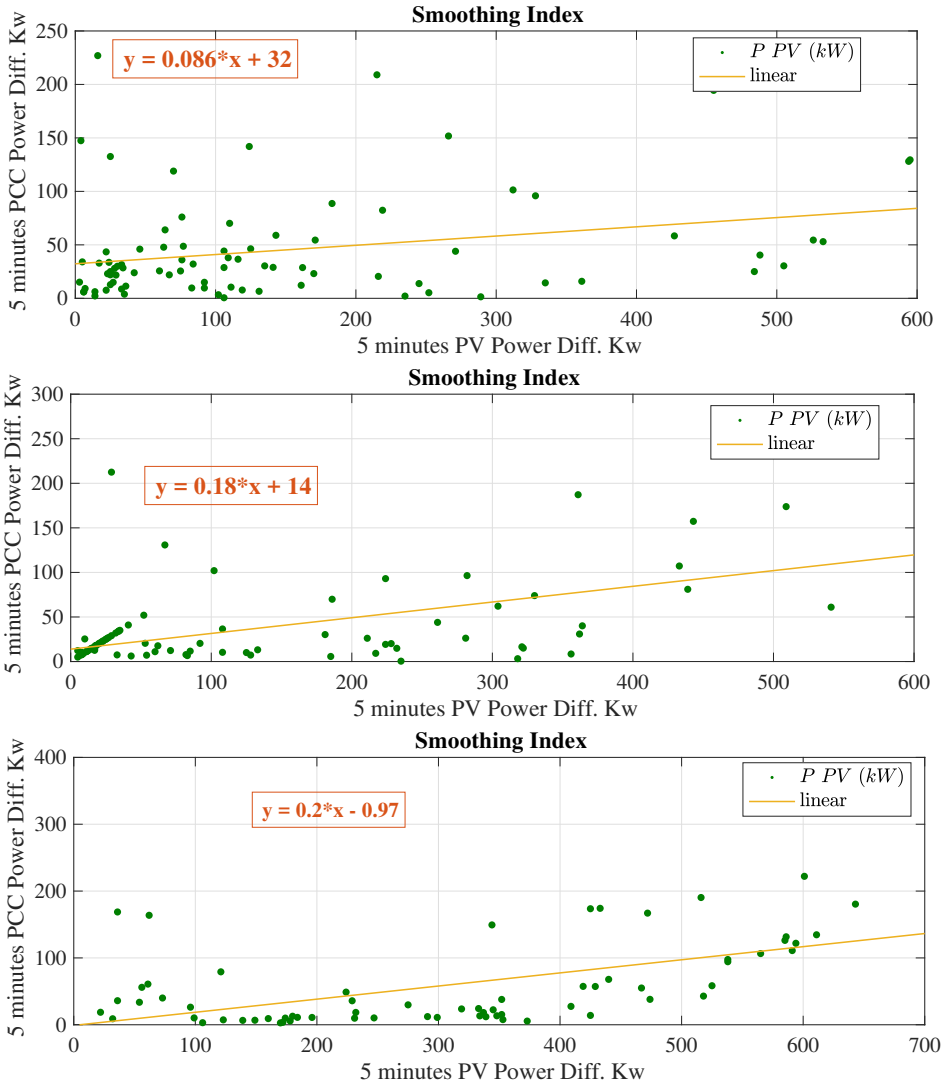

Fig. 2.10. Smoothing index Scatter.(a) Day-1; (b) Day-2.; (c) Day-3.

In regards to the other firming performance index, the least time step (5 seconds) rate of change for both PV and PCC power are just shown in table 2.1. As expected, method II has the least R_{PCC} for day 1 which is the mostly cloudy day. However, Method I shows equal performance for day 2 which is moderate cloudy day.

As shown in Fig. 2.12, BESS state of charge for both methods results are plotted

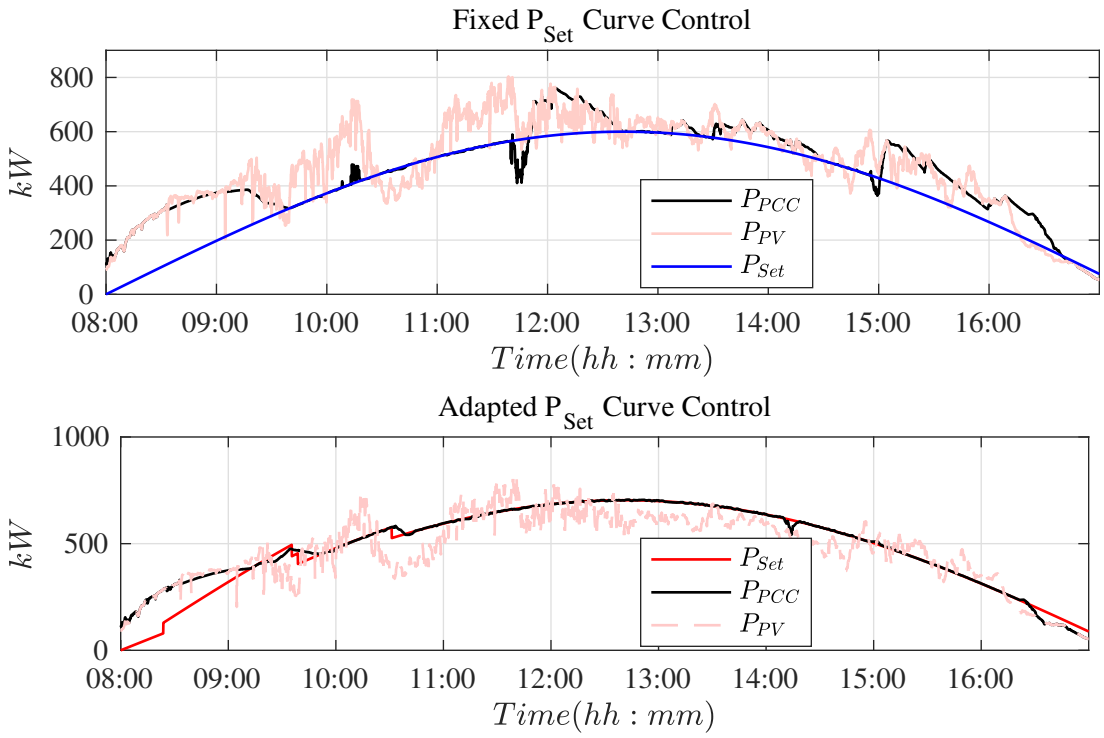

Fig. 2.11. Day 2 results comparison.(a) Constant P_{Set} curve.; (b) Controlled P_{Set} curve.

Table 2.1
PV and PCC 5 seconds time step rate of change

Day	Method	R_{PV} kW/5sec	R_{PCC} kW/5sec
Day1	Method I	49.4327	28.9717
	Method II	49.4327	21.176
Day2	Method I	57.8906	39.6021
	Method II	57.8906	38.3261
Day3	Method I	29.8617	16.3094
	Method II	29.8617	17.658

for both days of comparison. It is clear that method I SoC (0.799) at the end of the day 1 is significantly greater than method II SoC (0.645) which means that without SoC maximization being considered, method I could possibly take care of that more than method II. Because method I is much more looking at the PV level in the objective function itself, it preserves the SoC at higher level than method II does. vspace-10mm

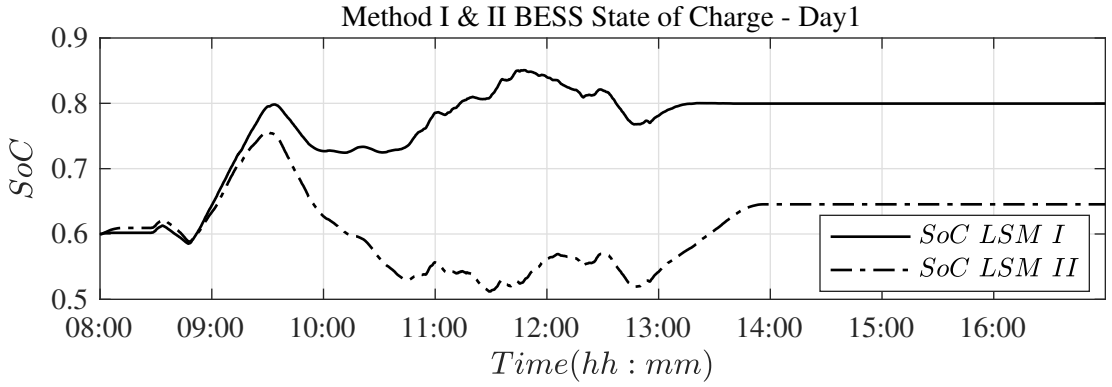

Fig. 2.12. Battery storage system state of charge evaluation

2.5 Summary

This chapter presented a local net active power management for the local point of common coupling (PCC) of utility-scale PV farms using energy storage systems. The proposed methodology is based on least squares minimization (LSM) technique. Error minimization technique aims to minimize the error between the total active power at the PCC and an optimal PV reference curve. Further, the proposed methodology uses the last minute average PV output feedback to adjust the positioning of the set-point curve P_{Set}. Results show a high level of PV firming to the very intermittent PV output power as the 5 minutes smoothing index (SI) was reduced from 450 kW/5min to 70 kW/5min.

CHAPTER 3: INTEGRATED NET ACTIVE POWER MANAGEMENT BASED ON OPTIMAL RAMP RATE AND PCC ERROR MINIMIZATION

This chapter presents a novel ramp rate control and active power smoothing for net-load profiles in large power distribution networks where high PV penetration levels exist. The novelty is to break large systems into virtual local net-load locations where energy storage systems (ESSs) technologies are installed to mitigate the severity of the anticipated shapes of system net-loads "Duck Curve."

3.1 Introduction

High penetration of PV farms develops the risk of over-generation in conventional generation units due to the timing imbalance between peak load and PV generation [4, 33]. PV penetration is expected to increase as the penetration level of distributed energy resources (DER) increases due to the inclusion of larger micro-grids and (BTM) based PV farms. PV power and the load changes during the day is significant especially when there is a high penetration of PV in the power grid. So, having the net-load (Load minus PV generation at a feeder location) ramp rate controlled in the middle of the day is an important application for reducing PV intermittency and load plus PV imbalances. With a moderate PV penetration level, combined-cycle technologies are used to address network ramping control [5]. However, at higher levels of PV penetration, these units are at the risk of shutdown due to steep change in the PV generation. Therefore, ESS technologies are considered essential tools for

controlling grid ramp rate and fluctuations of large-scale PV facilities. Active power management is now a basic primary term of energy storage applications in modern power distribution systems. This storage device can also help mitigate some of the issues related to time imbalance between load and PV generation. One of the most common active power management using energy storage systems is PV active power smoothing [11, 17, 29, 87, 108]. Ref. [17] presented a novel approach for PV system ramp rate control which used past time steps ramp rate control of PV to deduce the required ESS's ramp rate to achieve a certain level of smoothing at the point of common coupling (PCC) interface bus. Also, authors in [16] developed an error minimization based PCC active power smoothing using least squares minimization (LSM) technique. In [29], an active power curtailment based PV power ramp rate control (PRRC) was achieved utilizing short-term PV forecasting when the question nevertheless arises whether the free excessive power should be saved or curtailed. Similarly, given the applied restrictions on PV facilities ramp rate, authors in [88] developed PV ramp rate control by adjusting maximum power point tracking (MPPT) algorithm and by curtailing part of available potential power from solar PV facility. Nevertheless, most of the performed works considered installing the energy storage system at the PV solar facility bus where it is utilized to smooth the fast fluctuations generated during cloudy days. For system net-load active power to be controlled, energy storage systems are to be installed at distribution networks' substations. Active power supplied by a substation is also called "Net-load." Similar to PV active power smoothing, some research works are proposed for net-load smoothing and ramp rate control purposes as in references [50, 74, 83, 86]. Ref. [62, 83] studied all of the

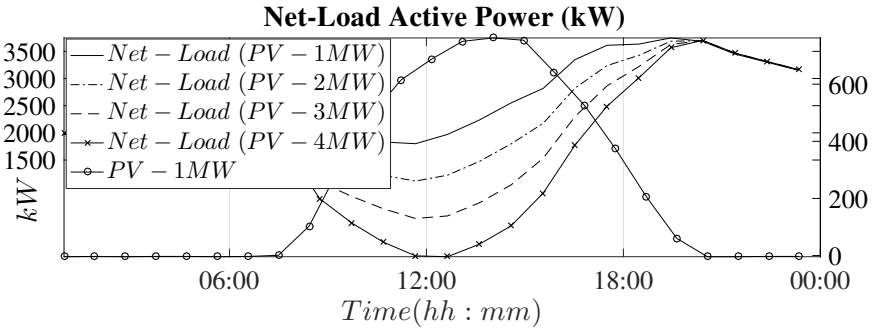

Fig. 3.1. Distribution Feeder Net-Load profile at of PV penetration

anticipated effects on distribution networks with high PV penetration levels. Results also raised the problem of net-load reduction and how energy storage systems usage along with conventional generation units are important to cope with this drastic change. Ref. [50] proposed an energy management system for high penetrated power grid with solar power plants, however fast changes active power were only considered. Besides, authors in [43] proposed an optimal unit commitment to solving the problem of 'duck curve.' However, as far as (UC) is concerned, there is still a significant amount of energy storage system for smoothing PV active power during cloudy days. Also, Ref. [74] proposed an economic dispatch optimization solution to solve Security Constrained Economic Dispatch (SCED) problem. The methodology is to optimize usage of all conventional power resources down- and up-ramping capability. References [70, 71] proposed a flexibility-oriented micro-grid optimal scheduling to control both hourly and intra-hour net-load variability. Using Plug-in Electric Vehicles (PEV) as a mean of controlling system net-load variability is mentioned in the literature as in [27, 38, 39, 69], because this form of energy storage is anticipated to be more commonly used in the future. A detailed study has been introduced in [69] where net-load variability was controlled by charging control strategy for PEV to

mitigate unit ramp-cycling operations (URC). However, the study was proposed for a high penetration level of wind power (WP). However, since wind generation does not have a fixed pattern that could cause a significant sag the total system net-load, it is more realistic to consider high penetration in PV power generation. Ref. [38] used dual splitting and gradient ascent to develop an optimal charging/discharging strategy for PEV to flatten the duck curve in California. In the current state-of-the-art methods, though solutions were provided, energy storage control methodologies were not addressed as an option for distributed control of net-load. In Ref. [39], authors, proposed customer incentives for EVs to be placed in the stations to aid load curve management. These swapping stations provide double discounts for those who can contribute during on-peak and off-peak periods for discharging/charging criteria. Ref. [18] presented two solutions for system net-load management; local management, and central management which recommends new fast response generation units. Methodology in [18] runs an optimal power flow which limits the two hours net-load change to certain value. This paper presents a methodology for system net-load active power control by controlling local locations of the system where high PV penetration is assumed to exist downstream those locations. The proposed method performs two separate applications: 1) net-load active power smoothing which aims to mitigate the fast fluctuations that happen due to the intermittent behavior of PV active power as well as randomness behavior in load profiles. 2) net-load ramp rate control over the short term and long term consideration to possibly minimize the expected steep ramp rate on conventional generators as well as avoiding over-generation events. Many factors are to be considered when energy storage systems (ESSs) are

used in such long-term applications. ESS sizing, optimal ramp rate during morning and evening times, the degree of flattening of the duck curve, and ESSs state of charge control schemes. Fast Fourier transform (FFT) based methodology is developed to considerably determine the optimal net-load reference curve from the original curve so that the existing energy storage system can bear charging/discharging schedule as far as active power (kW) and energy (kWh) capabilities are considered. This chapter is organized as follows: Section II explains the configuration of the system used to test the methodology. Section III presents in details an error minimization based active power control methodology for duck curve ramp rate control and associated ancillary services. Section IV discusses the simulation results, and section V discusses the summary and future work.

3.2 Problem Formulation and Methodology

In this section, net-load and reference curves definitions are provided. Also, least squares minimization based methodology to perform net-load ramp rate control, as well as active power smoothing, is provided in details.

3.2.1 Local Net-load and Relation to Local Duck Curve

For a certain power distribution network, feeder net-load P_{NL} is defined as the active power generation supplied by the main feeder substation. P_{NL} can also be defined as the result of subtracting renewable energy resources generation from total system feeder load as shown in Eq. (3.1). Similarly, local net-load P_{NLi} is the power generation at a local location in the distribution network such as the downstream part includes interconnected loads, solar farm facilities and energy storage units. As

PV penetration level increases, system net-load profile tends to have that shape of duck neck with a significant sag during the day and a steep ramp rate around it. The energy storage system is assumed to be installed at the net-load bus so that both fast changes and ramp rate of both loads and solar units are being controlled.

$$P_{NLi}(i = 1, 2, ..., n) = P_{Li} - P_{PVi} \tag{3.1}$$

where P_{NL} is the total net-load of the system, P_L is the total feeder load, P_{PV} total generation power by PV photo-voltaic plants, P_{WG} is all the generation supplied by the wind power resources existing in the system and P_{ESS} is the generation power supplied by energy storage systems installed in the system. Besides, active power profiles sub-scripted with the index i refer to the electrical quantities with respect to the i^{th} local net-load in the system.

3.2.2 Historical Days Based Net-load Reference Curve $P_{NL.Ref}$

To control ramp rate of local net-load locations of a distribution network, historical behavior and PV penetration level should be considered. Therefore, a smooth

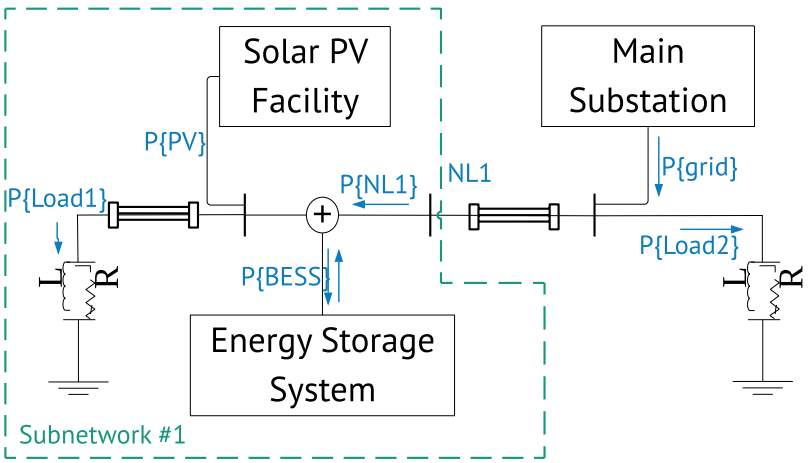

Fig. 3.2. Local Net-load and relation to local duck curve.

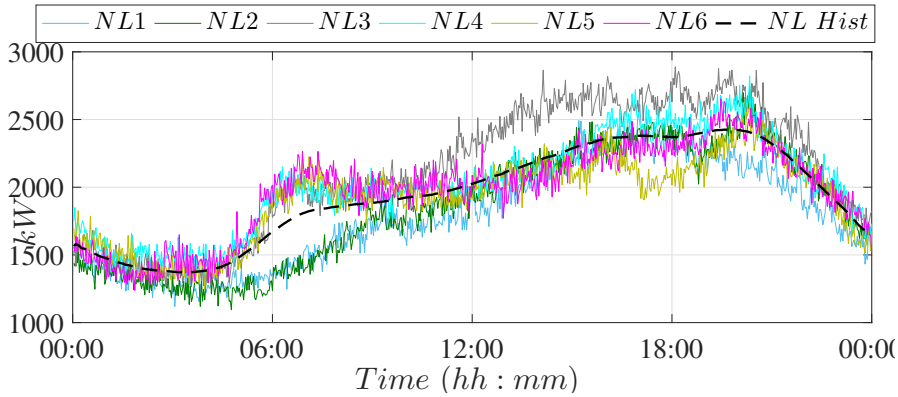

Fig. 3.3. Historical representation of net-load reference curve generation for ramp rate and active power smoothing purpose.

and controlled reference curve is required to the proposed optimization problem and constraints. Net-load historical curve is defined as the past week of average active power curve for all the downstream interconnected loads for a certain local net-load location with no PV solar facilities considered yet in a certain sub-network as shown in Fig. 3.3. One week selection is sufficient to capture the moving peaks according to load peaks PV peaks times. As PV penetration level changes and energy storage systems is selected, this reference curve requires control to manage changes due to different PV penetration levels. Fast Fourier transform (FFT) is used to divide net-load historical curve signal into its frequency components so that this curve is shaped in such a way that meets with energy storage sizing as well as reduced ramp rate. Net-load historical curve is expressed as follows:

$$P_{NLHist.} = average(P_{NL1}, P_{NL2}, P_{NL3}, ..., P_{NL7}) \tag{3.2}$$

where $P_{NLHist.}$ is historical representation of certain local net-load location. As shown in Fig. 3.5., reducing the frequency components by certain coefficient (α) controls level of the sag point in the net-load curve. Therefore, a frequency coefficient (α) is

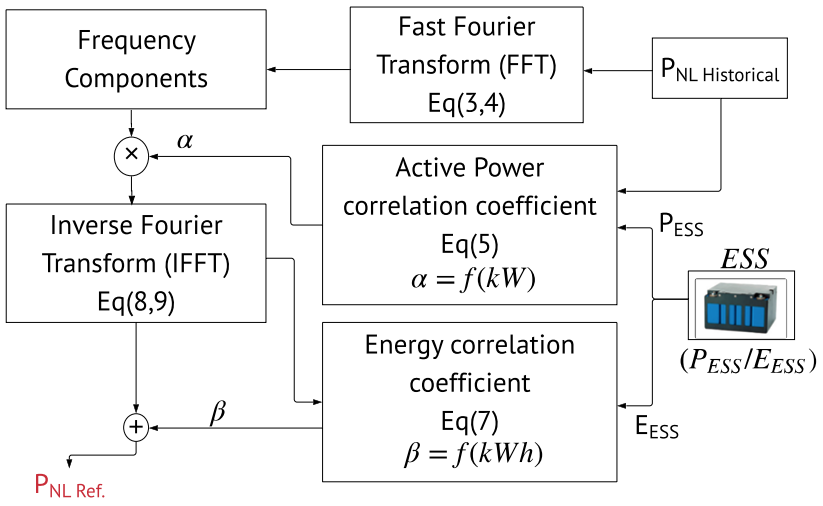

Fig. 3.4. Fast Fourier Transform based net-load reference curve generation flowchart used to develop a reduced ramp rate reference curve based on the historical curves and given energy storage active power capability as shown in Eq. (3.4. As energy capacity of energy storage is a second important aspect in active power management energy storage applications, Eq. (3.5 calculates the energy error between the charging area (E_2) and energy capacity of used energy storage system (E_{ESS}). Then, an average power offset is calculated based on energy error and charging time (T_2). An active power coefficient (β) is developed to adjust reference curve position so that charging and discharging areas are to be maintained within energy storage limits as shown in Eq. (3.6. For example, Fig. 3.5. shows a given net-load location with energy storage of [700kW/2100kWh]. Frequency coefficient is calculated as 0.6, whereas energy error brings the signal peak and up- and down-ramping rates by certain limits. Also, the correlation coefficient (α) has a direct proportionality with energy storage system sizing as the curve's sag points should only be brought up by the amount that the energy storage system could reach to perform active power smoothing. Hence, both wide span of (α) values, as well as corresponding controlled references curves, are

fitted so that an optimal (α) could be determined based on a given ESS's size. For example, an energy storage system with 140 kW active power capability would be enough to manage a controlled reference curve calculated by a correlation coefficient ($\alpha = 0.7$). Moreover, under the effect of PV intermittency level, the variable (α) could be a bit reduced so that ESS is able to bear smoothing the level of intermittency.

$$FFT(f(k)) = F(\omega) = \int_{-\infty}^{\infty} f(t)e^{j\omega}dx \tag{3.3}$$

$$\alpha = (P_{NL\ pk-pk} - P_{ESS})/(P_{NLpk-pk}) \tag{3.4}$$

$$e_2 = (E_2 - E_{ESS}) \tag{3.5}$$

$$\beta = e_2 * T_2 \tag{3.6}$$

$$P_{NL.Ref}(\omega) = \alpha * P_{NL}(\omega) \tag{3.7}$$

$$IFFT(F(\omega)) = \frac{1}{N} conj(FFT(conj(F(\omega)))) \tag{3.8}$$

$$P'_{NLRef.}(k) = IFFT[P_{NL.Ref}(\omega)] \tag{3.9}$$

$$P_{NLRef.}(k) = P'_{NLRef.}(k) - \beta \tag{3.10}$$

where α is the correlation coefficient between ESS active power capacity and the frequency components magnitudes, and β is the correlation coefficient between ESS energy capacity and the frequency components magnitudes.

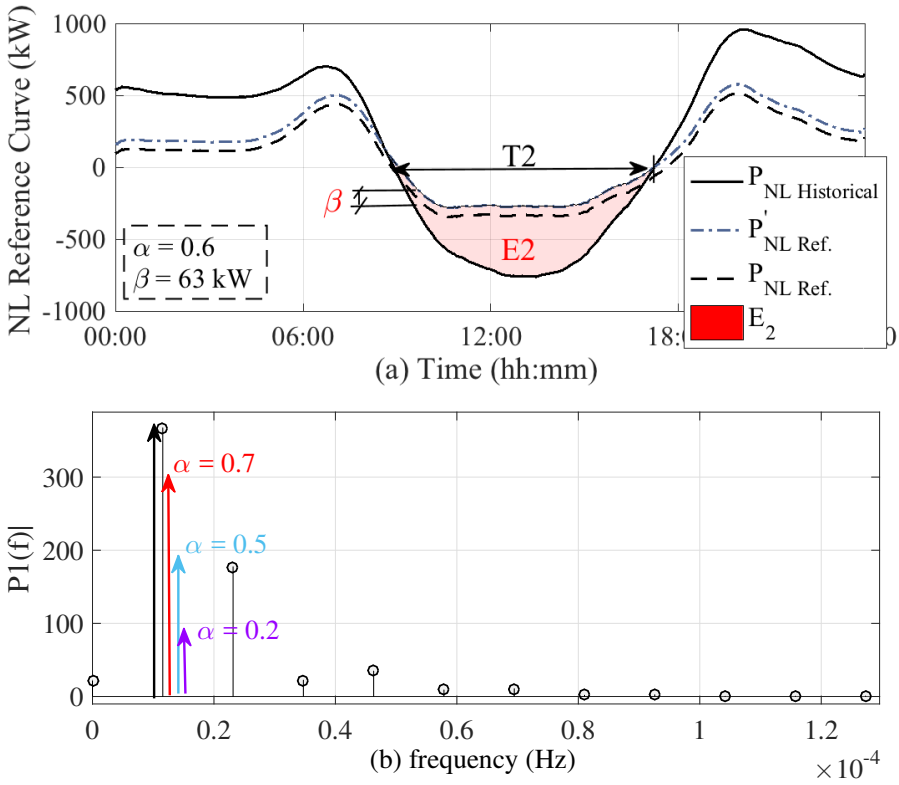

Fig. 3.5. Net-load reference curve control using fast Fourier transform (FFT) (a) controlled net-load curves using different values of correlation factor α ; (b) FFT Amplitude Spectrum.

3.2.3 Ramp Rate Threshold Generation

One of the crucial parameters in the proposed methodology is the net-load ramp rate threshold value. It is determined so that ramp rate of system net-load profile is reduced enough to bring the duck curve's sag point up to adequately prevents over-generation and steep ramp rate on conventional power generation units. Besides, ESS's State of charge (SoC) is a critical key factor in active power control applications as depleting or maximizing SoC at few hours of the day leads to algorithm termination which in turn stops the ESS from following the algorithm dispatch set-points. Therefore, ramp rate threshold value ζ is to be determined under the guidance and by the input of both net-load reference curve and energy storage system SoC status.

To dynamically control the constraint parameter ζ, two types of errors are calculated every time step; ramp rate error e_{rr} and state of charge error e_{SoC}. As shown in (3.12), the ramp rate error is the difference between net-load reference curve ramp rate and actual net-load profile ramp rate. Then, this ramp rate error is fed to a proportional controller which tunes the value for ramp rate threshold value ζ_{rr}. Also,

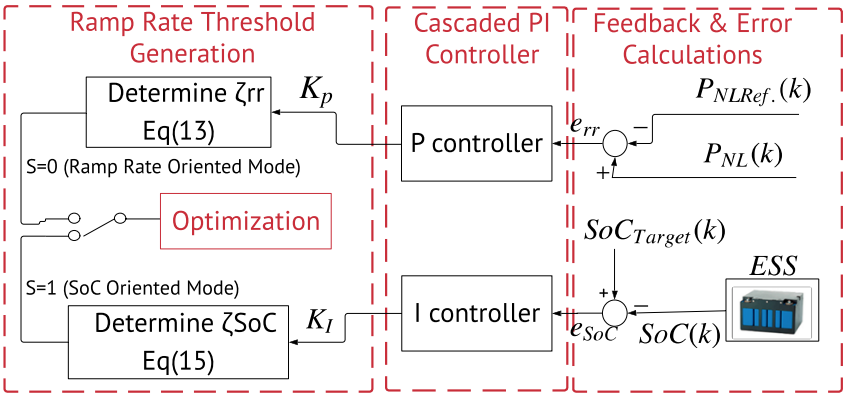

Fig. 3.6. Ramp rate threshold generation using cascaded PI controller

state of charge error e_{SoC} is the difference between the current SoC and the targeted SoC at time instant (k). In the regard of controlling SoC, ramp rate threshold value is generated so that energy storage system charges/discharges in the direction of approaching the targeted SoC. Therefore, e_{SoC} is then fed to an integral controller that calculates the SoC based ramp rate threshold value ζ_{SoC}.

$$\frac{dP}{dk} = (P(k) - P(k-1))/\Delta k \tag{3.11}$$

$$e_{rr}(k) = \frac{dP_{NLRef.}}{dk} - \frac{dP_{NL}}{dk} \tag{3.12}$$

$$\zeta_{rr}(k) = K_p * e_{rr}(k) \tag{3.13}$$

$$e_{SoC}(k) = SoC(k) - SoC_{Target}(k) \tag{3.14}$$

$$\zeta_{SoC} = K_i \int_{k}^{k+t} e_{SoC}\ dk \tag{3.15}$$

where $e_{rr}(k)$ is ramp rate difference between both net-load and net-load reference curves, $e_{SoC}(k)$ is difference between both current and targeted state of charge, K_p is proportional controller parameter, K_i is integral controller parameter, $\zeta_{rr}(k)$ is ramp rate based threshold value, and $\zeta_{SoC}(k)$ is SoC based ramp rate threshold value.

3.2.4 Optimal Power and Energy Management

As proposed by authors in Ref. [16], least squares minimization technique is proven to be valuable for PV active power smoothing application. In this study, least squares minimization performs the concept of reducing the error between the targeted power curve and a reference power curve so that controlled net-load profile is smoothed to prevent spread of intermittent solar PV power through the network. Also, based on the net-load reference curve selection, certain degree of ramp rate reduction is also achieved with a threshold value (ζ) which is discussed later in further details.

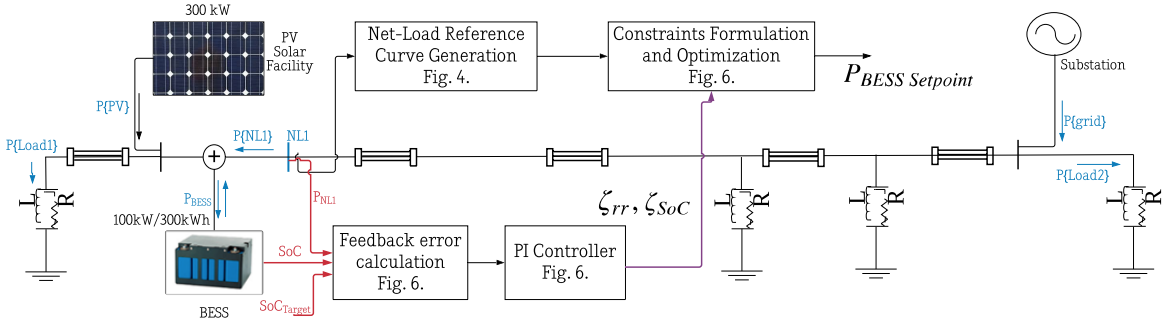

Fig. 3.7. Block representation of proposed methodology.

$$min\ U = \sum_{k=t}^{t-10} (1/2) * (P_{NL}(k) - m * P_{NLRef.}(k))^2 \tag{3.16}$$

$$P_{NLset-point}(k) = m(k) * P_{NLRef.}(k) \tag{3.17}$$

$$P_{ESSset-point}(k) = P_{NL}(k-1) - P_{NLset-point}(k) \tag{3.18}$$

Here $m(k)$ is a multiplication factor that derives the net-load active power set-point from the net-load reference curve such that all the following constraints are fulfilled.

$$P_{ESSMax.} \geq P_{ESS}(k) \geq P_{ESSmin} \tag{3.19}$$

$$P_{ESS}(k) = P_L(k) - m(k) * P_{NLRef.}(k) - P_{PV}(k) \tag{3.20}$$

$$m(k) \leq \frac{P_{ESSmin} + P_{PV}(k) - P_L(k)}{P_{NLRef.}(k)} \tag{3.21}$$

$$m(k) \geq \frac{P_{ESSmax} + P_{PV}(k) - P_L(k)}{P_{NLRef.}(k)} \tag{3.22}$$

Such that Eq. (4.2) is the algebraic inequality constraint for the energy storage system active power capability, and Eq. (3.20)-(3.22) are the inequality constraints for the multiplication factor $m(k)$ that achieves that algebraic constraint through the optimization formulation.

Also, net-load ramp rate control is controlled through an inequality constraint which derives limits for the multiplication factor ($m(k)$) based on the required thresh-

old value ζ for ramp rate of the net-load as shown in Eq. (3.23)-(3.26). Threshold value, zeta, of the net-load ramp rate is the targeted ramp rate for the net-load profile. This value depends upon season of the year, feeder capacity and PV Penetration level. Normally, zeta ζ is selected as the average ramp rate of the load demand curve at each certain location assuming that no PV generation exists. To cope with energy storage sizing and PV penetration level, zeta ζ is tuned and updated through net-load reference curve control. For example, a net-load profile with the 20% PV penetration level. The threshold ramp rate ζ is chosen as 20 kW/10 minutes which is the normal ramp rate for the same local net-load without PV generation existing. However, depending upon financial limitations with energy storage systems sizing, zeta is subjected to an increase as well as PV penetration increase. Results section presents a detailed study about trade-off between feeder capacity, PV penetration level and energy storage sizing.

$$-\zeta_{rr} \leq \frac{P_{NL}(k) - P_{NL}(k-1)}{\Delta k} \leq \zeta_{rr} \tag{3.23}$$

$$P_{NL}(k) \geq -\zeta_{rr} * \Delta k + P_{NL}(k-1) \tag{3.24}$$

$$m(k) \geq \frac{-\zeta_{rr} * \Delta k + P_{NL}(k-1)}{P_{NLRef.}(k)} \tag{3.25}$$

$$m(k) \leq \frac{\zeta_{rr} * \Delta k + P_{NL}(k-1)}{P_{NLRef.}(k)} \tag{3.26}$$

$$\zeta_{SoC} = \frac{P_{NL}(k) - P_{NL}(k-1)}{\Delta k} \tag{3.27}$$

$$P_{NL}(k) = -\zeta_{SoC} * \Delta k + P_{NL}(k-1) \tag{3.28}$$

$$m(k) = \frac{-\zeta_{SoC} * \Delta k + P_{NL}(k-1)}{P_{NLRef.}(k)} \tag{3.29}$$

where ζ_{rr} is ramp rate based threshold value of zeta, ζ_{SoC} is SoC control based threshold value of zeta, $P_{NL}(i)$ is the current value of net-load profile, $m(k)$ is the least squares minimization optimal coefficient.

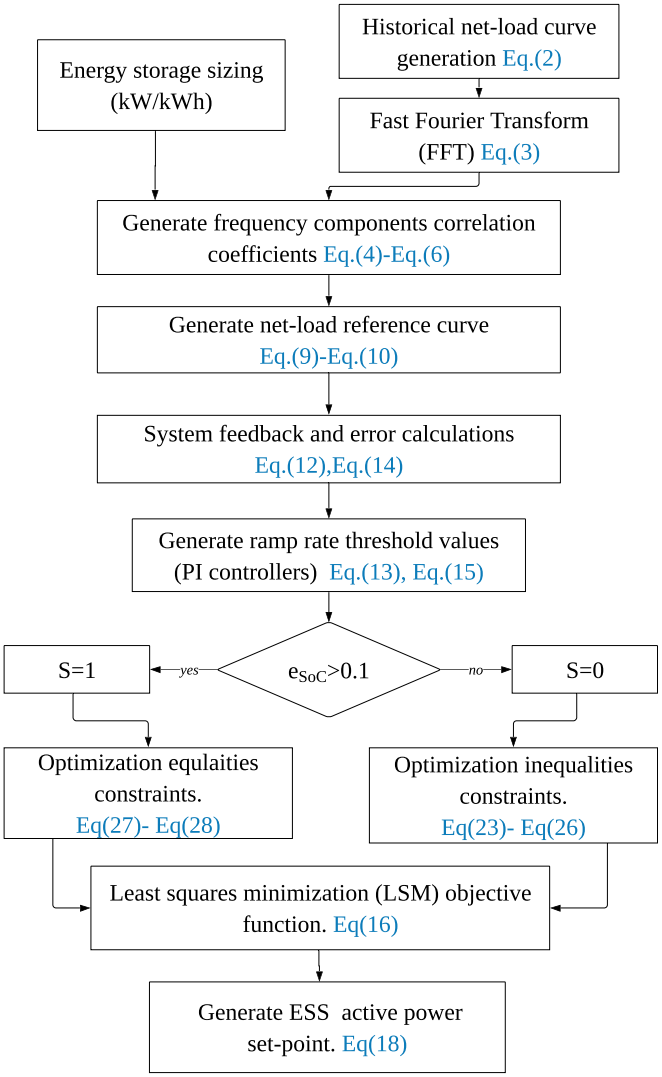

Fig. 3.8. Least Squares Minimization (LSM) based net-load control flowchart

3.3 Performance Index for Evaluation

This section presents and evaluates simulation results for the proposed net-load active power management methodology. The proposed methodology incorporates many crucial aspects of power distribution networks with higher renewable energy penetra-

tion levels. Results are discussed based on the following aspects:

Active Power Management Improvement: Active power management improvement incorporates active power smoothing, ramp rate improvement, and over-generation risk prevention. Due to the energy storage system's fast response, the proposed methodology incorporating active power smoothing for chosen local net-load locations. The main advantage of smoothing active power profiles is it smooths both PV out power intermittency and load profiles fluctuations. The smoothing index used in the proposed study is one-minute power differential R_{NL} as shown in Eq. (3.30). Also, as one of the essential applications, ramp rate improvement (RRI) is the long-term ratio of the overall controlled and uncontrolled net-load profile ramp rate which measures minimization of the imposed steep ramp rate on conventional power generation units as shown in Eq. (3.31) . Also, based upon selected energy storage system sizes, the risk of over-generation is evaluated as far as local locations and main system net-load location is concerned. Finally, system losses reduction is evaluated using power losses index (ILP) as shown in (3.32).

Voltage Profiles Improvement and Tap operations Savings: Another substantial metric of evaluation is voltage deviation index (VDI) which is a measure of how the system voltage span is reduced which in turns avoids voltage violations and voltage regulators.

Energy Storage Full Capacity Utilization: Besides, the methodology is evaluated based on how energy storage systems are utilized during the full day. ESS utilization is optimized so that full charge/discharge capacity is utilized taking into consideration

state of charge (SoC) within limits.

$$R_{NL} = \frac{P_{NL}(k) - P_{NL}(k-1)}{\Delta k} \tag{3.30}$$

$$RRI = \frac{RR_{controlled}}{RR_{basecase}} \tag{3.31}$$

$$ILP = \frac{P_{loss}^{controlled}}{P_{loss}^{basecase}} \tag{3.32}$$

$$VDI = \frac{V_{max} - V_{min}}{V_{mean}} \tag{3.33}$$

where (RRI) is the ramp rate improvement index, $RR_{controlled}$ is the ramp rate for the controlled local net-load profile, $RR_{basecase}$ is the uncontrolled profile for the same location, (ILP) is the power loss index, VDI is the voltage deviation index.

3.4 Test Feeder models

Two test feeder models are used in the proposed study.

Distribution Feeder 1: The first test feeder uses is an aggregated 16 bus system that includes substation, four load centers and two voltage regulators as shown in Fig.3.9. The feeder is aggregated from a real 720 nodes distribution feeder in the US, and the aggregated model is validated based on real measurements from the field. One PV facility and one energy storage system is installed in this feeder, and the assumed sizes are 300kW and 100 kW respectively. The load profile for one area is sized as 200 KW.

Distribution Feeder 2:The second benchmark distribution network for this study is IEEE 8500-node test feeder [21]. In this feeder, net-load ramp rate control algorithm

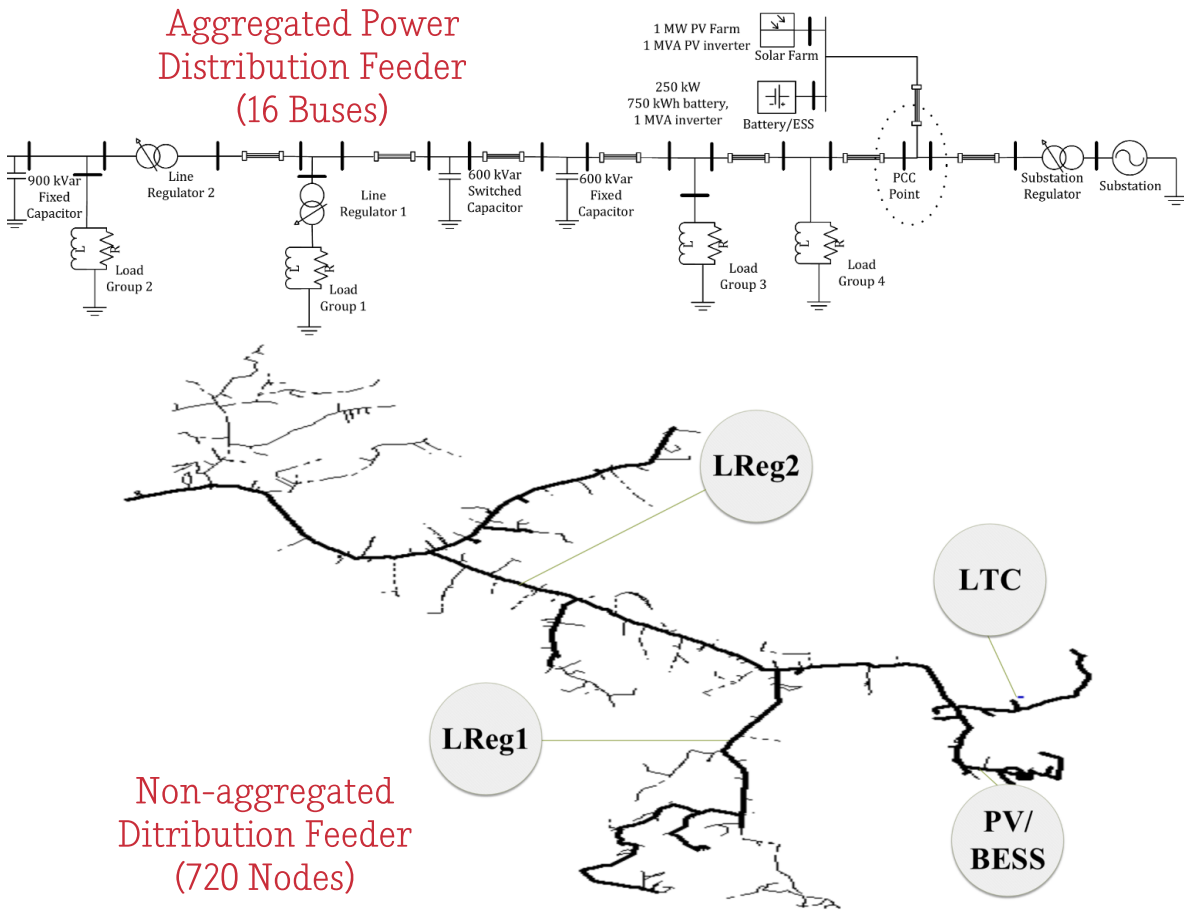

Fig. 3.9. Aggregated Power Distribution Feeder (16 Buses)

is applied independently on three different locations of local net-loads NL#1, NL#2 and NL#3. This feeder is selected as a more realistic feeder for testing the scalability of the proposed methodology. The model is developed in CYME including one online load tap changer (OLTC), three line voltage regulators, nine single phase and one three-phase capacitor. Sizing of developed PV facilities and energy storage systems is considered such that it is proportional to load percent of each zone of the whole feeder load. For example, PV penetration of 50% is 5.5 MW of the total load which is split between NL#1, NL#2 and NL#3 as 2500 kW, 1000 kW, and 2000 kW respectively. Similarly, energy storage systems sizing is selected 30% of PV ratings.

Hence ESS1/ESS2/ESS3 capacities are to be 750kW/2250kWh, 300kW/900 kWh, and 600kW/1800kWh respectively. In both these feeders, first, an offline study is performed to determine references curves. The results and analysis of the proposed algorithm on these feeders are discussed next.

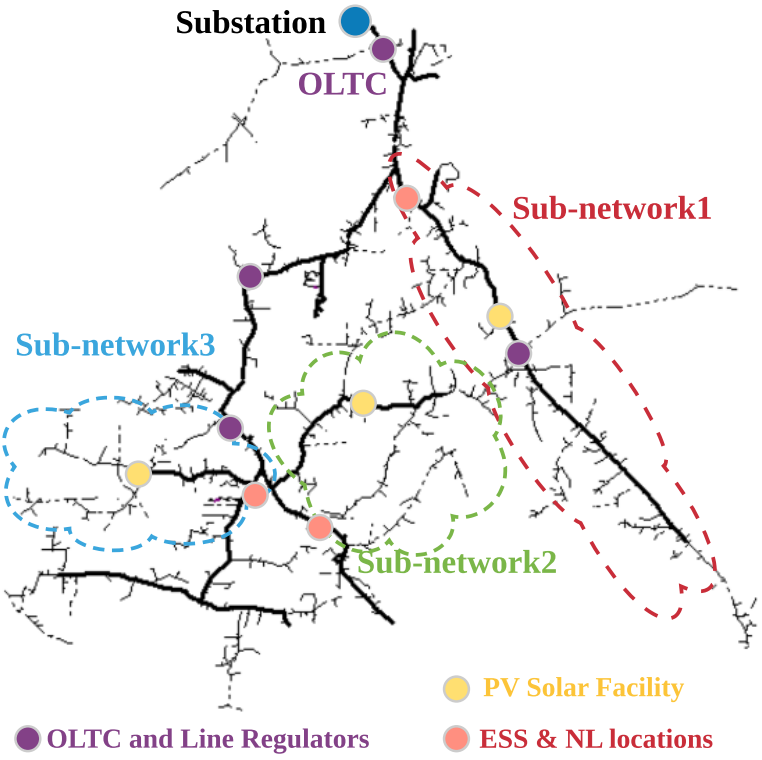

Fig. 3.10. IEEE 8500-Node test feeder

3.5 Simulation Results

3.5.1 Test-I: Distribution Feeder-I (Aggregated 16-Bus) Simulation Results

Fig. 3.11 shows results of active power smoothing and ramp rate control for net-load#1 location in test feeder presented in Fig. 3.7. This study is used as a proof of concept and to show the difference between using ramp rate based threshold value ζ_{rr}

using inequality constraints and state of charge based dynamic constraints ζ_{SoC} using equality constraints. Case-0 represents the original net-load profile without control is on, whereas case-1 is simulation results with ζ_{rr} controlled but without controlling ζ_{SoC}. Case-2 represents simulation with both thresholds applied and controlled, ζ_{rr} and ζ_{SoC}. Using ramp rate based zeta allows the methodology to set the ramp rate between ζ_{rr} and -ζ_{rr} through two inequalities constraints as shown in (3.25)-(3.26). Setting a wide range of ζ_{rr} controls the net-load profile with no SoC consideration which might make SoC hit any of maximum or minimum limit as shown in Fig. 3.11.(c). On the other side, generating SoC based threshold value ζ_{SoC} using error between current SoC and targeted SoC (which is incorporated through the set of equality constraints) will allow us to control net-load profile in the direction that adjusts SoC to the required level. Fig. 3.11.(a), case-2 shows better performance in both smoothing and ramp rate control using dynamic constraints formulation where ζ_{SoC} is controlled in steps from -5 to 5. Fig. 3.11.(c), SoC case 2 shows better control of SoC as it was kept within an average of 0.5, whereas SoC case 1 state of charge hit the limit of 0.9 and the algorithm is terminated.

3.5.2 Test-II: Distribution feeder II Multiple Net-load locations Management Simulation Results

In this subsection, more detailed results are presented for IEEE 8500-node test feeder [21]. System is divided into three sub-networks, where each sub-network includes a photo-voltaic PV solar facility, energy storage system unit at the net-load location and the sub-network load spots. To show improvement for each location

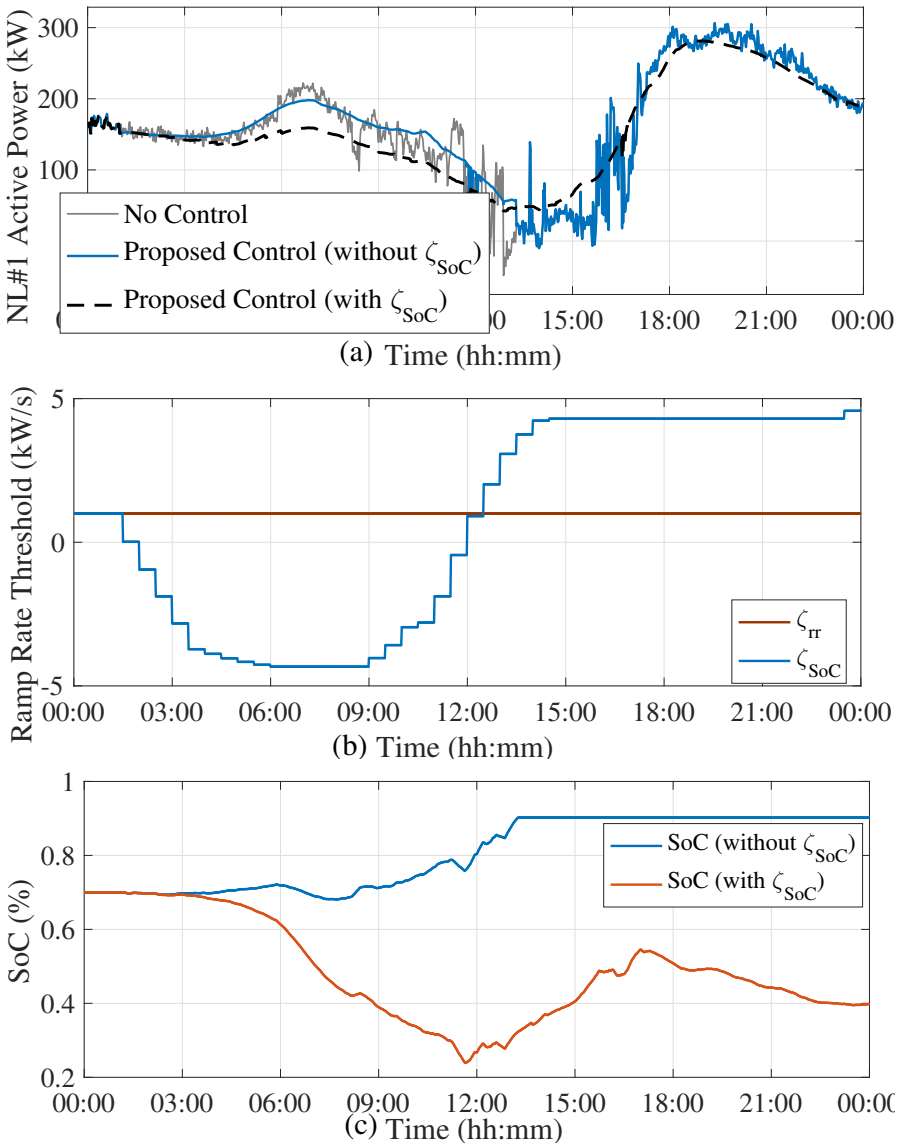

Fig. 3.11. Case-I simulation results with and without applying dynamic constraints. (a) P_{NL} Net-load profiles; (b) Ramp rate threshold values ζ.; (c) Energy storage system SoC profile.

control, study is developed on four cases as follows:

Case-1: This case incorporates net-load control at only net-load location#1, whereas both location#2 and location#3 remain uncontrolled. The purpose of controlling net-load location separately is to show significant improvement of different locations in the feeder.

Case-2: Also, as shown in Fig. 3.13, case-2 provides results for same tested feeder

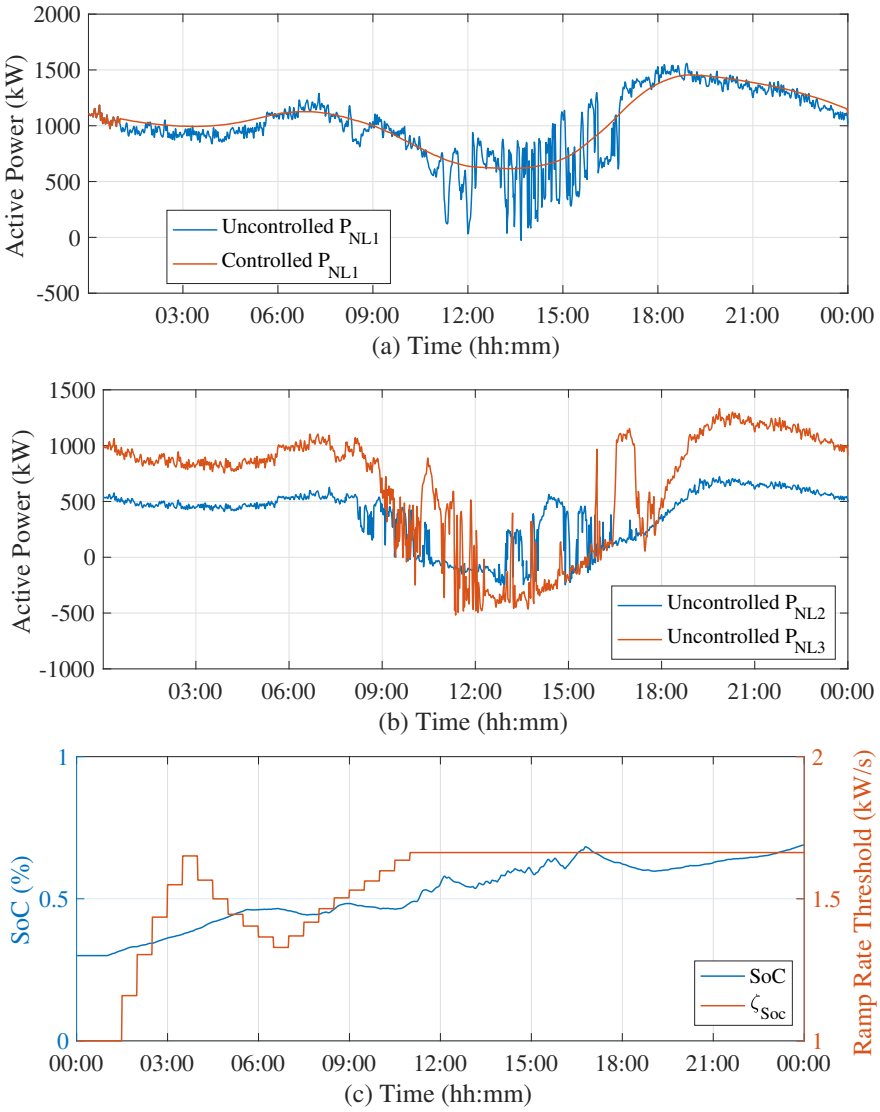

Fig. 3.12. Case-I simulation results. (a) Active power profile.; (b) state of charge (SoC) and ramp rate threshold value ζ_{SoC}

load and PV profile but with only net-load location#2 is controlled. Net-load2 ramp rate is successfully brought down by 31% which in turn prevented reverse power flow at this location as shown in Fig. 3.13.(a). Besides, Fig. 3.13.(b) shows other two uncontrolled net-load locations. Also, it could be seen in Fig. 3.13.(c) that state of charge was kept within limits under the control of state of charge based ramp rate threshold value ζ_{SoC} when ζ_{SoC} started decreasing around 10:00 AM when SoC

reached 40% which is less than targeted SoC by 10%.

Case-3: Similarly, case-3 provides simulation results for net-load control for loca-

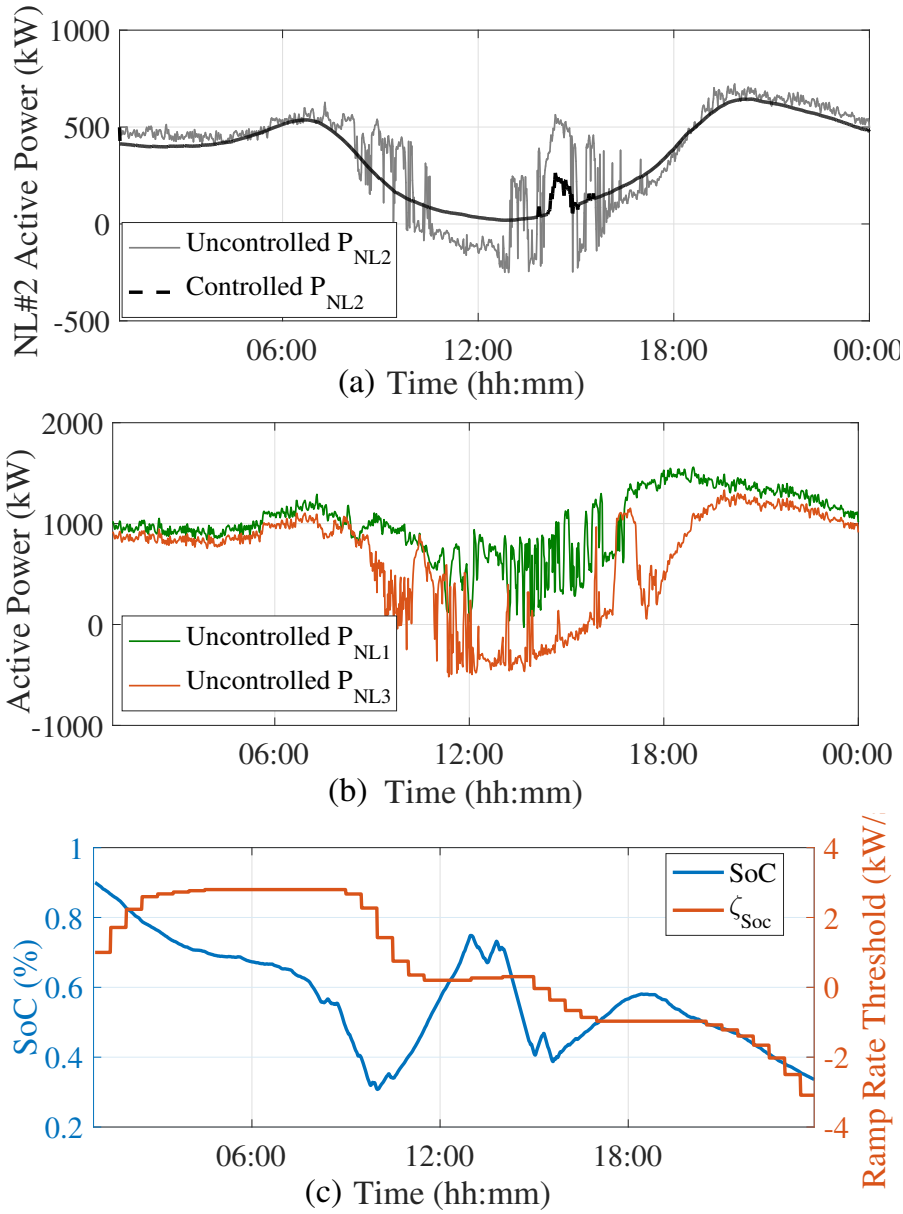

Fig. 3.13. Case-2 simulation results. (a) Active power profile.; (b) state of charge (SoC) and ramp rate threshold value ζ_{SoC}

tion#3 while keeping location#1 and location#2 uncontrolled as shown in Fig. 3.14. It could be seen that controlled net-load profile deviates from the following the reference curve by following the equality constraints to attain certain ramp rate threshold

value and hence targeted state of charge.

Case-4: Finally, case-4 presents simulation results for the system when all net-load

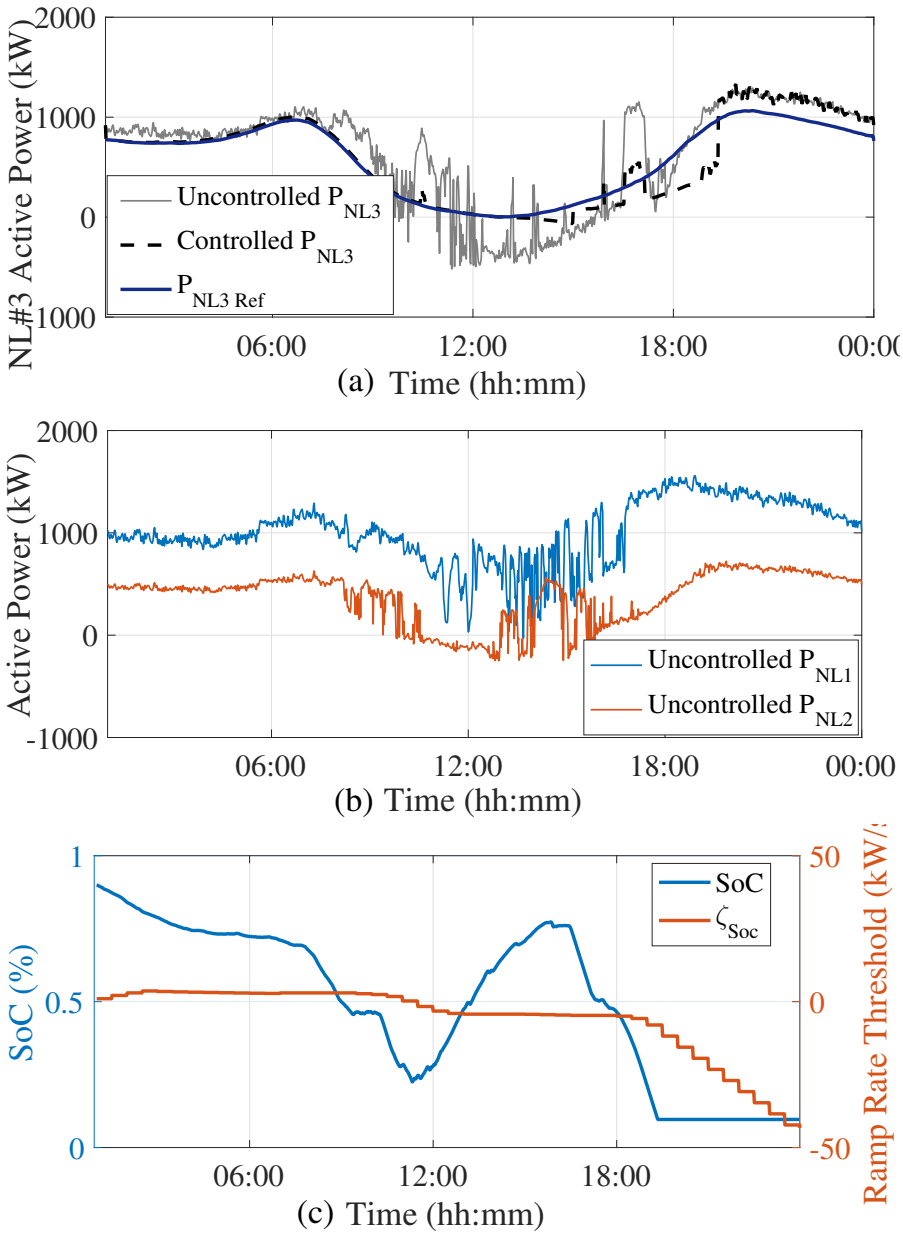

Fig. 3.14. Case-3 simulation results. (a) Active power profile.; (b) state of charge (SoC) and ramp rate threshold value ζ_{SoC}

locations are controlled. The results show overall ramp rate improvement and active power smoothing. Primarily, controlled substation active power profile is shown in Fig.3.15. The original ramp rate of the uncontrolled profile is reduced to 26.69% of

its original value. Also, short-term fluctuations are successfully mitigated by three installed energy storage systems. Performance indexes for this case are also presented and explained later in Table 3.1.

Voltage Profile Improvement: Moreover, system voltage profiles are shown in Fig.

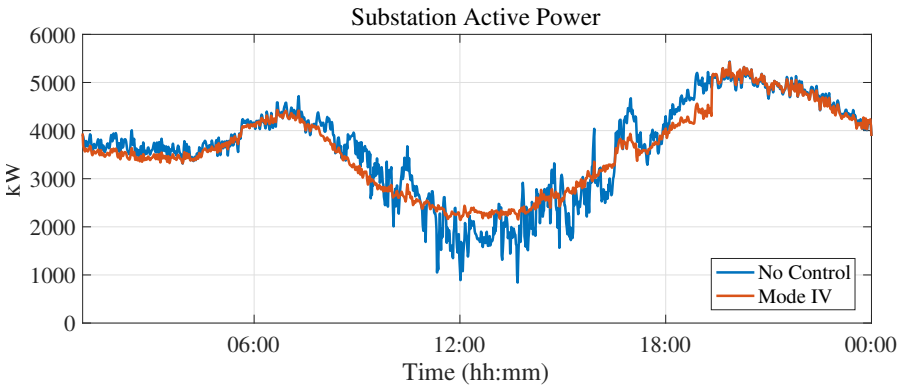

Fig. 3.15. Substation (main network net-load) simulation results.

Table 3.1
Summarized results for feeder-II considering PV penetration level as 50%

Proposed methodology evaluation								
Case	RRI				VDI			ILP
	NL#1	NL#2	NL#3	Substation	NL#1	NL#2	NL#3	
Case-1	33.81%	-	-	80%	90%	-	-	0.9338
Case-2	-	31%	-	90%	-	80%	-	0.98
Case-3	-	-	19%	63%	-	-	83%	0.96
Case-4	33.81%	31%	19%	26.69%	68.80%	48%	47%	0.93

3.16, where all of three net-load locations voltage profiles are considered as locations of interest for evaluation purpose. It is noticeable that the farther the location from the main substation, the smaller the voltage fluctuations are. For example, by controlling all locations (case-4), VDI is significantly decreased to 47%, 48% and 68% for Nl#1, Nl#2 and Nl#3 respectively. Nevertheless, the number of tap operations for OLTC and three line regulators are insignificantly reduced by 5 taps operations for case-4. However, OLTC and line regulator#2 have a significant improvement in tap

operations for all control modes. It is also worth mentioning that reactive power flow and switched capacitors have a higher effect on the voltage profile than active power flow due to R/X ration of the system under study. Finally, the voltage profile has a noticeable improvement due to smoothing application as well as significant ramp rate reduction. Fig. 3.16. shows V_{rmsA} for $NL\#2$ location through three control modes. Voltage deviation is minimized to (32.39%) of its original value. The results for 50%

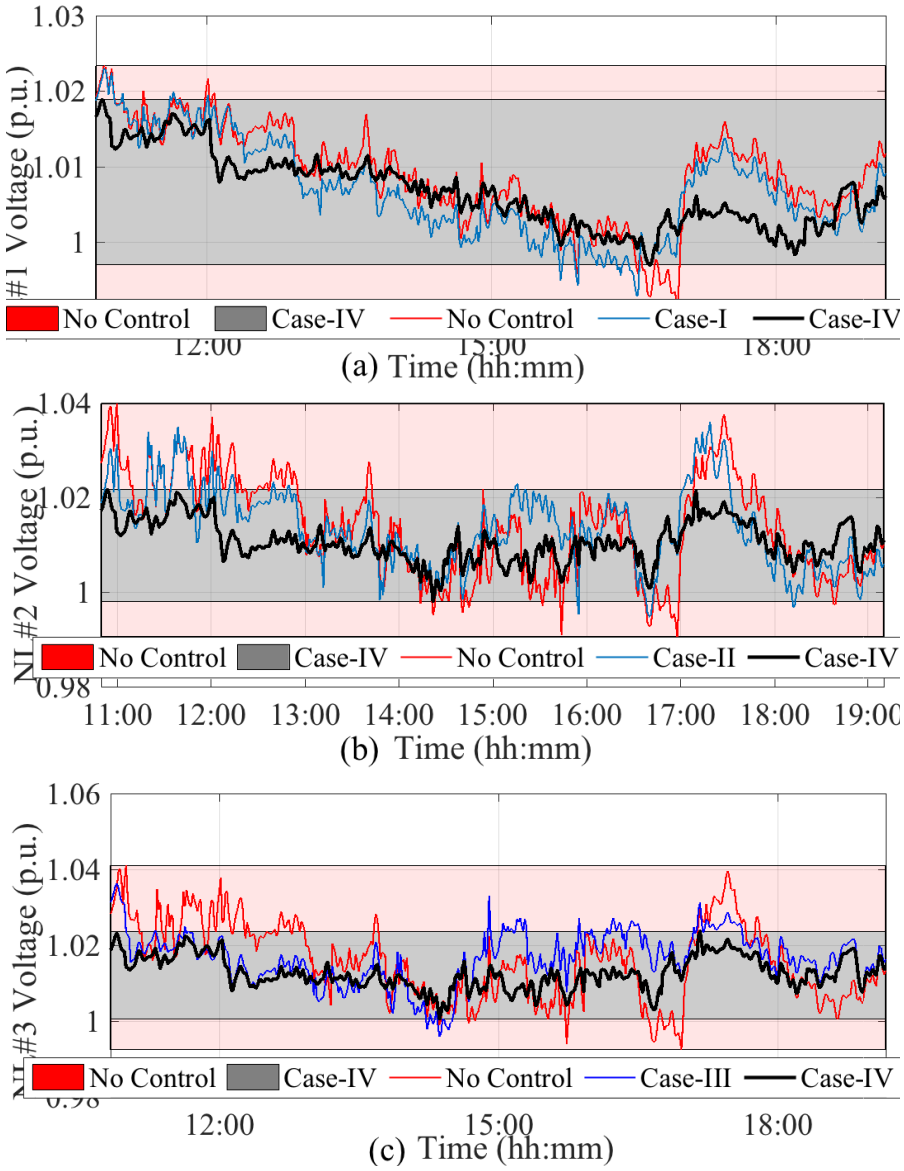

Fig. 3.16. Net-load locations voltage profiles. (a) $NL\#1$ location; (b) $NL\#2$ location; (c) $NL\#3$ location

Table 3.2
Substation OLTC and line regulator #2 taps operations for IEEE-8500 test feeder simulation results.

Substation Regulator (OLTC)					
Phase	No Control	All locations	NL#1 control	NL#2 control	NL#3 control
A	7	5	5	5	7
B	5	5	5	5	4
C	6	3	5	3	5
Line Regulator#2					
Phase	No Control	All locations	NL#1 control	NL#2 control	NL#3 control
A	7	3	6	5	4
B	3	4	5	8	4
C	5	2	6	2	3

PV penetration level are summarized in Table 3.1. All indexes are developed on the four cases as mentioned earlier to quantify the amount of savings and estimate the improvement in all possible shapes of PV active power profiles. Total system RRI is significantly reduced for all individual net-load locations 26% in case-4. Because of R/X characteristics of distribution networks, active power is remarkably contributing to voltage profiles changes which could be noticed through the number of taps operations savings. As shown in the table, voltage deviation index is decreased to 68%, 48% and 47% for net-load#1, net-load#2, and net-load#3 respectively. Also, system losses are decreased the most by 7% for case-4 when all locations are controlled. Losses savings are mainly due to mitigated intermittent active power flow from substation through controlled locations, not to mention the losses savings during the discharge period of ESS. Also, Table 5.1. shows the number of taps operations for both OLTC and line regulator #2.

3.6 Summary

This chapter proposed an active power control for local net-load location in distribution networks with high PV penetration levels. Fast Fourier Transformation (FFT) is applied to historical net-load profiles are used to generate reference profiles for each location. FFT is successful to generate reference curves that meet energy storage systems capabilities as far as active power and energy capacity are considered. Furthermore, proportional and integral controllers are introduced to control objective function constraints better. The main advantage of controlling local net-load locations is it prevents all active PV output power fluctuations and resulting voltage fluctuations to be propagated through the whole feeder. The methodology is tested and proved successful till 50% of PV penetration level. Moreover, depending up the degree of the resistive part in a particular distribution system, the proposed methodology optimizes voltage profiles regulation as well as voltage regulators tap operations reduction. The proposed method aims to optimally utilize the given energy storage system active power and energy capabilities by maintaining the state of charge between 0.5 and 0.7 with a 15 minutes step control action for PI controller so that ESS keep dispatching active power according to methodology set-points. Future work incorporates very high penetration of renewable energy which leads to the phenomena of "Duck Curve."

CHAPTER 4: INTEGRATED FEEDER LEVEL PEAK LOAD MANAGEMENT BASED ON ACTIVE LOAD PREDICTION USING WEATHER FORECASTING

This chapter presents a day ahead feeder load prediction approach based on the day ahead weather forecasts. The motivation is seeking an accurate estimate of feeder load profile patterns as well as peak load times. The proposed methodology aims to support energy storage ancillary services applications in power distribution networks.

4.1 Introduction

Several research works propose optimal management of renewable energy resource with energy storage for a changing feeder load conditions. For example, [8] discusses an energy time shift (ETS) application for energy storage systems to satisfy load shaving goals. The technique is proved efficient; however, the accuracy of peak load time prediction is critical for such applications. Therefore, it became necessary to utilize accurate and robust load predictions tools to aid these applications. In [96], additive and multiplicative decomposition techniques are applied for load forecasting after performing system identification on the load time series data. Similarly, [19] discusses load forecasting by applying moving average (MA) on a monthly, weekly and daily basis. In that work, load segmentation is performed by constructing contour lines through the time series cyclical peaks and dips to divide it into similar regions. Empirical Mode Decomposition (EMD) and Support Vector Regression (SVR) are also applied in [40] where load pattern is divided into trend component and some local

oscillations. Recently, [45] introduced the comparison between auto-regressive moving average (ARMA), the variation of exponential smoothing (DSHW) and echo state network (ESN). Also, several works proposed short-term load forecasting methodologies using artificial neural networks (ANN) and how it exploits weather variables for accurate forecasting. [30,95] performed a weather based-ANN load forecasting. Reference [95] uses weather ensemble prediction to predict from 1-10 days. The significance of this methodology is that weather ensemble prediction has multiple scenarios rather than what is produced by usual weather forecasting, whereas [30] uses ANN load forecasting taking human comfort index in consideration. This index is a function of three weather variables: temperature, humidity, and wind speed. Reference [67, 76] uses backpropagation for forecasting with different types of neural networks. The performance of these NNs is compared in this work as well with all three types of back propagation neural network (BP) considering temperature in the input layers. Combined genetic algorithm (GA) with ANN are provided by [28, 44, 93, 104], and results showed that evolutionary algorithms (EA) could help in fast calculation times and high precision which allow the ANN architecture and parameters to be easily optimized. Combining EA with ANN for prediction shows significant improvement over stand-alone ANN forecasting methods. The main disadvantage of all these methods is that earlier works did not take into account feeder load changes considering all the factors. This chapter presents weather forecasts and Artificial Neural Network (ANN) based methodology of day ahead feeder load prediction. The goal is to predict an accurate pattern of load profile for the day ahead as well as the load peak time instant so that methodology could be utilized in energy time shift (ETS) application.

Proposed prediction methodology uses load time series decomposition to distinguish between all types of loads and events on the feeder. Then, Back-propagation Neural Network (BPNN) technique is used to utilize the day ahead weather variables forecasting to predict weather dependent load component. The proposed algorithm has been evaluated on a real residential distribution feeder data. Results show very accurate prediction results for active power as well as the feeder peak load time instants. Moreover, implementation results on a real distribution feeder in North Carolina, USA are also provided.

This chapter is organized as follows: Section 4.2 discusses the proposed load decomposition method. Then, section 4.3 analyses the correlation between the feeder load and weather variables as well as back propagation neural network (BPNN) methodology to predict the weather-dependent portion of feeder load. Section 4.4 shows simulation results as well as implementation results for the proposed methodology to aid energy time shift (ETS) application on an existing controller in a real distribution feeder in North Carolina, USA. Finally, section 4.5 summarizes the methodology contribution in day ahead load prediction literature works as well as potential future work for accuracy improvement. In this chapter, an integral decomposition method is designed for load prediction. In this approach, first, a load time series is employed for load decomposition. This step removes all the constant and seasonal (weekly, daily) components from the original dataset. Then, after performing the forecasting, those components are added back. Also, a dynamic regression method is employed for weather-dependent load forecasting. Results showed great accuracy.

4.2 Feeder Load Decomposition

Electric grids have many different load types and inconsistent customer's behaviors which makes predicting feeder load prediction easy to be achieved. Load prediction methodology is based on time series decomposition of feeder load. As in (4.1), any time series is decomposed into three main components; trend component, seasonal component, and random term. Similarly, distribution feeders load profiles can be segregated into similar components; the however variable dependent component is added as it depends on feeder location weather conditions. Days are categorized into two weather-based categories; comfort days and discomfort days. Comfort days are the days when the temperature ranges from 65 to 70 °F and dew-point (DP) is less than 65 °F, whereas the discomfort days are the days with over/under temperature and air conditioning/heat devices are expected to be significantly loaded. This section presents load components definitions as well as load decomposition approach that is used in the proposed methodology.

4.2.1 Comfort Component (P_c)

Each distribution feeder usually has an almost constant average base load. This base load differs from season to another. Mathematically, this component is the trend component (mean value) of any given time series. For comfort component P_c to be estimated for certain day/season, comfort day needs to be used so that all weather dependent loads are almost negligible. Comfort day is defined as the day when weather conditions are comfortable enough with an average temperature of (70 °F) so that neither air conditioning (AC) or heating systems are expected to be in

service. This component is the average value (trend) of load profile in a comfort day. It could be determined for each season/month based on historical data analysis for any feeder under study.

4.2.2 Lighting Component (P_l)

Similarly, light component is defined as the portion of the feeder load that is associated with lighting loads at any given feeder load. Mathematically, this component is the daily basis seasonal behavior of any given time series. Therefore, the lighting component also represents the morning and evening peaks that appear in the feeder due to lighting loads for all residential, industrial and commercial buildings. Since weather discomfort causes a dominant peak load in the morning and the evening for the winter and the summer respectively, it is advised to use comfort days to estimate lighting component for each season/month.

4.2.3 Random Component (P_r)

This component represents the customers' random behavior in turning different loads on and off such as; lighting, kitchen equipment, and washing/drying equipment, etc. The random component has a certain pattern depends on the day of the week. It is also called plug loads. For accuracy, random components are also developed for each month with its standard comfort day.

4.2.4 Weather Component (P_w)

This component represents the overloading on the air conditioning/heating equipment due to over/under temperature. This component evaluation and prediction are discussed in the next section in all required details.

$$y_t = T_t + S_t + I_t \tag{4.1}$$

$$P_{total} = P_c + P_l + P_w + P_r \tag{4.2}$$

Such as P_{total} is the total feeder load profile, P_c is the comfort component, P_l is the lighting load component, P_w is the weather dependent component, and P_r is the random (plug load) load component.

4.2.5 Load Decomposition Approach

To develop the first three components of any predicted load profile, an additive load decomposition process is applied. First, time series the mean value of the load profile is calculated. Then, small window moving average (MA) is applied to the de-trended series to segregate the seasonal component from the random component. The

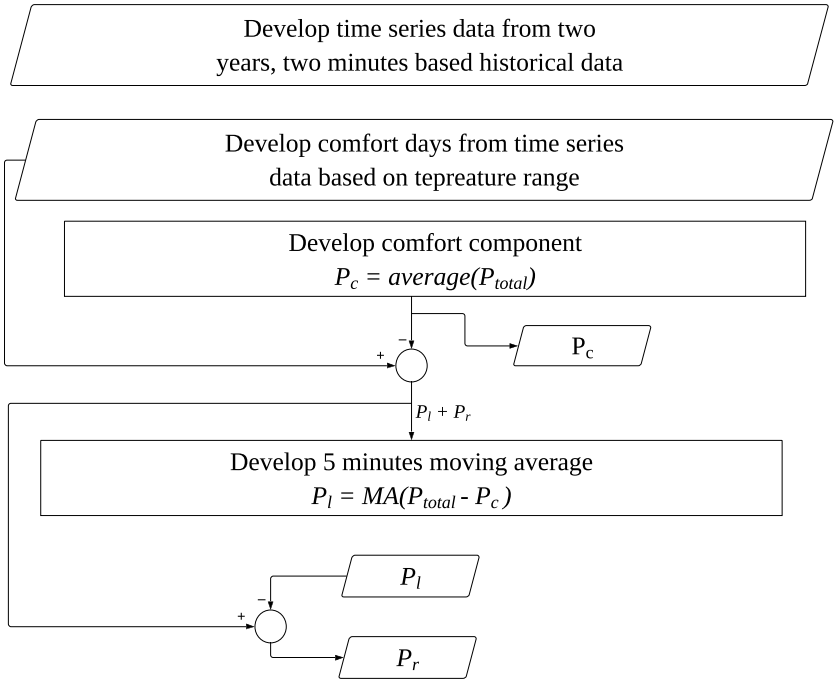

Fig. 4.1. Feeder load decomposition flowchart.

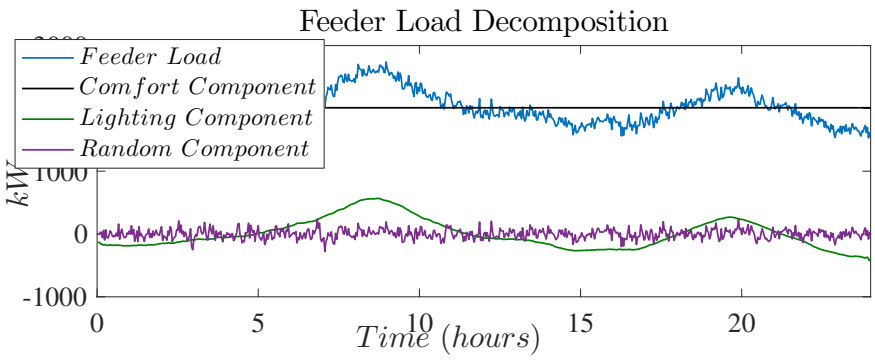

Fig. 4.2. Sample day load decomposition components.

moving average window aims to capture all short term fluctuations in the load profile, therefore, it was selected as 5 minutes, whereas the data is provided as 2 minutes based time series. Fig. 4.2 shows sample comfort day decomposed into comfort, lighting and random component. Also, load decomposition approach is shown in flowchart in Fig. 4.1 to show mathematical sequence of evaluation.

$$P_c = \frac{\sum_{i=1}^{n} P_{totali}}{n} \tag{4.3}$$

$$P_l = MA(P_{total} - P_c) \tag{4.4}$$

$$P_r = P_{total} - P_l - P_c \tag{4.5}$$

4.3 Day Ahead Load Prediction Methodology

This section presents core part of the proposed methodology, which is weather dependent load component prediction using Back-propagation feed-forward neural network (BPNN).

4.3.1 Active Power and Weather Variables Correlation

One year historical data of feeder load and weather variables underwent a detailed correlation study to find out the real significance of relative humidity (RH)/dew-point temperature in feeder load behavior especially during summer/winter days. Dew-point serves as a measure of relative humidity and it is the temperature below which water droplets start to condense. Table 4.1 shows correlation coefficients

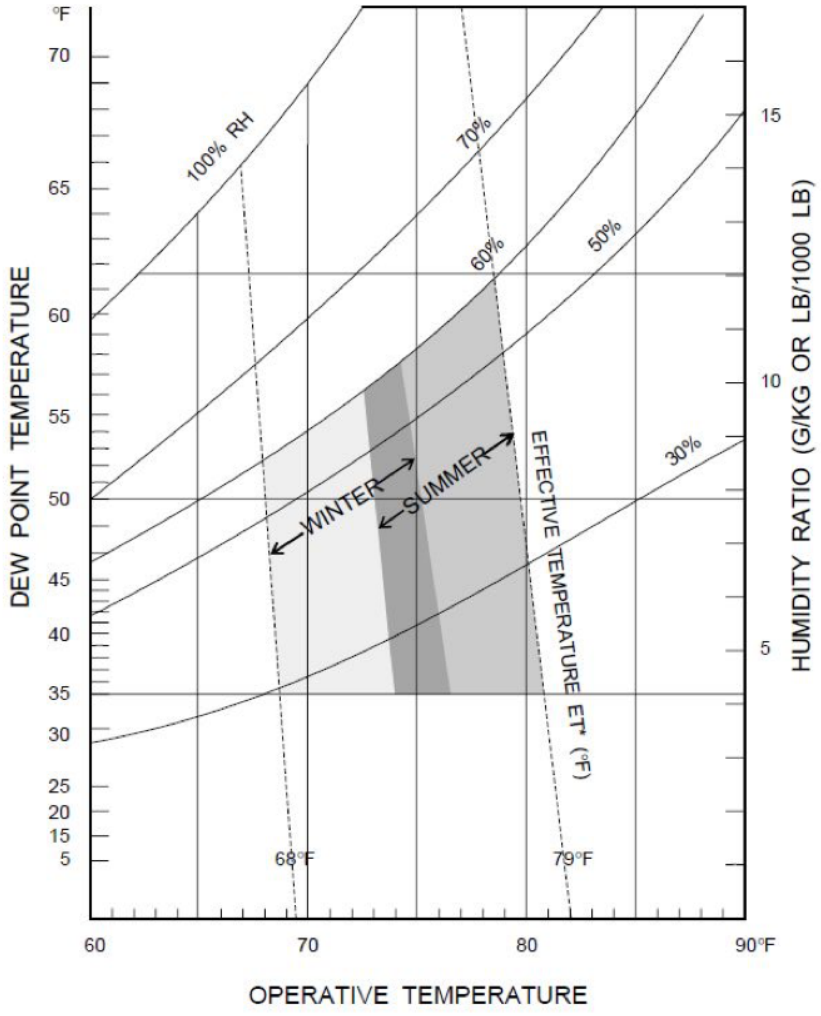

Fig. 4.3. ASHRAE chart of comfort. [1]

between both temperature and dew-point and feeder load at different seasons. In

such summer days when dew-point is greater than 65 °F, it is a measure of high relative humidity such that atmospheric temperature would feel quite higher than it is. Also, Fig. 4.3 shows the chart of comfort presented by The American Society of Heating, Refrigerating and Air-Conditioning Engineers (ASHRAE) [1]. This chart plots dew-point, operative temperature and effective temperature all together on one chart. The chart maps the effect of relative humidity (RH) to operative temperature and calculates the effective temperature. Therefore, it is concluded that dew-point

Table 4.1
Feeder load and weather variables correlation

Day	T-Correlation	Dew-point-Correlation
Summer Day-1	0.8	0.2
Summer Day-2	0.9	0.9
Summer Day-3	0.7	0.9
Winter Day-1	0.9	0.1
Winter Day-2	0.7	0.2
Winter Day-3	0.9	0.4

has to be incorporated in predicting the weather dependent component of feeder load and since temperature is the significant factor that impacts feeder load changes, it is challenging to develop a technique that analyzes the non-linearity between temperature, dew-point and feeder load. Findings showed a complex non-linearity between any given feeder load, temperature and dew-point as the certain range of dew-point values do not have any significant effect on feeder load. Fig. 4.4 shows how the feeder load could be more dependent on dew-point than temperature because of the higher level of relative humidity.

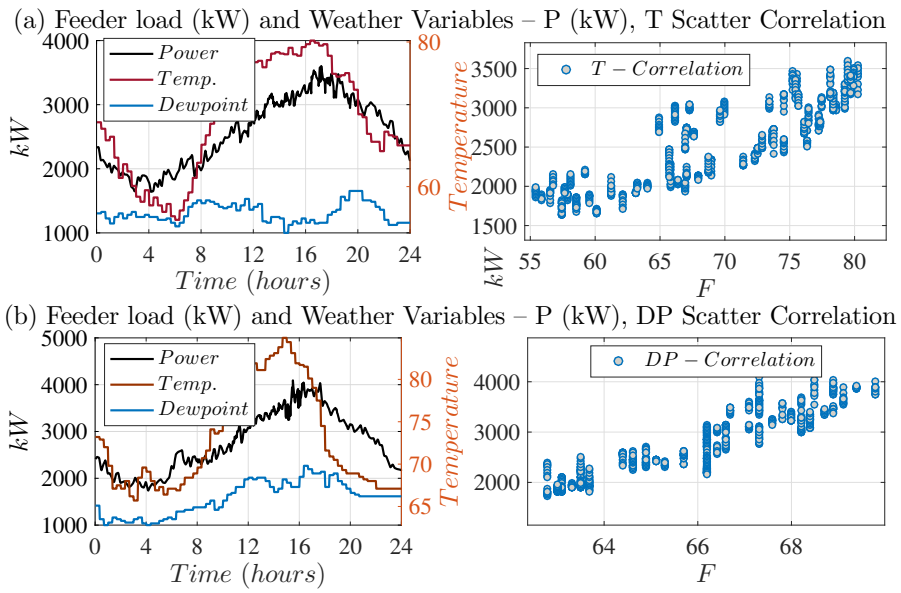

Fig. 4.4. Weather variables correlation with feeder load.

4.3.2 Back-propagation Feed-forward Neural Network (BPNN)

In the literature [72]- [80], the back-propagation neural network was used in a day ahead peak load forecasting, however, peak magnitude was only more of a concern, not peak load time. Also, authors in [77], and [20] presented day ahead peak load forecasting based on the back-propagation neural network where the only temperature was taken into consideration and all feeder's load components are predicted using one process which is not addressing the peak time very closely. Due to the complexity of non-linearity between feeder load and weather variables, it proved efficient that neural network regression applications are the best choice to fit this complex relationship. This subsection presents a back-propagation feed-forward neural network for regression purpose. Details of training and testing the network are also discussed. Ultimately, the proposed neural network technique is used to predict the weather-dependent load component P_w using day ahead weather forecasts ($T_{forecast}$,

$DP_{forecast}$) which are retrieved from weather service website. Details of the methodology are also explained later in this section. The feed-forward neural network is a machine learning technique that is commonly used for classification and regression purposes. Neural networks function based on learning methods that mimic the behavior of certain dataset (Training set) to be able to classify further or regress new set of data (Testing set). As shown in Eq.(4.4), all neurons transfer function is selected as tangent hyperbolic as it is recommended to be used for regression applications. Also, Eq. (4.6)-(4.7) show the process of back-propagation of feeding the error back into the network to estimate the participation factor of each weight in the training error, and hence, updating all network's weights correspondingly. Batch learning is an iterative offline learning process on the training dataset. It was considered sufficient to be selected in the proposed study since the methodology is developed to predict feeder load profile at each day's midnight.

$$net_{h1} = w_1 * i_1 + w_2 * i_2 + b_1 * 1 \tag{4.6}$$

$$out_{h1} = \frac{e^{net_{h1}} - e^{-net_{h1}}}{e^{net_{h1}} + e^{-net_{h1}}} \tag{4.7}$$

$$E_{total} = \sum (1/2) * (target - output)^2 \tag{4.8}$$

$$\frac{\partial E_{total}}{\partial w_7} = \frac{\partial E_{total}}{\partial out_{o1}} * \frac{\partial out_{o1}}{\partial net_{o1}} * \frac{\partial net_{o1}}{\partial w_7} \tag{4.9}$$

Neural network training phase has been developed through three versions as follows:

4.3.3 Recent Days Historical Data Based Learning $V-0$

This version of the methodology determines the day type based on the day ahead weather forecasts. Then, it extracts historical data for same day type for training purpose. As shown in Fig. 4.6, training process starts with random weights, then weights get updated at each iteration till certain stopping criterion converges to the optimal weights that fit the training batch. The drawback of this approach is that some days types are not experienced yet at the beginning of each season which causes an under-fitting issue.

4.3.4 Past Year Historical Data Based Learning $V-1$

Under-fitting neural network training exists due to the lack of comprehensive and inclusive training data set. Therefore, relying on past few weeks of historical feeder load profiles is not enough especially during the period in between seasons changes. Hence, one year of historical data underwent training process on a monthly basis, which successfully generated a set of optimal weights that entail all days weather/load fitting features for each month during the year. These optimal weights are expected to be used by itself for moderately accurate results. Nevertheless, this approach is missing load growth and all possible changes that might happen to any existing distribution feeder.

4.3.5 Combined Recent Days and Past Year Based Learning $V-2$

Instead of assigning random weights at the beginning of the learning process, this improved version of the methodology starts the first iteration with optimal weights

obtained from V-1 results for the same month during previous year. Then, recent days historical data is used to fine-tune the network weights, and adequately train the network on any new behavior. Intuitively, this approach adds all new fitting features from recent days historical data with all past year fitting features remained exist. Moreover, V-2 learning approach optimizes the number of epochs the stopping criterion needs for convergence. Fig. 4.5 shows pseudo-code algorithm for V-2 learning process. Prediction accuracy is also improved by developing categories concerning weather conditions (temperature range). Table. 4.2 shows day's categorization developed for this methodology. Summer categorization is based on maximum temperature, whereas winter categorization is based on minimum temperature.

Table 4.2
Temperature ranges based days categories

Bucket	Mean Temperature	Category
1	T 100	EX_H
2	90-100	V_H
3	80-90	M_H
4	75-80	H
5	60-75	C
6	50-60	L
7	40-50	M_L
8	30-40	V_L
9	T30	EX_L

4.4 Real Feeder Implementation and Simulation Results

This section provides both simulation and field implementation results for the proposed day ahead feeder load prediction. The proposed methodology is developed using Java programming. Both historical and day ahead weather forecasts data is retrieved through API protocol from a reliable weather service website (weather-underground), and then data is parsed using Java to extract temperature and dew-point data points

1: **procedure** START($P_{hist.}$, $T_{hist.}$, $DP_{hist.}$, $T_{forecast}$, $DP_{forecast}$, $P_{comfort}$)
2: *Generate weather dependent component training dataset ($P_{w\ train} = P_{hist.} - P_{comfort}$)*
3: *Normalize training dataset with respect to selected base values*
4: *Set random weights to three layers feedforward neural network*
5: *Test the network and check error between network output and actual output*
6: **if** *stopping criterion met* **then**
7: *Test the network using $T_{forecast}$ and $DP_{forecast}$*
8: *Predict day ahead weather dependent load component*
9: *Predict day ahead total feeder load profile*
10: **else**
11: *Back-propagate the error using the gradient descent method*
12: *Update weights based on their dependency with error*
13: *Go to 5*

Fig. 4.5. Algorithm for weather dependent load component prediction.

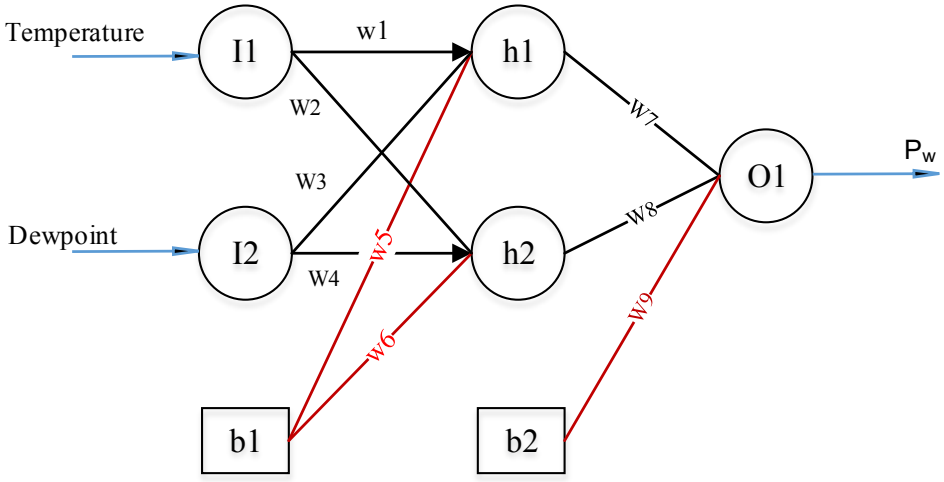

Fig. 4.6. Neural network layers layout.

in two minutes time stamp. By having access to recent days feeder load, weather variables, and historical comfort days, the methodology is run every midnight to predict 24 hours ahead feeder load profile. To evaluate the methodology performance,

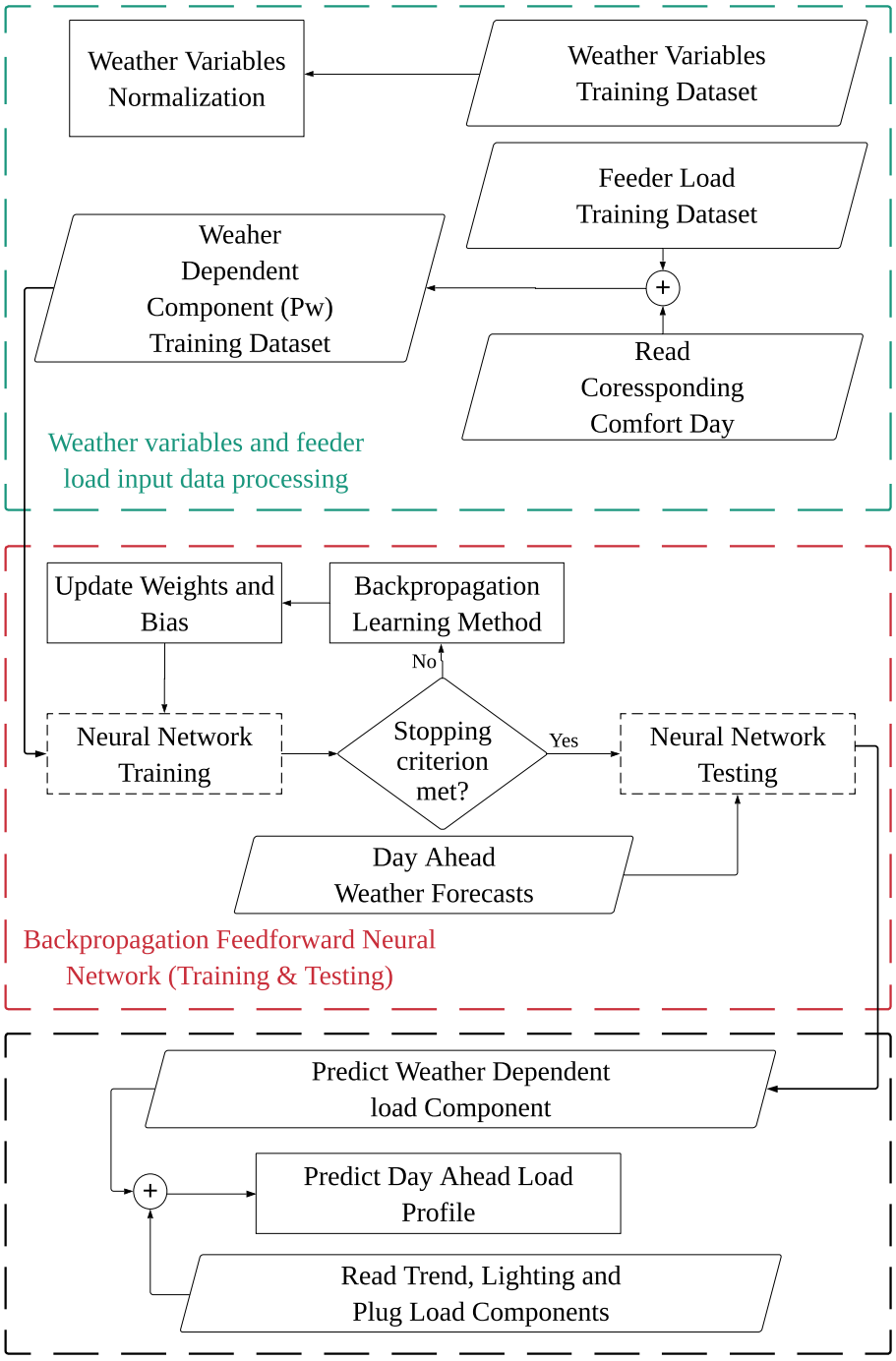

Fig. 4.7. Proposed day ahead load prediction methodology flowchart.

metrics are evaluated as follows:

4.4.1 Mean Absolute Percentage Error (MAPE %)

The mean absolute percentage error is the difference between the actual and predicted values divided by the actual values. Then, the outcome is divided by the number of data points to evaluate the mean value of the error value.

4.4.2 Peak-Load Time Error

The peak-load time error is a measure of the difference between the time of the predicted peak-load and the time of actual peak. This metric aims to evaluate the efficiency of the energy time shift (ETS) application as shown below in the implementation results.

4.4.3 Simulation Results

As a proof of concept, 2014 historical data of feeder load and weather variables are developed to test the algorithm using actual weather variables. Fig. 4.9 demonstrates day ahead load prediction for sample days of different seasons in 2014. Markedly, results indicate predicted feeder load profiles that follow the pattern of the actual feeder load with less MAPE 5.83%. Our methodology is also successful in minimizing peak-load time error to 6 minutes and maximum value as 30 minutes. Moreover, Fig. 4.10 shows the results of day 4 prediction results using day ahead weather. Remarkably, weather forecasts inaccuracy is recognized in Fig. 4.10.(b) which led to an error in the prediction during the same period of the day. It is seen that the temperature went more comfortable which, in turn, leads to less usage of air conditioning/heat load. Table. 4.3 shows summarized results for four days simulation

results.

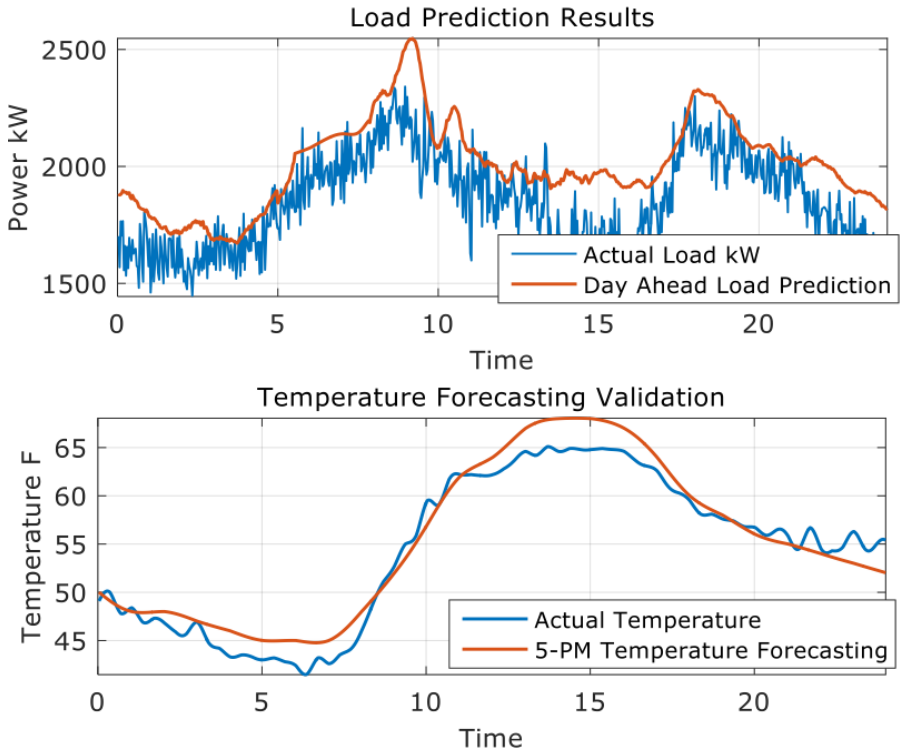

Fig. 4.8. Simulation results based using day ahead weather forecasts retrieved from weather-underground. Day-5, November 2015

4.4.4 Implementation Results

This subsection presents the implementation results of the proposed methodology. The methodology is integrated with an existing battery energy management system (BEMS) that manages a PV/BESS facility which is installed in a real distribution feeder. The day ahead load prediction is used to aid energy time shift (ETS) application by optimizing the time to initiate the energy storage active power set-point to dispatch with full capacity during load peak time. The main advantage of sending anticipated peak load time every midnight is that BEMS coordinate with state of charge (SoC) control algorithm. Also, weather forecasts accuracy level is a crucial factor in the load prediction results. Therefore, part of this methodology's inaccuracy

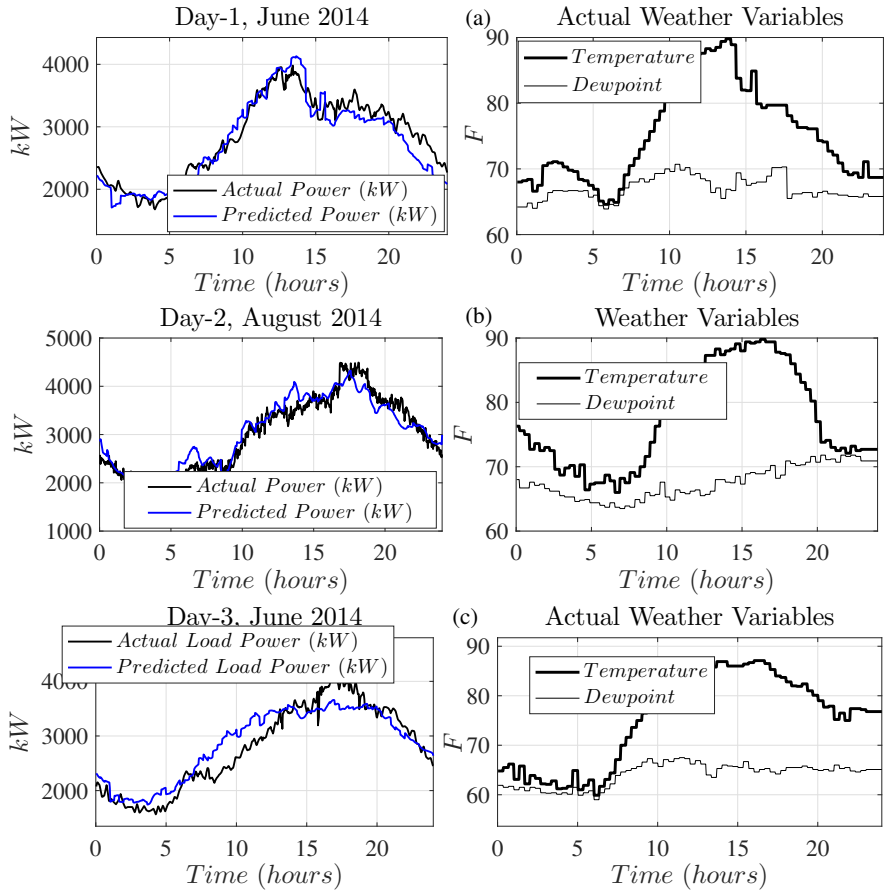

Fig. 4.9. Simulation results based on actual weather variables for historical days with no weather forecasts available. (a) Day-1, June 2014; (b)Day-2, August 2014, (c) Day-3 June 2014

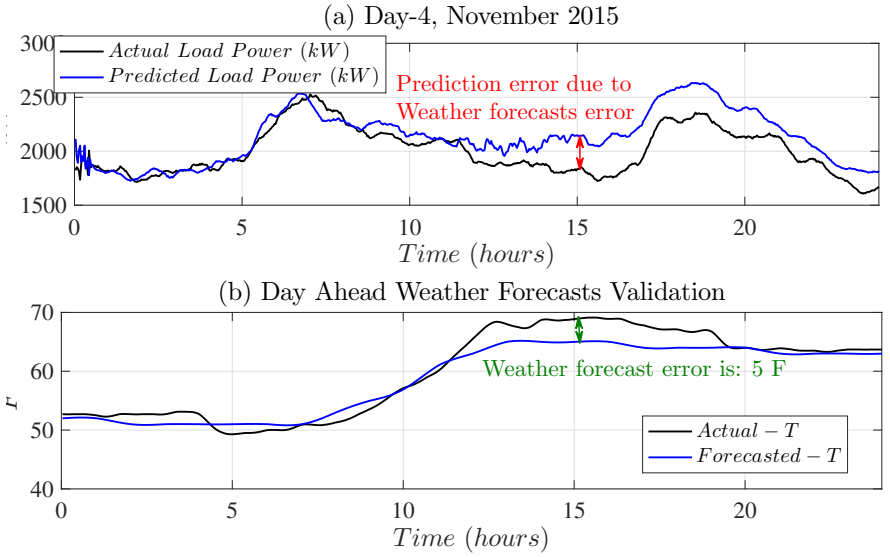

Fig. 4.10. Simulation results based using day ahead weather forecasts retrieved from weather-underground. Day-4, November 2015

is due to weather forecasts inaccuracy which could be easily addressed by addressing the forecasting error according to prediction errors. Fig. 4.11. shows implementation results for day-5 in November 2015. Fig. 4.11.(a) depicts actual feeder load profile versus predicted profile as well as point of common coupling active power profile. It is noticeable how energy storage system is dispatching with a full capacity around the anticipated peak time. Also, due to weather forecasts errors shown in Fig. 4.11.(b), there is an error offset between actual and predicted load profile. nevertheless, offset errors are not inversely affecting ETS application since peak time is the main concern. Similarly, Fig. 4.12. shows implementation for another in winter day when ETS application is initiated in the morning to cover the morning peak. It is also worth mentioning that MAPE is 7.8%. Finally, day 7 results are presented in Fig. 4.13 with as low MAPE as 4.3% due to the high level of accuracy in weather forecasting. Table Fig. 4.4. summarizes methodology evaluation as far as MAPE and peak time offset is considered.

Table 4.3
Historical days simulation results

	Simulation Results			
Day	Day-1	Day-2	Day-3	Day-4
MAPE (%)	6.19%	5.83%	9.1%	7.2%
Time Error(Morning Peak)	-	-	-	20 minutes
Time Error(Evening Peak)	6 minutes	10 minutes	31 minutes	0 minutes

Table 4.4
Real feeder implementation results

	Implementation Results		
Day	Day-5	Day-6	Day-7
MAPE (%)	11.5%	7.8%	4.3%
Time Error(Morning Peak)	-	32 minutes	16 minutes
Time Error(Evening Peak)	16 minutes	-	18 minutes

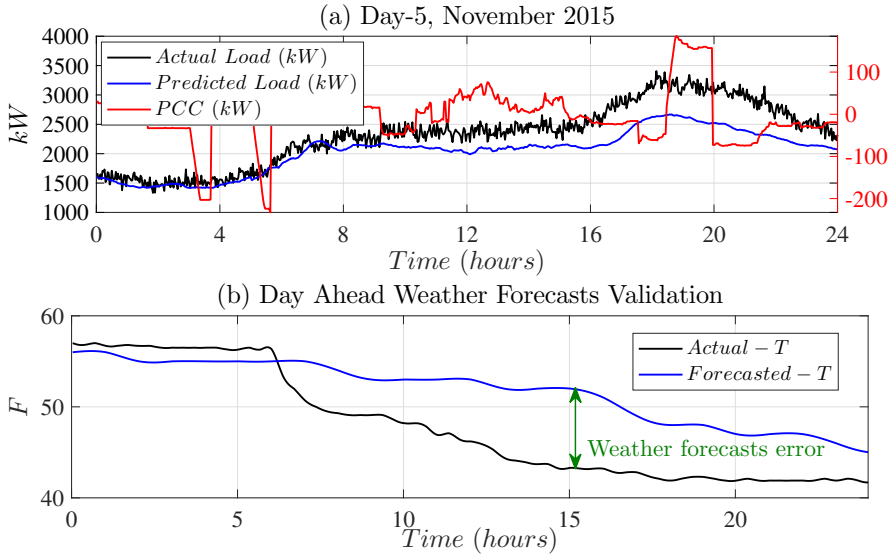

Fig. 4.11. Implementation results and weather forecasts validation. (a) Day-5, November 2015 feeder load prediction and point of common coupling (PCC) active power; (b) Weather forecasts versus actual weather variables validation (Day-5)

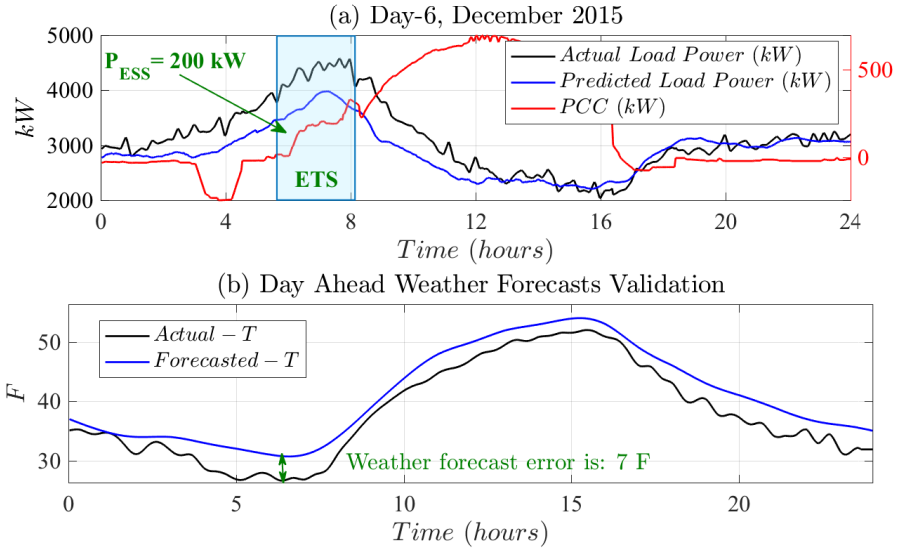

Fig. 4.12. Implementation results and weather forecasts validation. (a) Day-6, December 2015 feeder load prediction and point of common coupling (PCC) active power; (b) Weather forecasts versus actual weather variables validation (Day-6)

4.5 Summary

This chapter presented an intelligent day ahead feeder load prediction methodology to mainly aid energy storage applications in hybrid PV/BESS distribution networks. First, historical feeder load profiles are decomposed into certain distinct types of

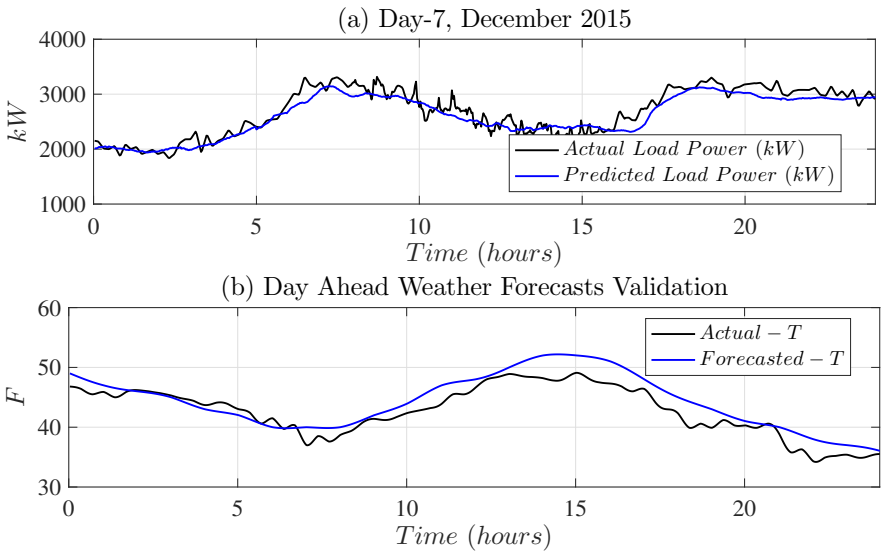

Fig. 4.13. Implementation results and weather forecasts validation. (a) Day-7, December 2015 feeder load prediction; (b) Weather forecasts versus actual weather variables validation (Day-6)

load types/behaviors so that they could be further predicted separately. Then, the back-propagation neural network technique is used to predict the weather-dependent portion of the load using day ahead weather forecasts. BPNN training stage is developed and improved in three different phases as follows: the first version trains the network based on past three weeks historical data, whereas the second version utilizes past year historical data of the same feeder, and finally the third version is fine-tuning past year's historical data weights with recent few weeks. The methodology was on some historical data and was implemented on an existing BMS controller, and both results showed high level of accuracy as far as load peak time as well as load full day load pattern are concerned. Methodology contribution is the ability to predict all types of load types/behavior separately so that both patterns and peak time are accurately predicted to fulfill battery management systems applications. Also, the state of charge could be better managed and more optimal dispatch during the day.

CHAPTER 5: CO-ORDINATED VOLTAGE CONTROL UTILIZING VOLTAGE SOURCE CONVERTERS IN PV/BESS HYBRID DISTRIBUTION SYSTEM

It is well known that most of distribution feeders have significant effect due to lines reactance over resistances. This fact mostly depends on medium voltage level, main feeder/lateral feeder proportionality and types of loads. These factors keep volt-var control (VVC) algorithms still exist for power distribution networks voltage support application. It became more vital and attractive since those feeders are now connected to such distributed energy resources (DER) with power conversion systems that are also capable of injecting/absorbing reactive power. This chapter presents an engineering solution to power distribution feeder in NC utilizing PV solar power plant/BESS converter system. Proposed methodology is looking at fast changes as well as slow changes in feeder load at different locations of interest.

5.1 Introduction

The voltage control coordination in the distribution feeder among various devices has been discussed and researched in the literature. Many volt-var control (VVC) algorithms are developed utilizing heuristic multi-objective optimization methodologies using feeder power losses and voltage regulators taps operations as objectives formulations. In [59], a co-ordinated control approach is presented to response coordination of DERs and substation OLTCs. However, the technique requires changing the compensation settings of the OLTC. Ref. [92] aimed to minimize power losses, average

voltage deviation for all buses and voltage collapse proximity indicator (VCPI) using Genetic Algorithms (GA). Similarly, [92,107] presented different volt-var optimization (VVO) techniques to maintain all buses voltages within limits. Also, [14] presented reactive power control methodology based on system voltage sensitivity analysis. The reactive power is dispatched in such a way to compensate for the voltage fluctuations due to active power changes from PV farms. References [47,84,90] discussed different VVC algorithms utilizing sensitivity analysis along with objectives functions based formulations. Ref. [84] presented dynamic adjustment of OLTC parameters (Line Drop Compensators LDC) for algorithm improvement. In references [46, 55, 56, 97] the importance of coordination between OLTC, Line regulators and distributed generation sources are discussed in detail. In [46], a distributed method for the coordination of these sources is shown based upon multi agent system (MAS) architecture. But implementation of the methods require communication between different devices which requires extension of the current architecture of distribution system costing utility large sum of money which makes them less attractive for industrial application. Other optimization based VVC algorithms do not target certain weak locations in the feeders since they consider all feeder voltages as constraints. Also the approaches are model dependent making the implemented architecture not giving desired results. Integrated volt-var control (IVVC) methodologies which use heuristics based adaptive control are proven to be successful in such distribution systems with large penetration of DERs as using optimal power flow to generate DMS control actions is complex with DERs. Reference [102] applied signal processing and adaptive control volt-var optimization methodology where distribution system operation decisions were made

based on system measurements observation and processing rather than depending on the circuit models. Reference [103] presented 11 different distribution voltage optimization projects using measurement and verification method. In references [9,10,12] field measurements have been used to implement active power control for performing applications like peak load shaving and photo-voltaic active power smoothing. This work is along the similar direction of using feeder measurements and being aware about the feeder voltage situation for a better control and operation of distribution system without adding new variables to the conventional optimization problem used for distribution system management.

5.2 Co-ordinated Voltage Regulation

This section discusses the proposed co-ordinated control strategy for the various voltage regulation devices and reactive power sources in the distribution system. The primary focus is to utilize the reactive power capability of VSCs in the distribution feeder to support the operation of the existing legacy controllers such as line voltage regulators and substation OLTCs. Fig. 6.1 illustrates the voltage regulation approach in the distribution system. In general, as it can be seen in fig. 6.1, the voltage regulation in the distribution system is currently achieved by using on-load tap changers (OLTCs), Line Regulators (LRs) and SCADA based Distribution Management System (DMS) (this varies from utility to another) along with the reactive power supporting devices like static and switched capacitors. These controllers are placed in various location in the distribution feeder based on the design criteria and once in operation, there is no direct co-ordination among these devices. This can lead to

voltage regulation problem, when the components and power flow in the distribution system is changing at a fast pace especially with the increase in DERs integration. Modern distribution system, thus needs changes in the voltage regulation approach.

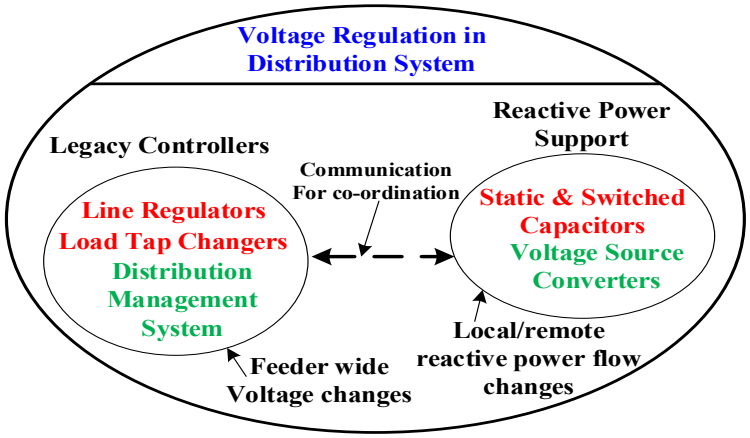

Fig. 5.1. Voltage regulation paradigm for the distribution system.

These changes could be achieved using DMS and VSCs as shown in green in fig. 6.1 while the components in red are the ones that are the part of the legacy system. In general, utility does not appreciate major changes in the legacy systems because:

- They are still the major devices which can regulate both voltage and reactive power demand of the consumers and the technology is mature.
- Cost involved in un-installing these devices are a critical factor and the uncertainty about the reliable operation of the distribution system without these legacy devices is a major concern.

5.2.1 Proposed Approach

The proposed algorithm utilizes the information from the line regulators about the current status of voltage of the load end of the feeder and then supplies/absorbs

reactive power from the VSCs in order improve the voltage profile in the feeder. The information gathered is based on the line regulator warning status. As the warning from line regulator is a pre-cursor for actual regulator operation (it may take few seconds for regulator to operate after the warning is issued), the approach can co-ordinate well with the actual regulator operation. During the time period between a warning and actual regulator operation, the VSCs in the distribution feeder can supply/absorb the reactive power from the feeder so that the voltage in the feeder can be improved. In many cases, line regulators operations are no longer needed. This helps in increasing the overall lifetime of the line regulators, while minimizing operational and maintenance cost to the utilities. This faster reactive power control from the VSCs also regulates the voltage in the load end of the feeder and reduces the chances of damaging the voltage sensitive devices as the transients caused by the tap changes is minimized. The algorithm is presented in fig. 5.2. Fig. 5.3 shows the Fig. 5.2. Algorithm for proposed co-ordinated linear voltage regulation.

flowchart for the proposed voltage regulation algorithm designed to co-ordinate the substation regulators, line regulators and the battery SMS deployed in the feeder. The substation LTC regulates the overall voltage profile in the feeder and is dependent on the load profile variation throughout the day (which is assumed to be periodic with time period of 24 hrs- slow frequency changes) whereas line regulators are primarily controlling voltage on their load ends which may vary at faster frequency than the overall load profile and do not directly impact on the voltage upstream. Based on the above mentioned assumption about load in the feeder, two components of reactive

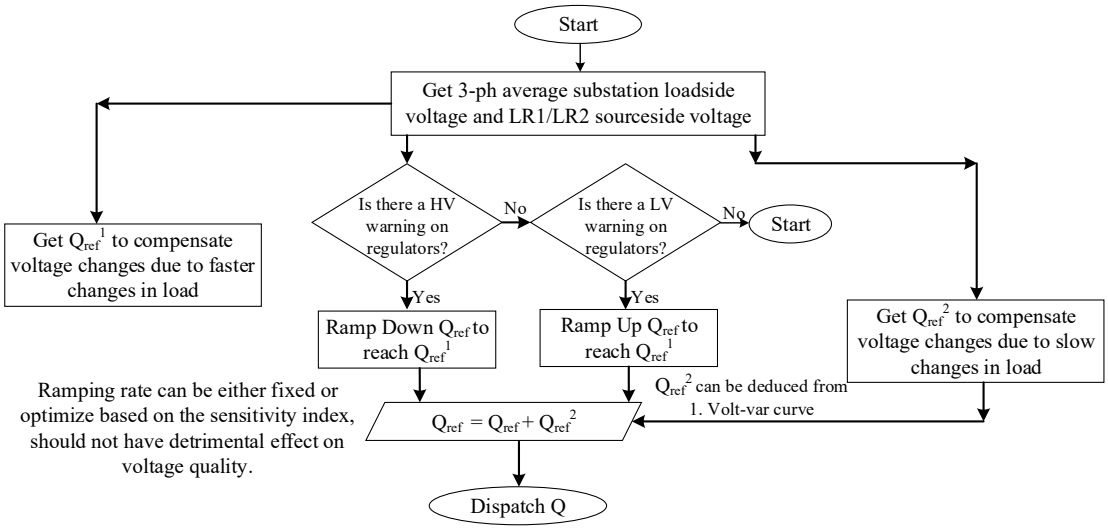

Fig. 5.3. Voltage regulation framework for coordinated volt/var control.

power is generated from the battery SMS that co-ordinates the regulators with the battery SMS. The first component of reactive power Q^1_{ref} is generated based on the instantaneous demand of load centers which are downstream of line regulators. These instantaneous demand of load centers after line regulators are determined based on the voltage warnings of the line regulators. If the high voltage warnings is detected, it is assumed that the load demand is dropping downstream and if low voltage warning is detected the assumption is that the load downstream is increasing and reactive power is to be supplied to maintain the voltage. Q^2_{ref}, however is determined based on the forecasted load for next day (if available) or based on the measurement of substation OLTC load side voltage. In the following subsections, a brief explanation about the rationale of each of the steps in the algorithm is discussed.

5.2.2 Line Regulator Warning Acquisition

Fig. 5.4 shows the high voltage (HV) and low voltage (LV) warning data collected from the utility feeder. The warning signals are issued by the line regulators whenever the load-side voltage of line regulators goes out of the preset voltage band. If the voltage is lower than the lower limit of the allowed band, a low voltage warning signal is issued and if higher than the upper limit of allowed band, a high voltage warning is issued. These warnings are good indicators of the voltage status in the load end. Utilizing warnings as an indicator of voltage status and reactive power needs of the system makes the proposed control scheme situational aware. i.e. the controller acts only if a situation where it needs to act arises. Utilization of warnings for reactive power control also eliminates the need to place the voltmeters to measure the load end voltages in the feeder. As line regulators tend to isolate the load downstream of it from the feeder upstream, it is crucial to determine the upstream side voltage of the feeder when reactive power is dispatched from VSCs to support the load. To

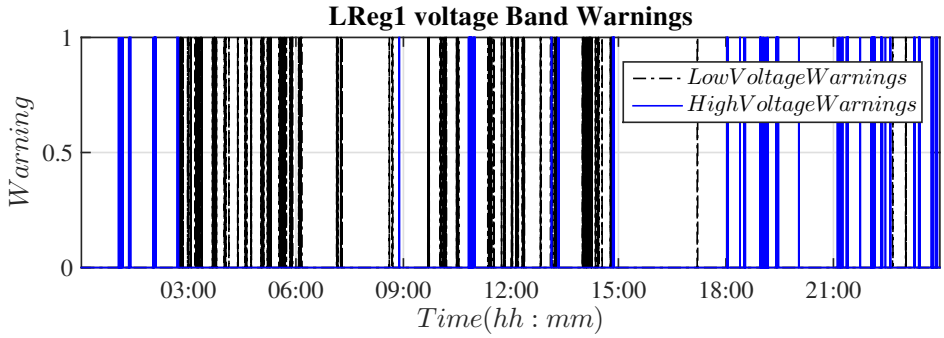

Fig. 5.4. LV/HV warnings for proposed feeder real measurements.

illustrate the above mentioned situation, consider fig. 6.3. Consider a case, where the primary side voltage of the line regulator is close to the upper limit of the allowed

band, whereas due to a lower tap position used in the line regulators and increasing load, the secondary side voltage now reaches close to its lower band, which then starts to generate low voltage warning. If the reactive power injected from the VSCs do not consider the primary side voltage of the line regulator on its control action and inject reactive power solely based on warnings, the primary side voltage might go higher, which might trigger operation of substation OLTC, which is regulating the primary side voltage of the line regulators. Thus injection/absorption of reactive power from the VSCs based on the warnings should also consider the source side voltage of the line regulators.

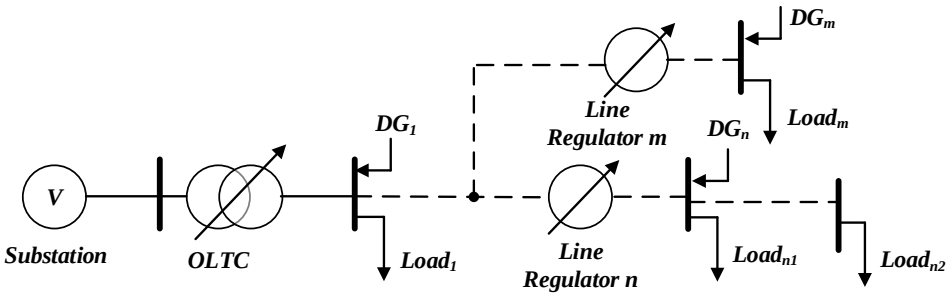

Fig. 5.5. Simplified model of distribution system.

5.2.3 Local Load Fast Changes based Q^1_{ref} Generation

This reactive power reference is generated based on fast changes in feeder voltage in the vicinity of line regulator 2. When the line regulator warnings are received, the proposed controller first access the line regulator source side voltage and compares in which of the range it falls as shown in fig. 5.6. For example, if the line regulator source side voltage lies within 119.5 V to 120 V, which is the lower range of the substation OLTC regulation, more emphasis is given to reactive power generation as compared to reactive power absorption. A large quantity of reactive power if absorbed in that

range due to high voltage warning can cause the substation OLTC to act which is not desired. The reactive power ranges for other voltages is also shown in fig.5.6. Also, it should be noted that, the controller should regulate the rate at which the reactive power is injected to the feeder. A faster change in reactive power in the feeder causes steep changes in voltage which is not desirable in the DS operation and may result in voltage flickers. So, a ramp rate controller is also placed in this control scheme to limit at the rate of change of voltage occurs in the field. The reactive power reference

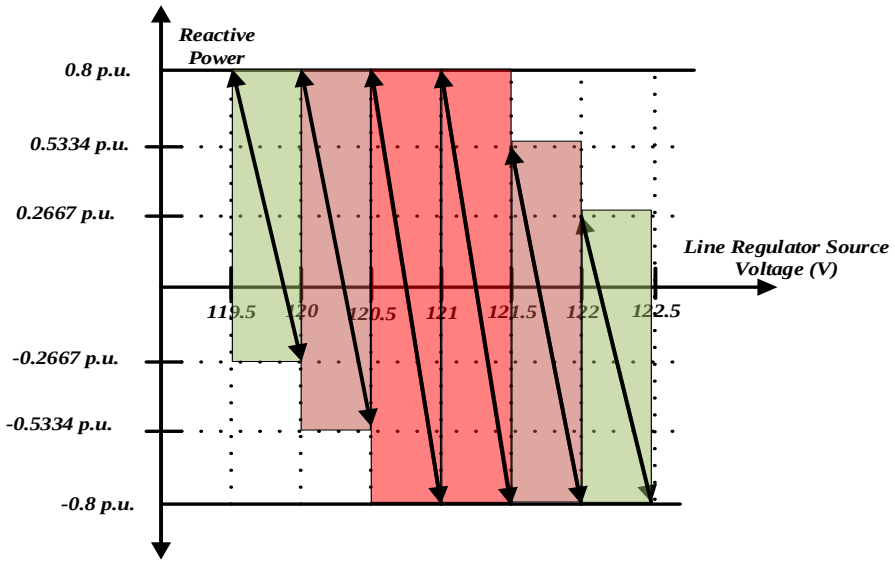

Fig. 5.6. Plot showing region for reactive power generation based on voltage.

Q^1_{ref} can be mathematically considered in the form shown in 5.1 where a is -1 for High Voltage warning and 1 for Low Voltage warning, t is time and the k is the ramp rate at which the reactive power is injected.

$$Q_{ref} = Q_{ref} + a * k * t \tag{5.1}$$

Note: ***limit with the*** Q^1_{ref} ***range shown in fig. 5.6***

5.2.4 Line Regulators Voltages Warnings Based Q^1_{ref} Ramp rate Correction

As mentioned, line regulators warnings issue voltage violations at the regulator terminal point in the form of binary signal. Also, Q^1_{ref} generates reactive power reference points according to only fast changes in voltage. Consequently, voltage warnings are being used to ramp up/down Q^1_{ref} to mitigate voltage profiles fast changes as well as going out of band. In this work we have considered a fixed ramp rate for the reactive power injection in the feeder. If we assume $K1 = \frac{\Delta V}{\Delta t}$ to be rate of change of line regulator source side voltage and $K2 = \frac{\Delta V}{\Delta Q_{vsc}}$ to be the sensitivity of the line regulator source voltage with respect to reactive power from VSC, the optimal ramp rate for reactive power injection can then be obtained by (5.2).

$$k = \frac{K1}{K2} \tag{5.2}$$

For field implementation of sensitivity based technique, it might be easier to find the rate of change of voltage, $K1$, based on measurements, however, computing sensitivity coefficient online is a daunting task. The feeder topology is constantly changing with load variations and a real world feeder has large number of variables which make computing online sensitivity a difficult task. This can still be achieved with large number of measurements and line admittance's information of the feeder, but such methods are computationally expensive and may not be feasible for real world applications as of now.

5.2.5 Slow changing local load Based Q^2_{ref} Generation

Load profiles generally have a certain periodic pattern throughout the days and seasons. To exploit such predictable behavior of load, another reactive power component Q^2_{ref} is generated by applying a second volt-var curve considering LTC load side voltage as a point of interest.Q^2_{ref} in this work is generated using the substation OLTC secondary side voltage which changes in inverse proportion of the load increment in the feeder. The purpose of generating Q^2_{ref} is also to limit the line regulator source side voltage as close to the middle of the allowed band of the substation OLTC so that during the case of HV and LV warnings, a larger range of reactive power can be utilized to avoid the tap operation of line regulators.

5.3 Test system Modeling

This section explains characteristics of the distribution feeder which is used for evaluating the proposed co-ordinated voltage control methodology. The non-aggregated model of the distribution feeder consists of 720 nodes of 12.47 kV medium voltage level. The feeder has three capacitor banks, two line voltage regulators and one on-load tap changer (OLTC) on the substation side. The feeder is connected with 250 kW/750 kWh battery energy storage system (BESS) integrated with 1-MW PV solar plant. The voltage source converters from battery energy storage and PV farm are both rated at 1 MVA capacity. The maximum reactive power absorption/generation capacity of the VSC used for the battery is limited to 800 kVAR. The non-aggregated model of the system was aggregated and modeled in PSCAD/EMTDC platform (see Fig.5.7). The aggregation of the model into different load centers was done based on

the power flow measurements at each of the line regulators, RER's point of common coupling and the substation power flow readings. The power flow and voltage data was provided by the utility on a 5 sec basis which was utilized to compute the effective line impedances for the aggregated model. Further the aggregated model is validated with the field data measurements available from the utility. The aggregated model uses a voltage source modeled as the substation and consists of all the legacy systems in the actual feeder. The substation voltage is fed based on the field data which varies in time as per the overall changes in the load in all of the feeders supplied by the substation. The loads are modeled by variable resistive and inductive components that provides same load profile obtained from the field data. The substation OLTC is modeled using an ideal transformer with provision to change its transformer ratio using an external signal which is computed based on the tap position. The OLTC has a potential transformer (PT) with a ratio of 60:1 and operates at a nominal voltage of 120V which corresponds to 7.2 kV phase voltage. The OLTC is also equipped with a current transformer with ratio of 500:1. The substation OLTC is working based on line drop compensation (LDC) settings which R and X compensation of 5. This means if the substation source side voltage is at its nominal value of 120 V and supplies the load at the nominal value of 500 A, the load end voltage perceived by the LTC is equal to 120 - 5 = 115 V. The OLTC has provision for correcting the voltage in the range of ± 10%, and by adjusting the tap positions from -16 to +16 with each tap change resulting in 0.625% change in voltage. The time delay for the substation OLTC tap operation is 50 s. The voltage band used for the substation OLTC is 119.5 to 122.5 V. The voltage regulators use the same model as the OLTC, however the line

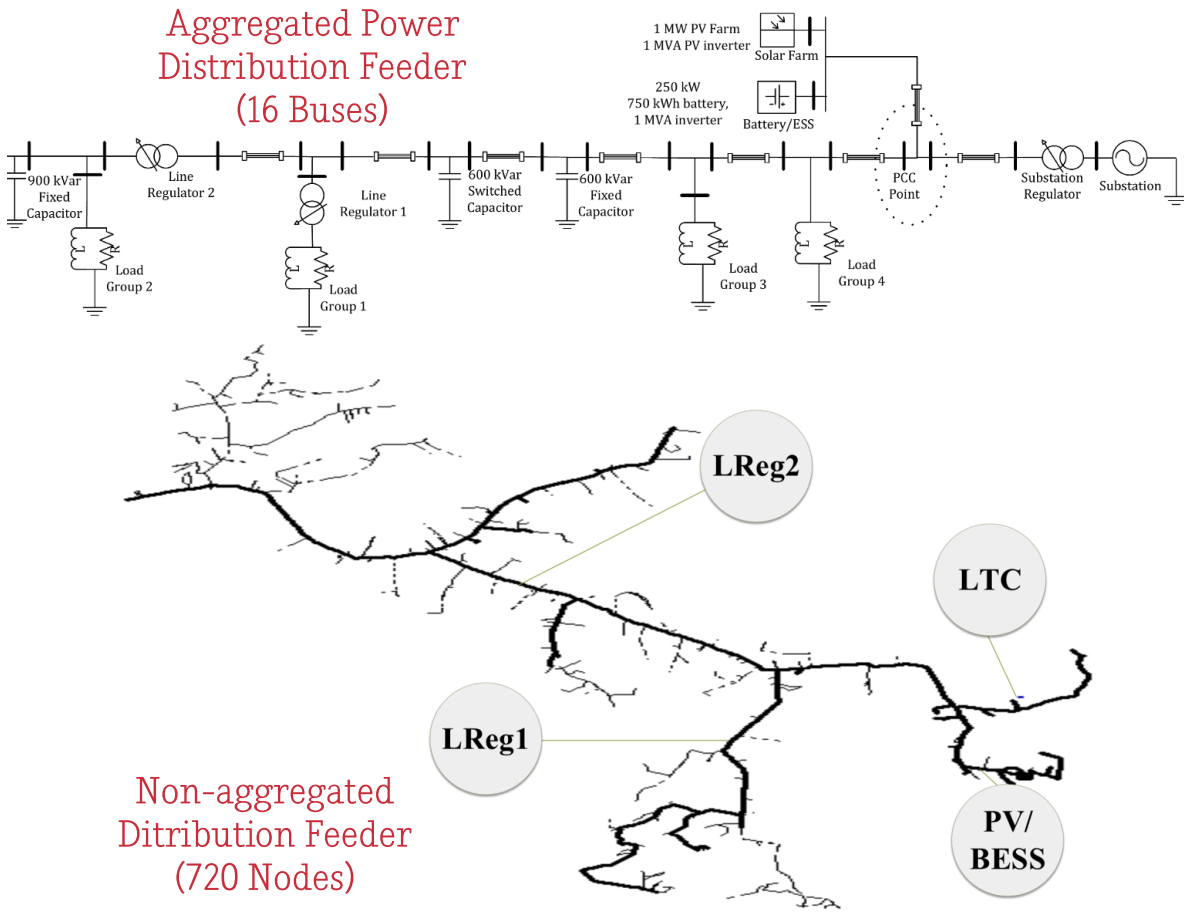

Fig. 5.7. Aggregated Power Distribution Feeder (16 Buses)

voltage regulators have R and X settings of zero, meaning they regulate the voltage based on their secondary side voltage, not based on a point in the downstream. Also, the time delay for the line regulators is 45 s and the voltage regulation band used for the line regulators is between 123 to 125 V. These settings for the substation LTC and the line regulators are based on the utility data.

5.4 Simulation Results

This section presents simulation results which is performed using five seconds intervals based real time measurements from utility feeder collected through server-based communication technology (PI System). The utility provides the research team with

data such as warnings from the line regulators and substation OLTC, associated current tap positions, voltages at the primary and secondary side of line regulators and OLTCs, active and reactive power flowing from the line regulators and OLTCs and PCC point, voltages at the point of common coupling (PCC) point where both energy storage system and solar PV facility are installed. Based on the available data from the utility and the feeder information from the utility, the PSCAD/EMTP model was first validated. The system inputs to the validated model are: substation voltage profile, substation active and reactive power, line regulators locations active and reactive power and initial tap positions for all voltage regulators (all obtained from utility data). Fig. 5.8 shows the field obtained load and substation source voltage profile used for the simulation study. In the study that follows :$Case-0$ is the case with no reactive power support from the VSCs and $Case-2$ is the case with co-ordinated voltage control using the VSCs. Aggregated model for the feeder is developed on PSCAD/EMTDC platform. Full days simulations are run on PSCAD with and without proposed co-ordinated voltage regulation. The proposed methodology is evaluated based on total number of taps operations for three voltage regulators as well as weak locations voltage profiles improvement. Fig. 5.8 also shows the periodic characteristics of the load as previously explained. The proposed controller exploits such periodicity in the load behavior for a better voltage regulation as well as reduction in voltage fluctuations at the locations of interest. As it can be seen from fig. 5.8, the substation voltage obtained from the field data varies in inverse proportion with the load supplied from the substation. The sharp changes in the voltages in fig.5.8 is due to tap changes in the upstream side of the substation (DMS).

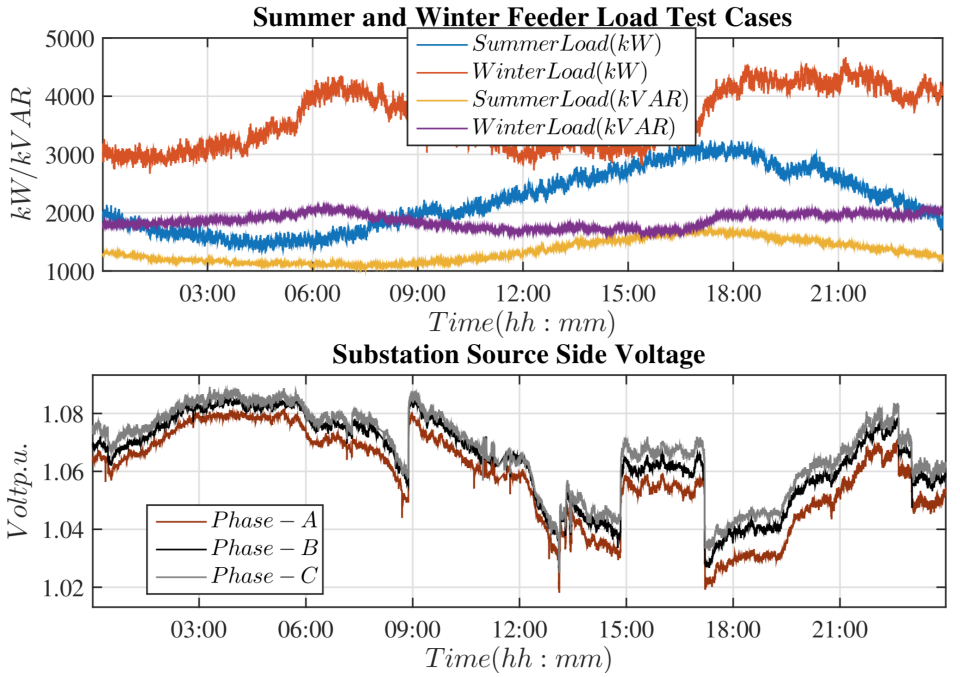

Fig. 5.8. Feeder measurements data. (a) Feeder load active and reactive power; (b) Summer real measurement LTC source side voltage and real DMS actions.

5.4.1 Case-I: Summer Day Simulation Results

Fig. 5.10 shows voltage regulators tap operations with and without using the proposed co-ordinated control. It can be observed that a significant number of tap operations is avoided due to the use of proposed co-ordinated control to dispatch reactive power from VSCs. Since substation voltage is constant throughout both cases durations, OLTC had less taps savings and delays than other line regulators. Intuitively, having both line regulators warnings observed by the control algorithm, the proper amount of reactive power was being injected/absorbed accordingly to bring the voltage back to normal level and prevent such real taps operations.

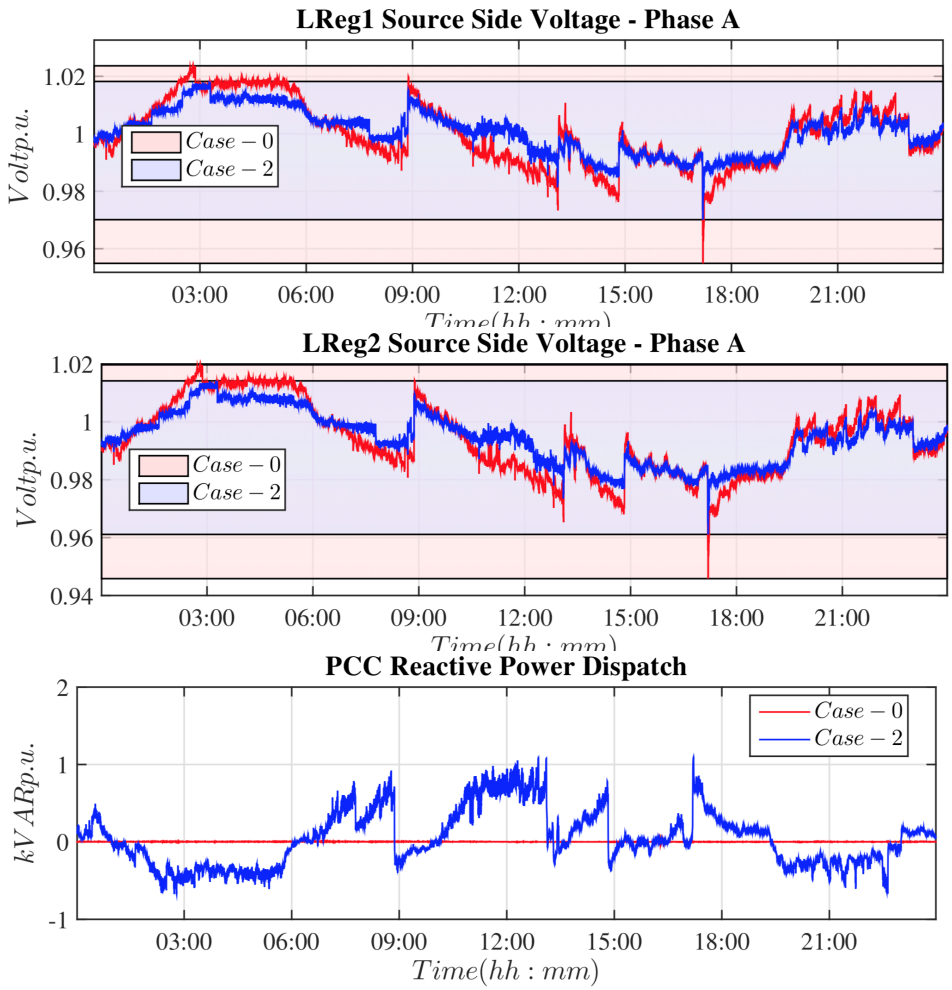

Fig. 5.9. Case-I: Summer day feeder voltage profiles and PCC reactive power dispatch. (a) LReg1 source side voltage - Phase A; (b) LReg2 source side voltage - Phase A; (c) PCC reactive power.

5.4.2 Case-II: Winter Day Simulation Results

Also, Fig. 5.12 shows taps operations results for simulating a winter day which has big number of taps in the morning due to demand peak.

5.4.3 Comparative Simulation Results

Table 5.1 shows the comparison of the total number of tap operations for substation OLTC, Line Regulator 1 and Line Regulator 2 within 24 hours with/without the use of

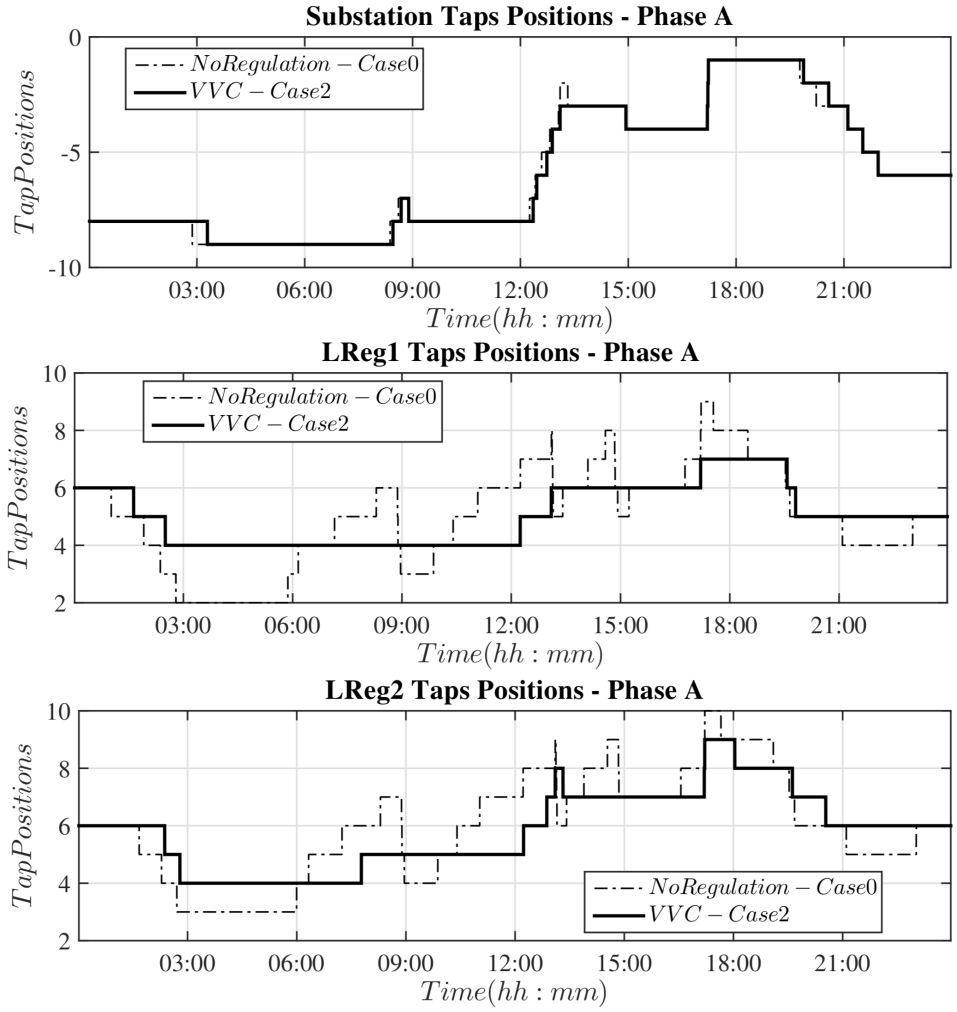

Fig. 5.10. Case-I: Summer day taps operations savings.(a) LTC taps - Phase A; (b) LReg1 taps - Phase A; (c) LReg2 taps - Phase A.

proposed voltage regulation for another summer day. As the proposed methodology is

Table 5.1
Summer day total number of tap operations for three voltage regulators.

-	OLTC		LReg1		LReg2	
	Case-0	Case-2	Case-0	Case-2	Case-0	Case-2
Phase-A	20	18	35	7	32	12
Phase-B	23	17	30	9	31	9
Phase-C	20	14	29	5	31	7

acting to reduce the number of tap operations, both line regulators source side voltage is always kept within limits which results in decreasing number of taps operations as

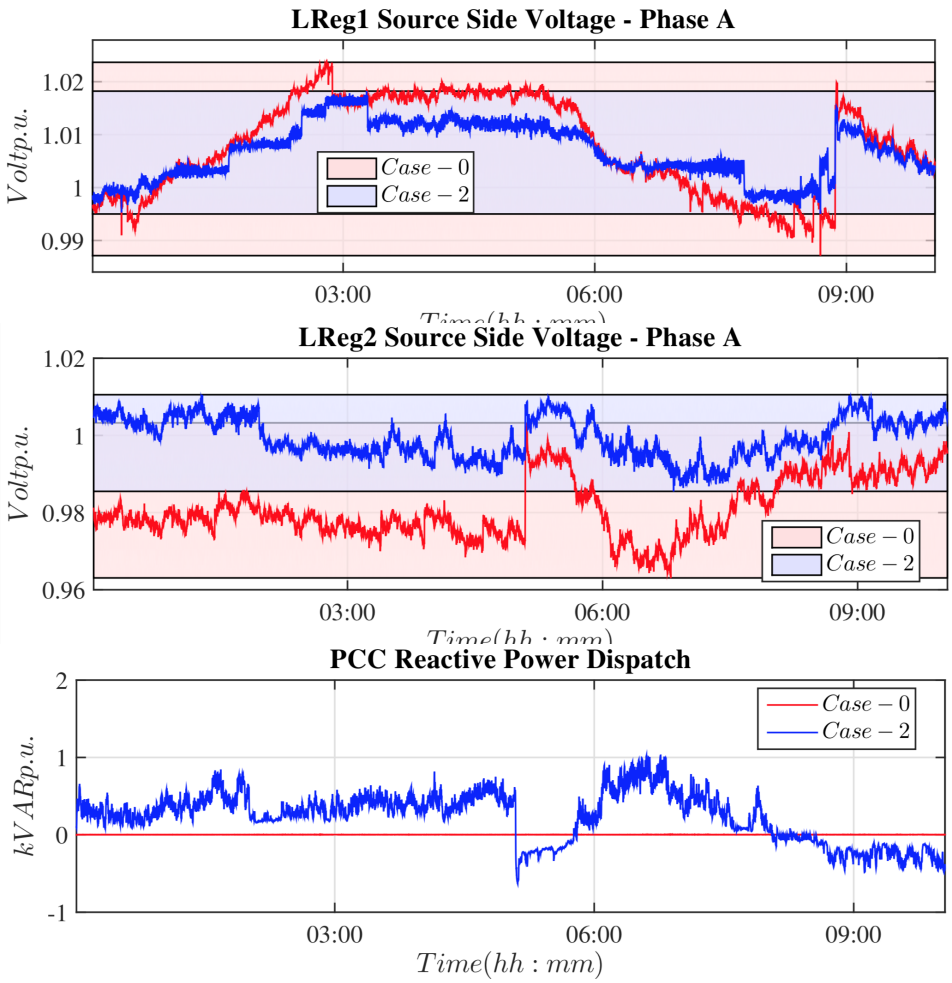

Fig. 5.11. Case-II: Winter day feeder voltage profiles and PCC reactive power dispatch.(a) LReg1 source side voltage - Phase A; (b) LReg2 source side voltage - Phase A; (c) PCC reactive power.

in feeder base case. Fig. 5.9 and Fig. 5.11 show line regulator 1 and line regulator 2 source side voltages and dispatched reactive power from point of common coupling. As it can be seen, with the proposed co-ordinated control, the overall voltage variation of source side of line regulator 1 and 2 is narrowed down as compared to the case with no regulation. Also, from the reactive power profile injected from PCC point, it can be seen that the proposed control helps in regulating the voltage better by absorbing reactive power during light load conditions, when tendency is to have high voltage in

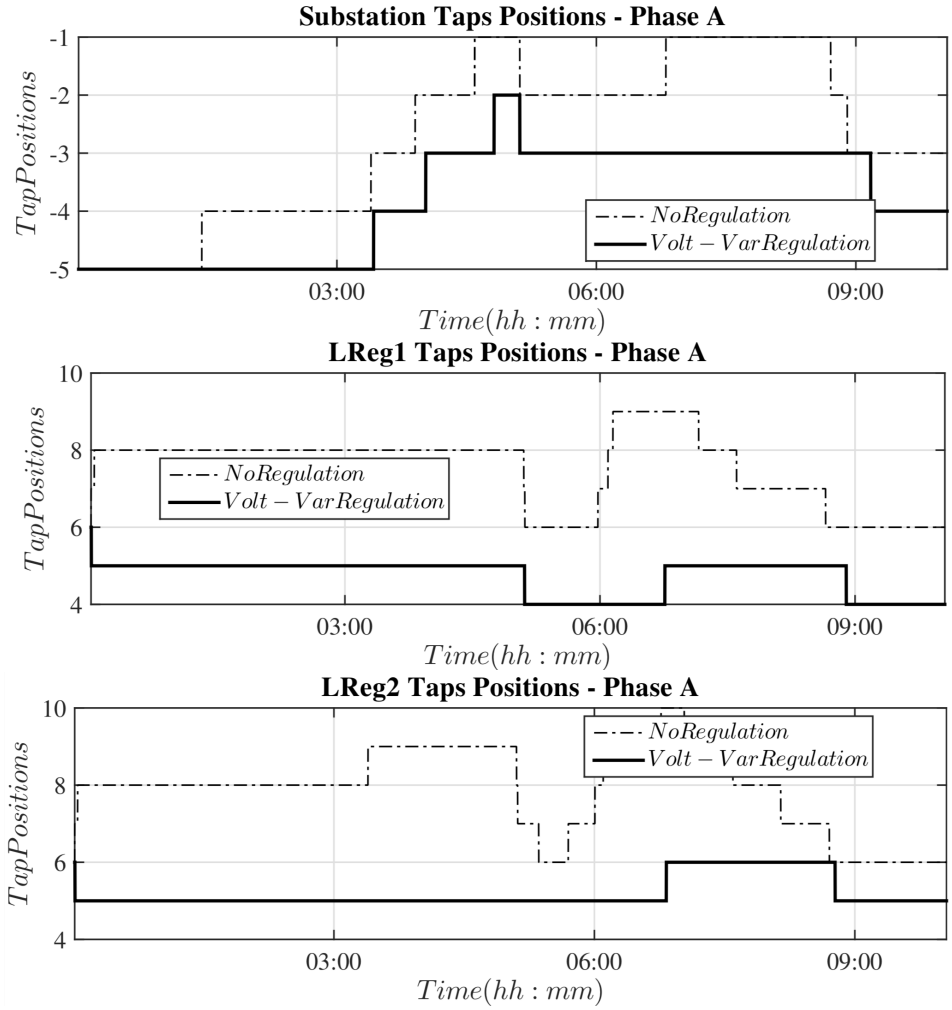

Fig. 5.12. Case-II: Winter day taps operations savings.(a) LTC taps - Phase A; (b) LReg1 taps - Phase A; (c) LReg2 taps - Phase A.

the feeder and supply reactive power during peak load conditions, when feeder tends to have lower voltage. Finally, point of common coupling voltage span of fluctuations is also narrowed down by applying the proposed voltage regulation methodology as in Fig. 5.13. It can be observed that the overall band of voltage changes throughout the day has been narrowed down in the feeder suggesting a more stricter regulation of voltage.

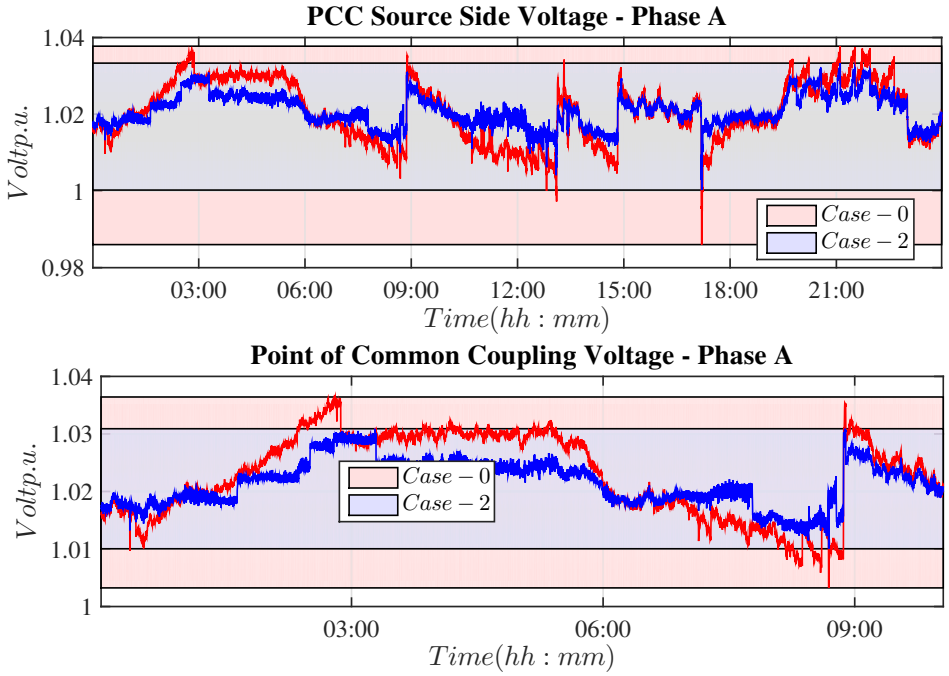

Fig. 5.13. PCC Voltage for both summer and winter test cases. (a) Summer test case.; (b) Winter test case.

5.5 Summary

The chapter proposed a coordinated control approach to co-ordinate the operation of currently used legacy control devices along with the newly integrated VSCs in the distribution system. The proposed technique is generic, situationally aware and can be utilized in any utility system as the method is based on real-time feeder measurements as opposed to the system model based on an operating point. The proposed method reduces the need for adding DER components as another variable in the distribution system management optimization problem, which means the complexity of the distribution system management is not worsened. The proposed technique has economic benefits as well as power quality benefits due to the significant number of tap operation savings they provide. The proposed control technique is being devel-

oped in a micro-controller framework for the test in the real world feeder for which the study presented in performed and the cost benefits of the proposed technique is being performed in terms of improvement of power quality, the number of tap savings and reduction in system losses etc.

CHAPTER 6: DYNAMIC VOLTAGE PROFILE MANAGEMENT OF POWER DISTRIBUTION SYSTEM BASED ON ONLINE SENSITIVITY BASED VOLT-VAR CONTROL

This chapter presents a situational awareness, data-driven, and agnostic coordinated control methodology for voltage regulation in the active distribution systems (DS). Considering voltage source converters (VSCs) as reactive power sources that work in conjunction with the existing legacy controllers.

6.1 Introduction

The approach uses time-scale coordination based on regulator warnings such that the voltage support from regulators is time separated from the reactive power support using VSCs. Two types of voltage changes are considered; a slow changing one based on the feeder load and a fast-changing one based on sudden changes in load or PV output. The reactive support for both these changes is then designed based on the voltage to reactive power sensitivities. The combined reactive support is then used as a set-point to dispatch reactive power from the VSCs. The proposed control technique is tested in the field verified model of a real feeder. Results show that the proposed coordination approach has major economic values as well and power quality benefits in the operation of distribution systems. It also shows that this can be achieved without major changes in the existing communication framework currently utilized by the utility. The utility-scale photovoltaic (PV) farms and battery

energy storage are growing in numbers, as the integration of large-scale renewable energy resources (RERs) has become a mandate initiated by the Renewable Portfolio Standards (RPS) [57]. However, these RERs impose challenges in the control and operation of the distribution system, especially on voltage profile management. One source that can provide additional reactive power support is the VSCs. VSCs are primarily connected to the distribution system to convert active power from the RERs and feed generated power into the network. Recently, grid codes in many countries have been modified such that the reactive power capability of grid-connected VSCs can be utilized to support the grid [78]. Even though utilizing VSCs as additional voltage control devices is promising, coordinating the existing legacy controllers in the feeder (such as on-load tap changing transformers (OLTCs), voltage regulators, capacitor banks, etc.) with the VSCs is very challenging. Thus, there is a need to intelligently provide reactive power support from the VSCs without affecting the operation of legacy controllers.

State-of-the-art work in this direction mainly focuses on either a fully model base or a fully measurement-based approach. For example, [51] proposed a multi-timescale based coordinated VVC algorithm which aimed to schedule reactive power dispatch for a given distribution system on two-time horizons; an hourly and 15-minute interval basis. Conventional voltage regulation devices like OLTC and capacitor banks (CBs) are controlled on an hourly basis, whereas RERs integrated voltage source converters (VSCs) are compensating reactive power in a 15-minute basis, based on the fast changes in voltage profiles due to renewable resources output power intermittencies. However, it is practically proven that fast fluctuations in voltage profiles could exist in

the order of a few seconds. Ref. [26] presents a distributed control of voltage profiles using both active and reactive power compensation, where the required reactive power dispatch is a function of the PV output power ramp rate change in the opposite slope. As the main application of system losses reduction, [73, 105] applied coordinated reactive power control to significantly reduce capacitor banks switching and system losses.

Much volt-var control (VVC) algorithms are developed utilizing heuristic multi-objective optimization methodologies. With [59], a coordinated control approach is presented to coordinate DERs and substation OLTCs. However, the technique requires changing the compensation settings of the OLTC. Similarly, [107] presented different volt-var optimization (VVO) techniques to maintain all buses voltages within limits. Ref. [47,84,90] discussed different VVC algorithms utilizing sensitivity analysis along with objectives and functions based formulations. Ref. [84] presented dynamic adjustment of OLTC parameters (Line Drop Compensators LDC) for algorithm improvement. In [46, 55, 56, 97] the importance of coordination between OLTC, line regulators and distributed generation sources are discussed in detail. In [46], a distributed method for the coordination of these sources is shown based upon multi-agent system (MAS) architecture. But implementation of the methods requires extensive communication links between different devices.

Integrated volt-var control (IVVC) methodologies which use heuristics based adaptive controls are proven to be successful. In such distribution systems with large penetration of DERs, using optimal power flow to generate DMS control actions is complex with the DERs. Ref. [102] applied signal processing and adaptive con-

trol volt-var optimization methodology, where distribution system operation decisions were made based on system measurements, observations, and processing rather than depending on circuit models. In ref. [9, 10, 12] field measurements have been used to implement active power controls for performing applications like peak load shaving and photovoltaic active power smoothing.

References [42, 63] and [13, 23, 64, 99] used a utility-scale distribution feeder to design a centralized volt-var control to keep voltage profiles within tight ranges, as well as for conservation voltage reduction (CVR). In ref. [22] the impact of bulk volt-var control on transmission systems by using a co-simulation framework with tight coupling control is designed and illustrated. Also, [31] presented fuzzy logic combined with the heuristic algorithm to implement volt-var coordination to minimize voltage violations, and [100] presented an assessment for both volt-var and volt-watt controls to avoid energy curtailment from renewable resources. All of the above work has demonstrated centralized control actions not coordinated with both OLTC and line regulators.

In [15], a control strategy is presented for coordinating the operation of OLTC, line voltage regulators and VSCs of battery energy storage. This technique aims to maintain the load end voltage of the feeder within the allowed band while minimizing the operation of the line regulators. The realization of the control depends on the knowledge of the regulator voltage out of band warning signal from the line regulators. Based on this, VSCs inject/absorb the reactive power to/from the feeder, such that the feeder load end voltage is at the allowable voltage band. The architecture is implemented using a communication network already available at the utility.

6.2 Problem Formulation

Conceptual representation of an active distribution system for volt-var profile management with both legacy and inverter based controllers is shown in Fig. 6.1.

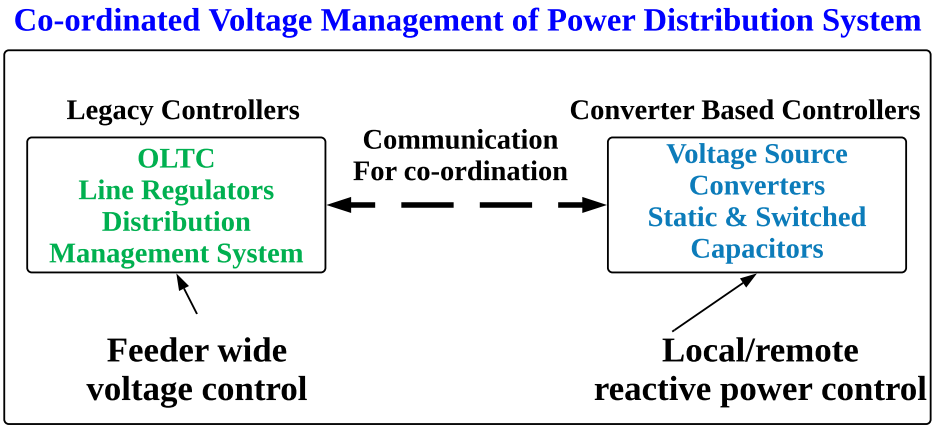

Fig. 6.1. Voltage regulation paradigm for the distribution system.

As illustrated, voltage regulation in the legacy power distribution system is achieved using on-load tap changers (OLTCs), Line Regulators (LRs) and static/switched capacitors. The location and the size of these devices are designed in the planning stage. A Supervisory Control and Data Acquisition System (SCADA) based Distribution Management System (DMS), is used to control the source side voltage of OLTCs. When voltage source converter (VSC) based systems are integrated, coordination between VSCs and DMS legacy system controllers are required. This coordination can be achieved using DMS and VSCs (marked in green) based on the information extracted from the legacy controllers (marked in red).

The proposed approach is a data-driven based methodology utilizing distribution feeder data obtained at regular time intervals. In the proposed algorithm, meter and controller information from line regulators, OLTCs and VSC based devices are utilized

(see Fig. 6.2). Specifically, load and source side voltage of line regulators, regulator tap information and warnings, OLTC tap information, DMS initiated OLTC source side voltage, active and reactive power from the regulators, VSC driven devices, and the substation, are measured at regular intervals.

For time scale separation, regulator warnings are used. The warning from line regulator is a pre-cursor for actual regulator operation (it may take few seconds for a regulator to operate after the warning is issued). The approach can coordinate well with the actual regulator operation. During the time period between a warning and actual regulator operation, the VSCs in the distribution feeder can supply/absorb the reactive power from the feeder so that the voltage can be improved. This approach can reduce the line regulator operation, thus saving the asset life and minimizing maintenance cost and time. Also, this faster reactive power control from the VSCs can regulate the voltage at the load end of the feeder and reduces the chances of damaging the voltage sensitive devices as the transients caused by the tap changes is minimized. The details are as follows.

6.2.1 Sensitivity Calculations

Consider a generic and simplified power distribution system represented in Fig. 6.3. Let us consider bus j for analysis purpose. From Fig. 6.3, V_j could be represented as:

$$V_j = V_i + \frac{P_j R_{th} + Q_j X_{th}}{V_j} \tag{6.1}$$

where P_j and Q_j are the active and reactive power at bus j.

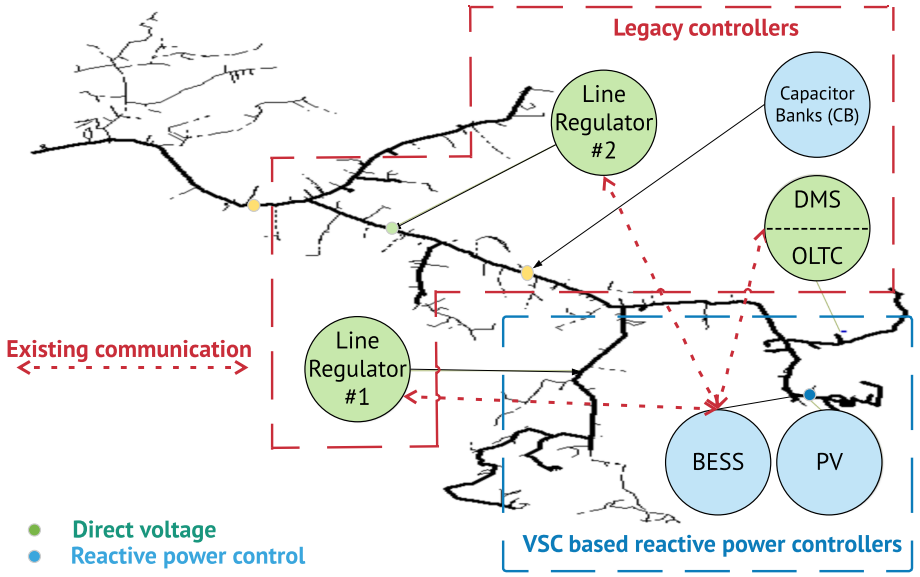

Fig. 6.2. Voltage regulators and PV/BESS systems location on the feeder.

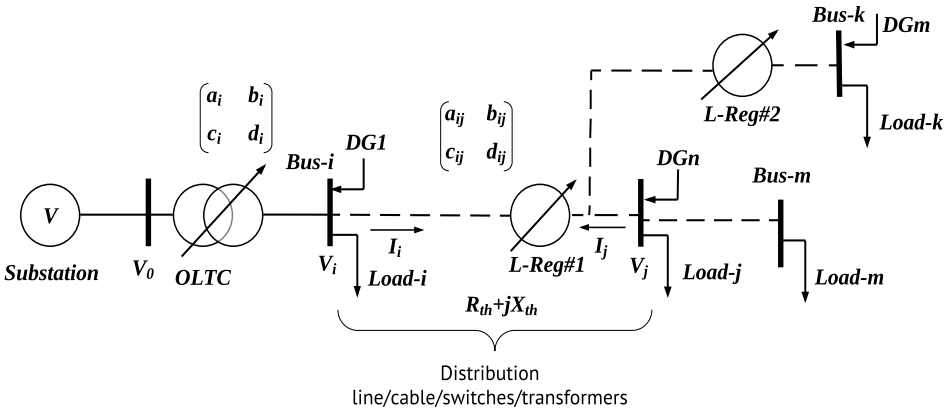

Fig. 6.3. Simplified model of distribution system.

Therefore, voltage rate of change with respect to both active and reactive power could be represented as follows:

$$\frac{\partial V_j}{\partial P_j} = \frac{R_{th}}{V_j} \tag{6.2}$$

$$\frac{\partial V_j}{\partial Q_j} = \frac{X_{th}}{V_j} \tag{6.3}$$

This can be extended to single phase and three phase loads as

$$V_j = a_j V_i + b_j I_i \tag{6.4}$$

$$I_j = c_j V_i + d_j I_i \tag{6.5}$$

$$V_i = A V_j + B I_j \tag{6.6}$$

and thus

$$R_{th} = -Re(B_j) \tag{6.7}$$

$$X_{th} = -Im(B_j) \tag{6.8}$$

It has been discussed and proved in [106] that if the reactive power source is at bus-k instead of bus-j and if it is a single phase load, then (B_j) can be replaced as $[A_{ij}[B_j]_{phase}]$. A similar representation can be made for other phases as well.

In order to find effective reactive power contributions from the VSC device point to maintain the voltage profile optimal, we should calculate the voltage to reactive power sensitivity of the feeder. Consider a power distribution radial feeder model as represented in Figure. The voltage at node j can be represented as [106]

$$\frac{\partial V_j}{\partial q_j} = \frac{X_{eq}}{V_j} \tag{6.9}$$

For a voltage sensitivity of the change of taps in a line regulator, we can represent

that

$$\frac{\partial V_{ssr}}{\partial V_{lsr}} = Tr \tag{6.10}$$

where V_{ssr} represents the source side voltage of the regulator, V_{lsr} represents the load side voltage of the regulator and Tr represents the tap ratio. For a total of 32 steps tap with a 10% regulation of voltage Tr can be represented as $1/(1+0.00625n)$ where n is the regulator tap. From (6.10) it can be derived that

$$\frac{\partial V_r}{\partial n} = \Delta V_r * [-0.00625/(1 + 0.00625 * n)^2] \tag{6.11}$$

From the above discussion, for a given feeder, the change in the voltage can be derived as

$$\Delta V_j = K_{Q_j} \Delta Q + K_{n_j} \Delta n + K_{P_j} \Delta P \tag{6.12}$$

where ΔV_i is the change in the voltage at the ith node, K_{Q_i} is the i^{th} row of the reactive power sensitivity matrix which is $\frac{\partial V_j}{\partial q_j}$ for a measurement period of 5 seconds, ΔQ is the reactive power changes vector, K_{n_i} is the i^{th} row of tap position sensitivity matrix which is $\frac{\partial V_r}{\partial n}$ for a measurement period of 5 seconds and Δn_{sbs} represents the deviation of substation tap position, K_{P_i} is the i^{th} row of the active power sensitivity matrix which is $\frac{\partial V_j}{\partial p_j}$ for a measurement period of 5 seconds,ΔP is the active power changes vector .

In this work, we do not consider the active power sensitivity matrix separately,

as the control variable under consideration is reactive power from inverters. But, the effect of active power on voltage changes are captured through the measured values. Also, because of the slower time scale of OLTC action, only the reactive power sensitivity at the various locations in the feeder is considered. The first term in (6.12) represent the changes in the voltage due to reactive power support and second terms consider the changes in voltage due to tap operation of regulators. As mentioned before, we can separate this as a two-time scale problem as the tap change occurs at a slower rate than reactive power support, especially if the support is from VSC based devices. Considering this, we can rewrite (6.12) as

$$\Delta Q = (K_{Q_j})^{-1}(\Delta V_j - K_{n_j}\Delta n - K_{P_j}\Delta P) \tag{6.13}$$

such that K_{Q_j} is the online sensitivity index between reactive power of VSC and voltage of location of interest, ΔV_j is the step change in voltage at that location, K_{n_j} is the sensitivity index of voltage change due to taps operations changes, and $\Delta n is the number of changed taps per time step.$

From the generic formulation in (6.13) it can be seen that the change in reactive power at PCC is a function of sensitivity between the voltage at bus j to the DG in bus j or bus k, voltage deviation at bus j, voltage change because of active power and, the tap operation of the regulator. Let us assume that the regulator-1 taps are set based on a specific rate of voltage change at the load-side, and a tap operation has happened. Then (6.13) can be written as

$$\Delta Q = \frac{\Delta V_j^{new}}{K_{Q_j}} \tag{6.14}$$

where V_j^{new} is the new voltage at the bus j after a tap operation which includes the change in voltage because of both active and reactive power changes.

Let us assume that the rate of change of voltage on the regulator is set based on the number of tap positions and the volt-var curve is designed using the controller setting. Then (6.14) will be

$$\Delta Q = [\frac{\frac{\Delta V_j^{new}}{\Delta t}\Delta t}{K_{Q_j}}] \tag{6.15}$$

6.2.2 Fast Changing PV/Load Based Q_{ref}^1 Generation

As mentioned, line regulator warnings issue voltage violations at the regulator terminal point in the form of binary signal. The first reference point generated at the PCC terminal is termed as Q_{ref}^1. This reactive power reference dynamically changes due to fast changes in voltage. The voltage warnings are also used to ramp up/down Q_{ref}^1 and to mitigate fast voltage profile changes. From (6.15), let us assume that ΔV_j^{new} is the load-side voltage of the line regulator-1, then we can represent the optimal ramp rate for reactive power injection as

$$k = \frac{K1}{K2} \tag{6.16}$$

where $K1 = \frac{\Delta V_{reg1}}{\Delta t}$ is the rate of change of line regulator source side voltage (which can be determined from the data obtained from the field) and $K2 = \frac{\Delta V_{reg1}}{\Delta Q_{vsc}}$ to be the sensitivity of the line regulator source voltage with respect to reactive power from VSC, the optimal ramp rate for reactive power injection can then be obtained by (6.16).

For field implementation first the equivalent reactance is calculated as discussed previously. Once an equivalent reactance is obtained, the sensitivity of the voltage at one particular node with respect to the reactive power injection from another node can be obtained. Once the sensitivity is obtained for that particular instant of time, the ramp rate for reactive power dispatch can be obtained as well using (6.16). Substituting (6.16) in (6.15), and considering two time steps t and $t-1$ we can derive the reactive power reference Q^1_{ref} in the form shown in (6.17) where a is -1 for High Voltage warning and 1 for Low Voltage warning, Δt is time elapsed after the warning has been received, which is $t-(t-1)$and k is the ramp rate at which the reactive power is injected/absorbed obtained from (6.16).

$$Q^1_{ref}(t) = Q^1_{ref}(t_0) + a * k * \Delta t \tag{6.17}$$

6.2.3 Slow changing local load Based Q^2_{ref} Generation

Load profiles generally have a certain periodic pattern throughout the days and seasons. The substation OLTC changes normally consider the load change based on the DMS calculations every 15 minutes either through power flow or state estimation. OLTC secondary side voltage changes in inverse proportion to the load increment in

the feeder. The load-side voltage of the OLTC can be computed as follows.

$$V_{ldsd} = V_{sec} - I_f * (R + jX) \tag{6.18}$$

where V_{ldsd} is the OLTC load-side voltage, V_{sec} is OLTC secondary side voltage, I_f is the current flowing towards the feeder from substation and (R, X) are the line drop compensation settings. From (6.18), current I_f can be represented in terms of active power P and reactive power Q. The magnitude of the substation load-side voltage can thus be computed as shown in (6.22). In (6.22), T_p is the tap position, CTR is the current transformer ratio, PTR is the potential transformer ratio, and P and Q are the active and reactive power flowing through the substation respectively.

$$a = (\frac{V_p}{1 - 0.000625 * T_p}) \tag{6.19}$$

$$b = \frac{(P * R + Q * X) * (1 - 0.000625 * T_p)}{V_p * CTR * PTR})^2 \tag{6.20}$$

$$c = (\frac{(P * X - Q * R) * (1 - 0.000625 * T_p)}{V_p * CTR * PTR})^2 \tag{6.21}$$

$$V_{ldsd} = \sqrt{a - b + c} \tag{6.22}$$

By utilizing (6.22), based on the forecasted load profile and OLTC source side

voltage from DMS, the voltage profile for load-side of OLTC can be obtained for any tap position. Representing the sensitivity of OLTC load side voltage V_{ldsd} with the ΔQ_{vsc} as K_{Q_i} similar equation for reference reactive power as in (6.17) can be derived for slow load changes supported by OLTC

$$Q^2_{ref}(t) = Q^2_{ref}(t_0) + a * k1 * \Delta t \tag{6.23}$$

where $k1 = K3/K4$ and $K3 = \dfrac{\Delta V_{ldsd}}{\Delta t}$ is the rate of change of load-side voltage of OLTC (which can be determined from the data obtained from the field) and $K4 = \dfrac{\Delta V_{ldsd}}{\Delta Q_{vsc}}$ to be the sensitivity of the line regulator source voltage with respect to reactive power from VSC, the optimal ramp rate for reactive power injection can then be obtained by (6.16).

From ((6.17)) and ((6.23)) the output reactive power from VSCs can be calcuated as follows.

$$Q_{BESS}(t) = Q^1_{ref}(t) + Q^2_{ref}(t) \tag{6.24}$$

6.2.4 Line Regulator Warning Acquisition

Line regulator warning signals are issued by the line regulators whenever the load-side voltage of line regulators goes out of the preset voltage band. If the voltage is lower than the lower limit of the allowed band, a low voltage warning signal is issued, and if higher than the upper limit of an allowed band, a high voltage warning is issued. These warnings are good indicators of the voltage status at the load end. Utilizing warnings as an indicator of voltage status and reactive power needs of the

system makes the proposed control scheme situational aware. i.e., the controller acts only if a situation where it needs to act arises. Utilization of warnings for reactive power control also eliminates the need to place the voltmeters to measure the load end voltages in the feeder. As line regulators tend to isolate the load downstream of it from the feeder upstream, it is crucial to determine the upstream side voltage of the feeder when reactive power is dispatched from VSCs to support the load. To illustrate the above mentioned situation, consider Fig. 6.3. Consider a case, where the primary side voltage of the line regulator m is close to the upper limit of the allowed band, whereas due to a lower tap position used in the line regulators and increasing load, the secondary side voltage now reaches close to its lower band, which then starts to generate low voltage warning. If the reactive power injected from the VSCs do not consider the primary side voltage of the line regulator on its control action and inject reactive power solely based on warnings, the primary side voltage might go higher, which might trigger operation of substation OLTC, which is regulating the primary side voltage of the line regulators. Thus injection/absorption of reactive power from the VSCs based on the warnings should also consider the source side voltage of the line regulators.

6.2.5 Local Load/PV Fast Changes based Ramp Rate Limits

This reactive power reference generated is modified with the limits based on regulator warnings. When the line regulator warnings are received, the proposed controller first access the line regulator source side voltage and compares in which of the range it falls. For example, if the line regulator source side voltage lies within 119.5 V to

120 V, which is the lower range of the substation OLTC regulation, more emphasis is given to reactive power generation as compared to reactive power absorption. A large quantity of reactive power if absorbed in that range due to high voltage warning can cause the substation OLTC to act which is not desired. Also, it should be noted that the controller should regulate the rate at which the reactive power is injected into the feeder. A faster change in reactive power in the feeder causes steep changes in voltage which is not desirable in the DS operation and may result in voltage flickers. So, a ramp rate controller is also placed in this control scheme to limit the rate of change of voltage occurs in the field. The ramp rate of reactive power generation in this paper is time varying and is dependent on the sensitivity as well as the rate of change of voltage variation.

6.3 Test System Modeling

The second benchmark distribution network for this study is IEEE 8500-node test feeder. This feeder is selected as a more realistic feeder for testing the scalability and showing the methodology contribution to the existing methodologies in the literature. The model is developed in CYME including one online load tap changer (OLTC), three line voltage regulators, nine single phase and one three-phase capacitor. There is one PV facility installed in the middle of the feeder, whereas energy storage system is installed at two different locations for two different case studies as shown in Fig.7.3.

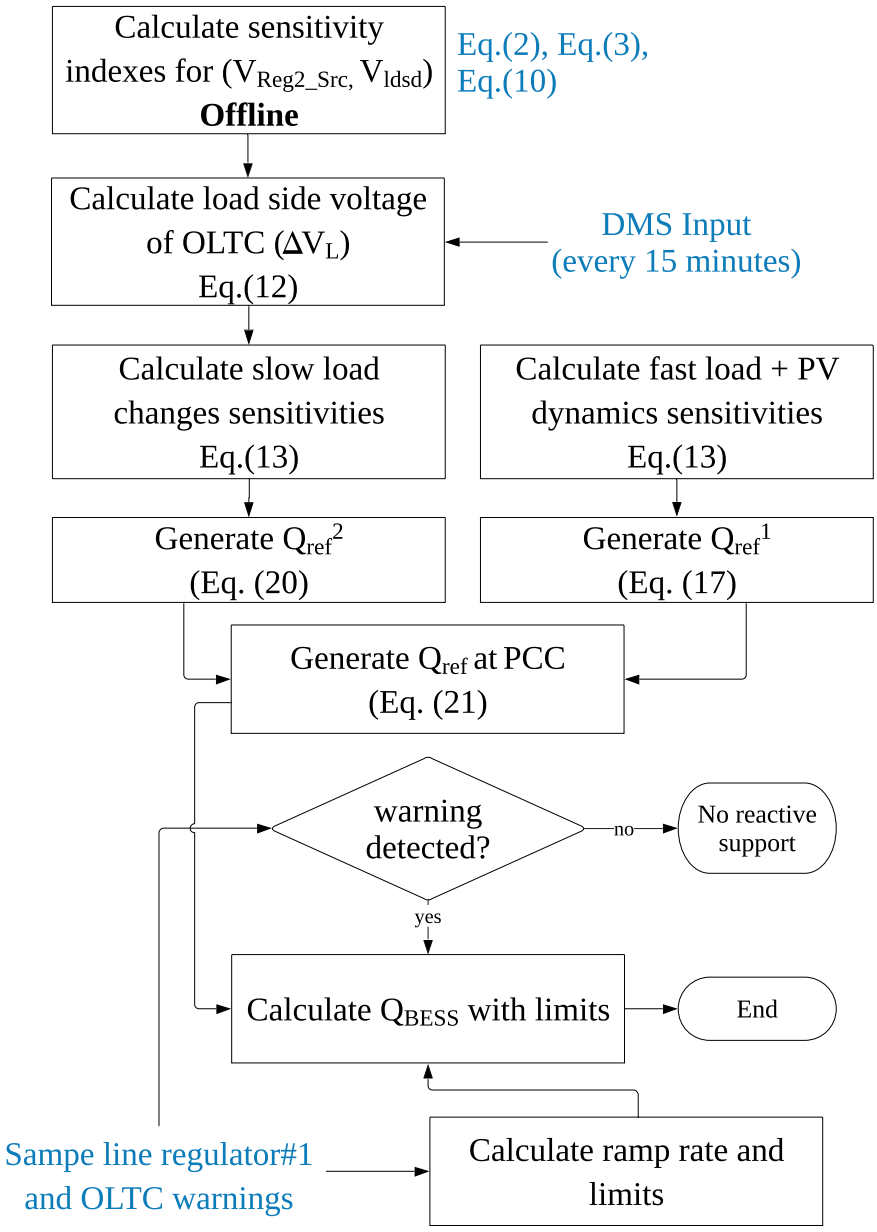

Fig. 6.4. Proposed approach flowchart.

6.4 Simulation Results

Using historical data of a certain feeder from North Carolina, IEEE 8500-node model is used to test the performance of the proposed volt-var control. The proposed sensitivity analysis based volt-var coordination is developed in Python pro-

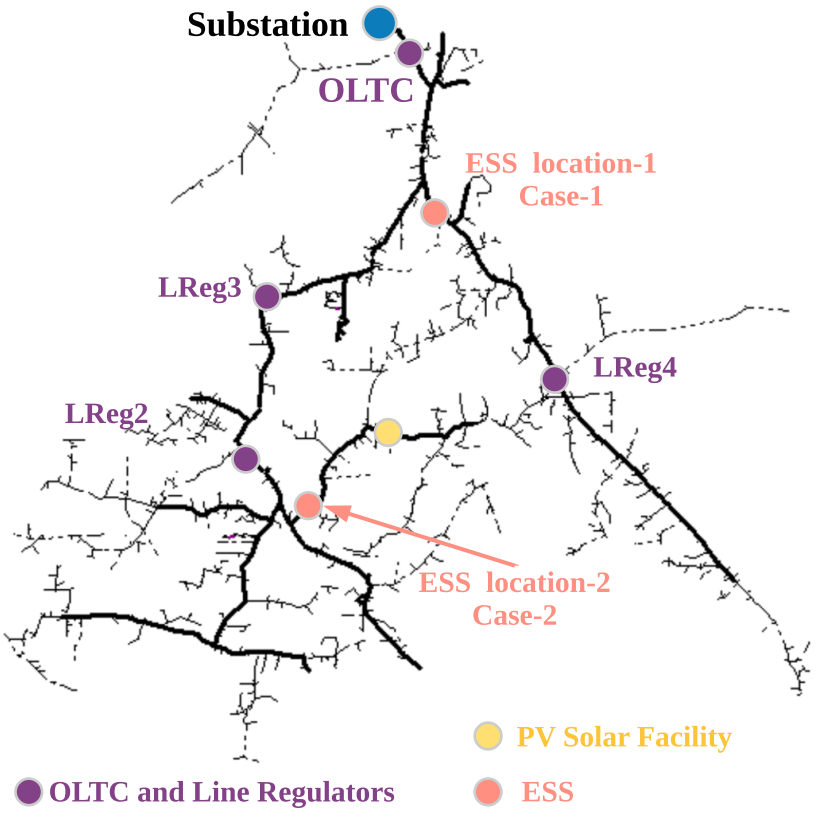

Fig. 6.5. IEEE 8500-Node model used for methodology validation.

gramming language and interfaced with Long-Term Dynamics (LTD) simulations through CYME platform. The advantage of using CYME for such study is that the feeder is represented in more details as far as load spots, line regulators locations, capacitors locations, and finally all lines parameters. Therefore, outcome results are quite realistic and most similar to what would happen in a real feeder circumstance. It is worth mentioning that communication time delay between PI server and the energy storage management system (SMS) is insignificant enough ($<$ 1s) to cause conflict between SMS reactive power set-points and regulators operation times after

warnings have already been issued. The controller generates reactive power set points every 5 seconds, whereas voltage regulators take 45 seconds to change the tap positions. Therefore, as far as implementation is considered, the communication delay is not expected to be a technical issue needing to be addressed. A summer day real data measurements are considered for the performed simulations in this section as shown in Fig. 6.6. This section is mainly analyzing the proposed methodology results as well as comparing the newly developed methodology with the volt-var curve based VVC methodology. Also, the energy storage system's location is being analyzed throughout three different locations; close to the substation, in the middle of the feeder, and at the furthest end of the feeder. Also, an additional case is added to analyze the contribution of the active power voltage changes that reactive power could possibly mitigate. For each case to be studied, four scenarios are plotted against each other; base case (no control), only volt-var curve control, sensitivity analysis based control without ramp rate control on reactive power reference points, and sensitivity analysis based control with ramp rate control. Results are evaluated based on a number of saved taps operations as well as the voltage profiles improvement comparing the base case with each control case. Figure. 6.6 shows system feeder load for a summer day used in methodology validation. Also, PV solar photovoltaic active power profile is depicted in Figure. 6.7

6.4.1 OLTC Load Side Voltage Analysis

In order to present more conclusive results for the proposed methodology, each subsection discusses certain location/feeder equipment for all performed cases and

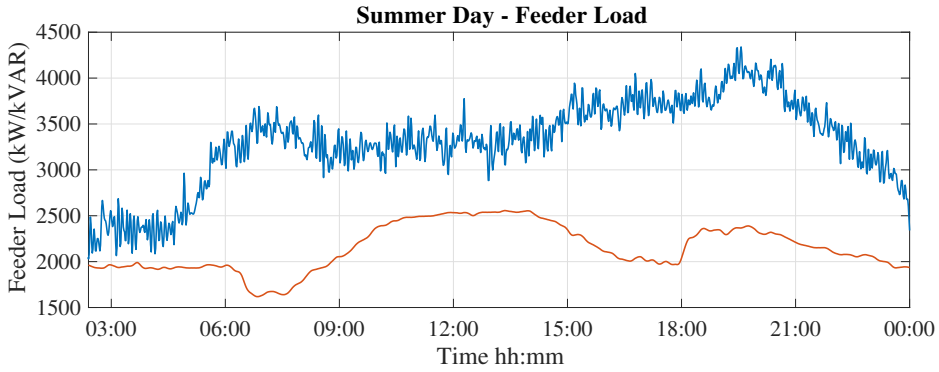

Fig. 6.6. Feeder load - Summer day.

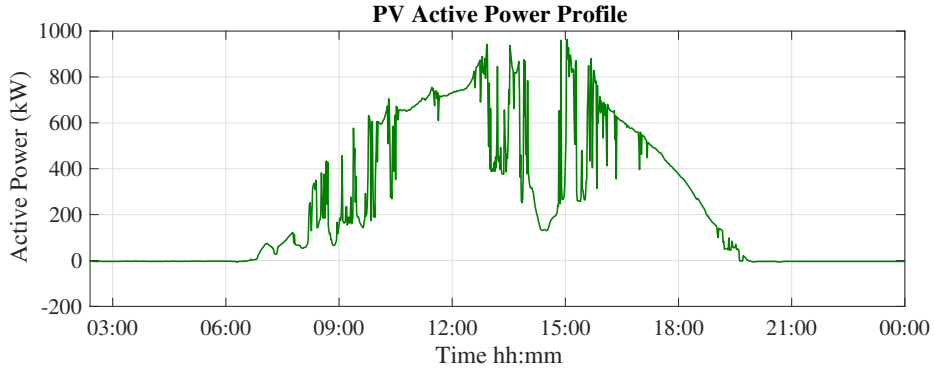

Fig. 6.7. PV active power profile.

scenarios. This subsection presents the OLTC load side location's voltage improvement and reactive power quantities for all cases. Figure. 6.8. shows OLTC load side voltage $V_{oltc-ld}$ for four cases/four scenarios. It is quite noticeably observed that $V_{oltc-ld}$ is better controlled and maintained at a constant targeted level (1.015 p.u.) by the improved sensitivity analysis based volt vat control methodology. However, results for case 2 shows more accurate control of average targeted voltage which is (1.015 p.u.) as shown in Figure. 6.8.(b). Even though volt var curve based methodology seems to improve voltage profiles in most cases, the voltage profile tends to have swings following swings due to load changes. This is due to volt-var curves are equa-

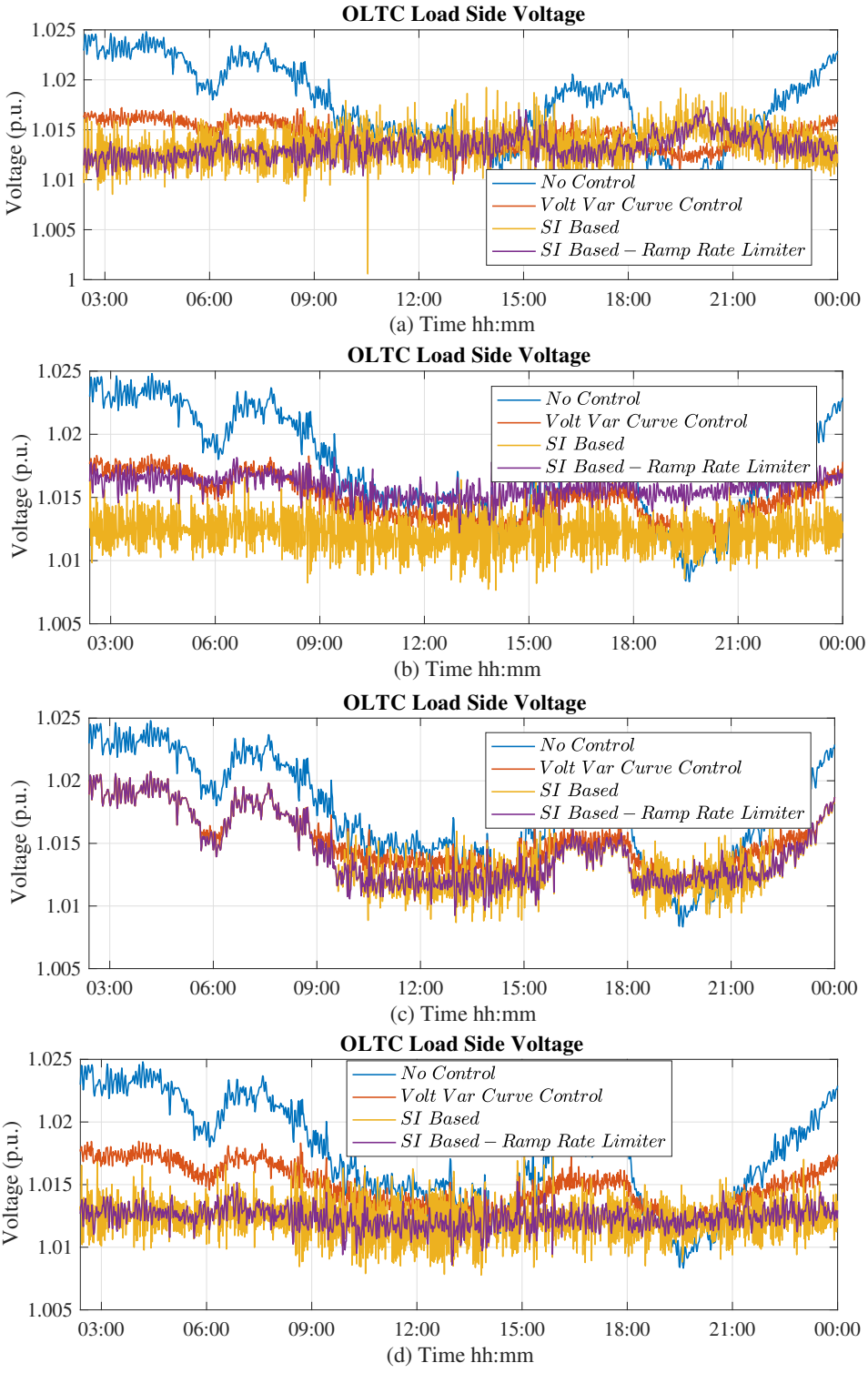

Fig. 6.8. OLTC load side voltage for four scenarios; base case, volt-var curve control based and sensitivity analysis based control without and with reference point ramp rate control.(a) Case-1; (b) Case-2; (c)Case-3. (d)Case-4

tion oriented rather than being targeted oriented. It is also clear that the farther the energy storage unit is from the substation, the less the volt-var curve based methodology could control $V_{oltc-ld}$. Furthermore, Figure. 6.9. shows OLTC taps operations for Phase-C where taps positions were fixed at (-5). This is due to having a constant voltage source from the substation side, therefore OLTC taps positions tend to be quite stable throughout the simulation duration.

6.4.2 Line Regulator-2 Source Side Voltage Analysis

In this section, line regulator2 source side voltage $V_{lreg2-src}$ is analyzed. As shown in Figure. 6.10.(b) and Figure 6.10.(d), $V_{lreg2-src}$ is better controlled due to being placed in the middle of the feeder. It was more achievable for the energy storage converter system to control this location whether it is placed in the middle of the feeder or at the end of the feeder. Additionally, Table. 6.1 presents a conclusive summary for the number of taps operations for LReg2. It is observed that line regulator 2 taps operations has the least number of taps operations - 2 taps - during case-1 whether with or without ramp rate limiter applied. Nevertheless, other cases seem to run within the same average of number of taps.

Table 6.1
Number of taps operations for line regulator 2.

LReg2 Taps Operations				
-	Case-1	Case-2	Case-3	Case-4
Base Case	15	15	15	15
Volt Var Curve	9	4	4	4
Sensitivity Index Based	2	6	3	6
SI with Ramp Rate Limiter	2	5	5	6

6.4.3 Line Regulator-3 Source Side Voltage Analysis

Similarly, line regulator3 source side voltage $V_{lreg3-src}$ shows similar results compared to $V_{lreg2-src}$ as shown in Figure. 6.14. Furthermore, Table. 6.2 shows minimal taps operations that could possible takes place during with SI based control with ramp rate limiter applied.

Table 6.2
Number of taps operations for line regulator 2.

LReg3 Taps Operations				
-	Case-1	Case-2	Case-3	Case-4
Base Case	10	10	10	10
Volt Var Curve	6	5	5	5
Sensitivity Index Based	5	6	5	6
SI with Ramp Rate Limiter	5	4	6	7

6.4.4 Reactive Power and Voltage Correlation

This subsection presents the scatter diagram (correlation) between both the voltage and reactive power profile at the locations of interest; source side of line regulator-3 and load side of OLTC. As shown in Fig. 6.18 (a), the V-Q curve for source side of line regulator-3 for sensitivity analysis based Volt-Var control. The curve is developed based on the simulation measurements which are linearly fit to calculate the estimate of the volt-var curve settings for this case. Fig. 6.18 (b) is, however, showing the V-Q curve for source side of line regulator-3 for sensitivity analysis based Volt-Var control.Similarly, both V-Q curves are depicted for load side voltage of OLTC as per Fig. 6.18 (c), and Fig. 6.18 (d).

6.5 Summary

This chapter presented online sensitivity analysis based Volt-Var control methodology for power distribution networks using system's legacy systems and voltage source converter (VSC) of energy storage systems. First, locations of interests are determined, they are usually OLTC load side voltage and source side voltage for all line regulators due to the availability of measurements at all of these locations. Then, an online sensitivity analysis calculation is performed between reactive power changes at the point of common coupling (PCC) location and voltage changes at these locations. The proposed methodology then aims to maintain these targeted locations at a tentative constant value (1 p.u.) such that voltages violations are mitigated as well as unwanted taps operations are less likely to occur. Furthermore, maintaining the OLTC load side voltage at a narrow band of changes proves the ability of the proposed algorithm to better coordinate with the distribution management system (DMS).

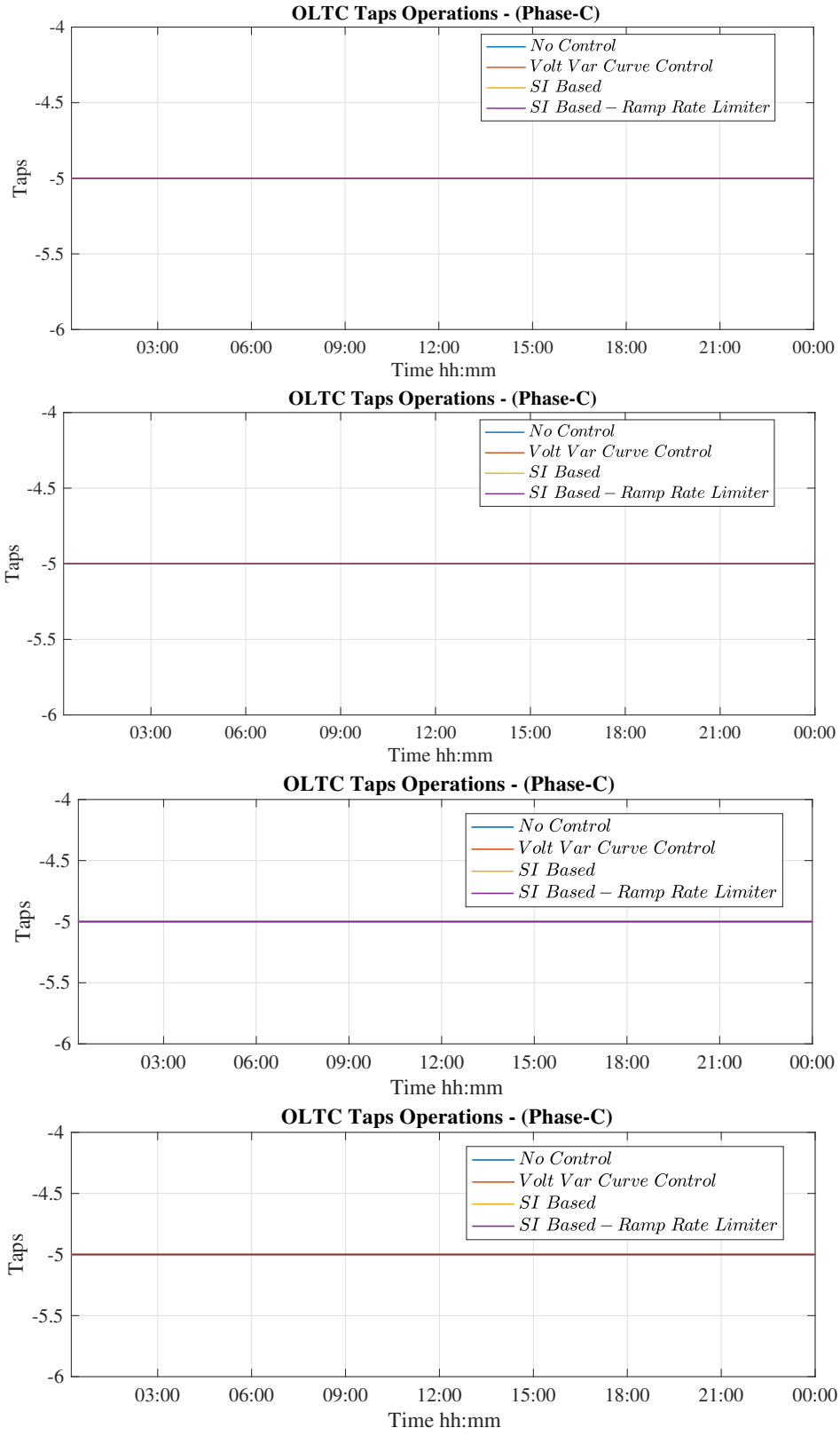

Fig. 6.9. OLTC taps operations for four cases - Phase (C); base case, volt-var curve control based and sensitivity analysis based control without and with reference point ramp rate control.(a) Case-1; (b) Case-2; (c)Case-3. (d)Case-4

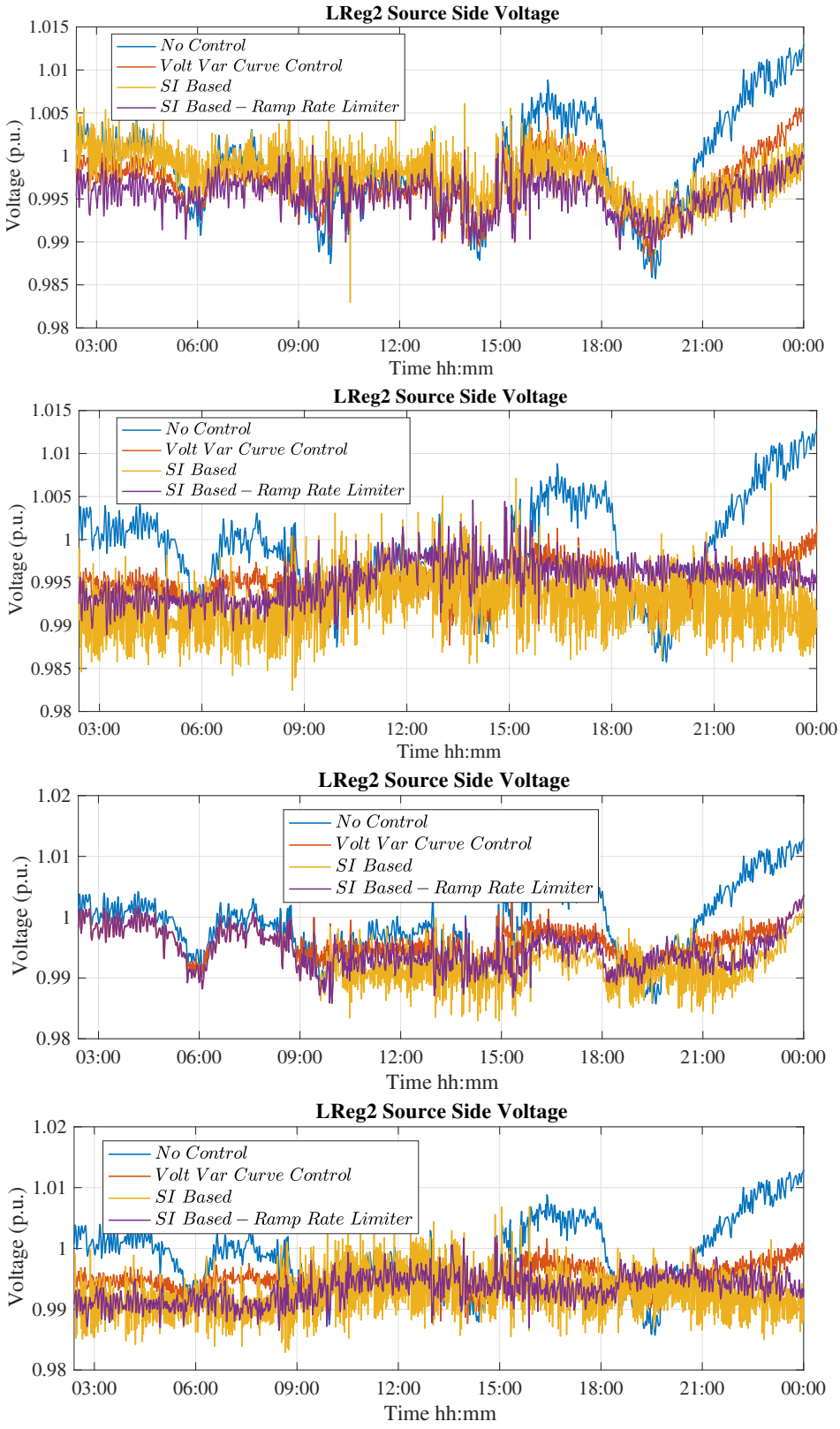

Fig. 6.10. LReg2 source side voltage for four scenarios; base case, volt-var curve control based and sensitivity analysis based control without and with reference point ramp rate control.(a) Case-1; (b) Case-2; (c)Case-3. (d)Case-4

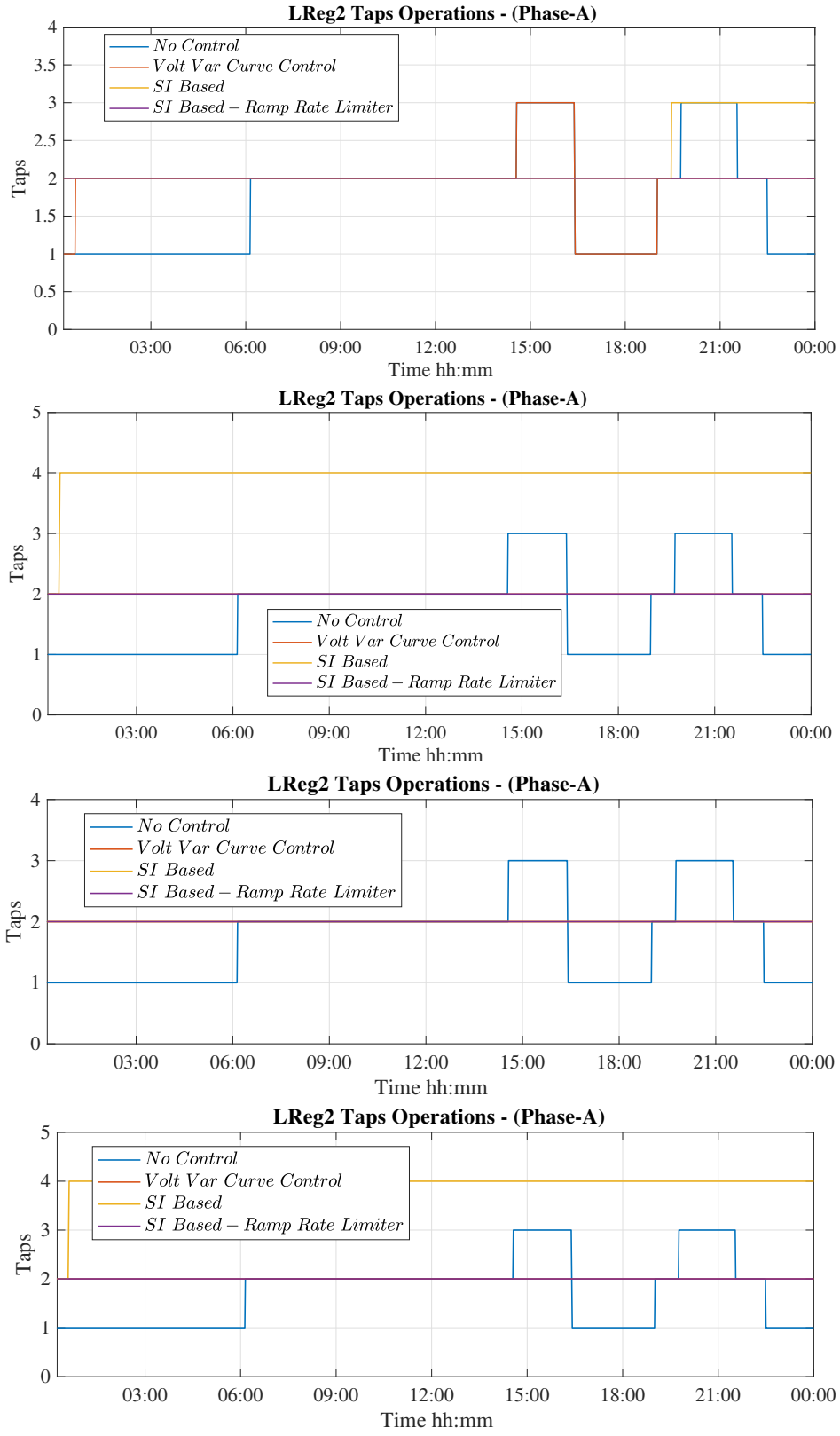

Fig. 6.11. LReg2 taps operations for four cases - Phase (A); base case, volt-var curve control based and sensitivity analysis based control without and with reference point ramp rate control.(a) Case-1; (b) Case-2; (c)Case-3. (d)Case-4

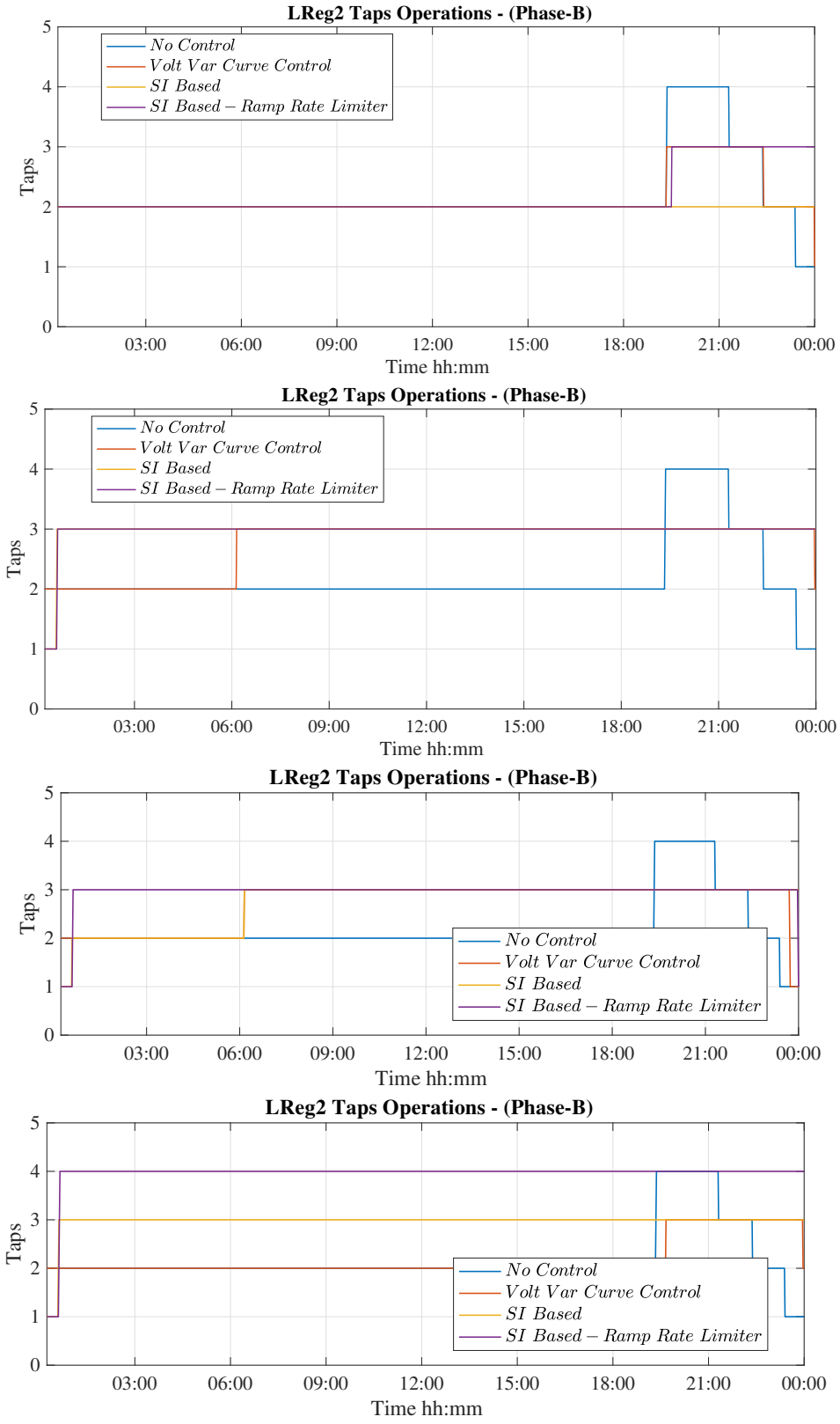

Fig. 6.12. LReg2 taps operations for four cases - Phase (B); base case, volt-var curve control based and sensitivity analysis based control without and with reference point ramp rate control.(a) Case-1; (b) Case-2; (c)Case-3. (d)Case-4

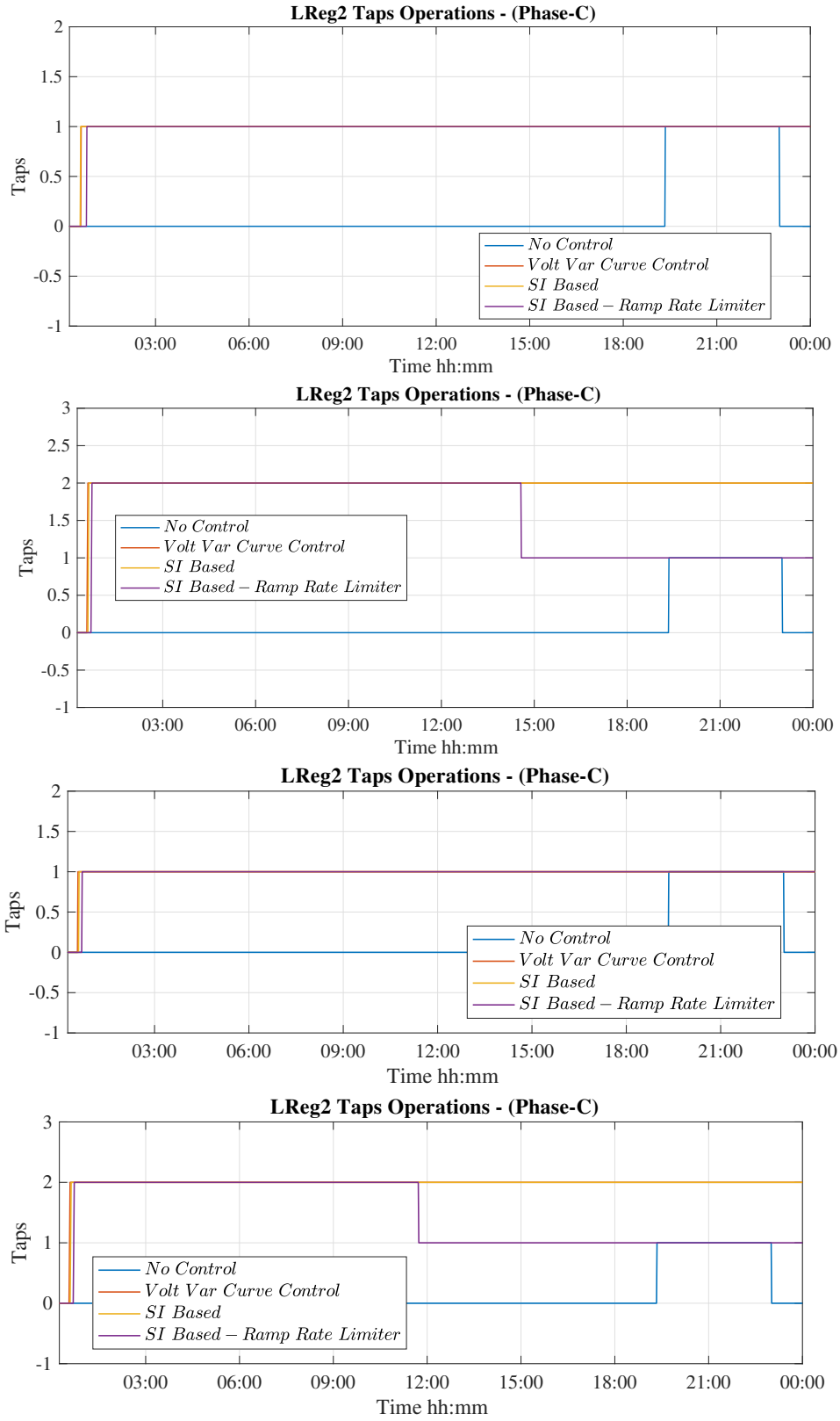

Fig. 6.13. LReg2 taps operations for four cases - Phase (C); base case, volt-var curve control based and sensitivity analysis based control without and with reference point ramp rate control.(a) Case-1; (b) Case-2; (c)Case-3. (d)Case-4

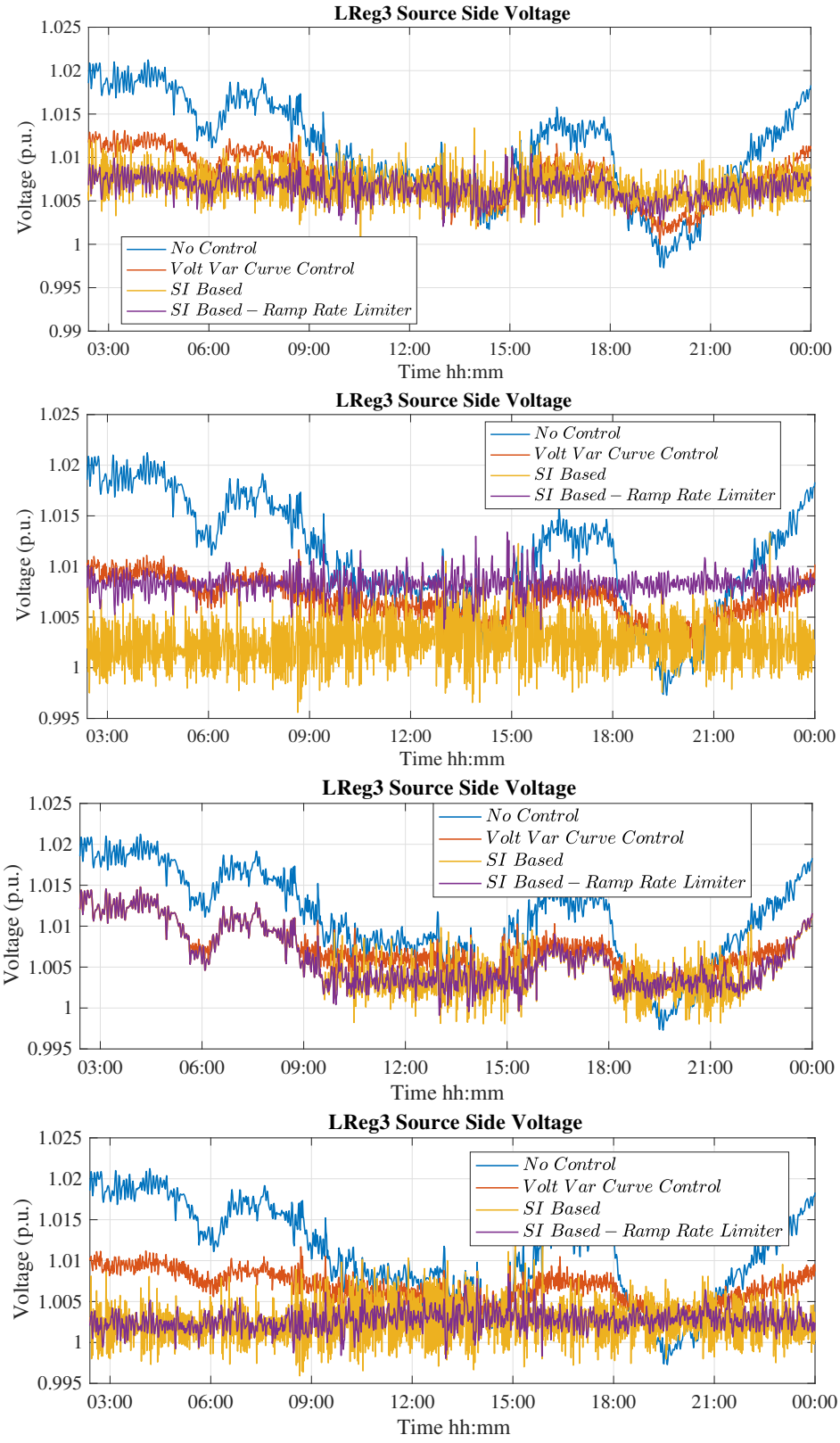

Fig. 6.14. LReg3 source side voltage for four scenarios; base case, volt-var curve control based and sensitivity analysis based control without and with reference point ramp rate control.(a) Case-1; (b) Case-2; (c)Case-3. (d)Case-4

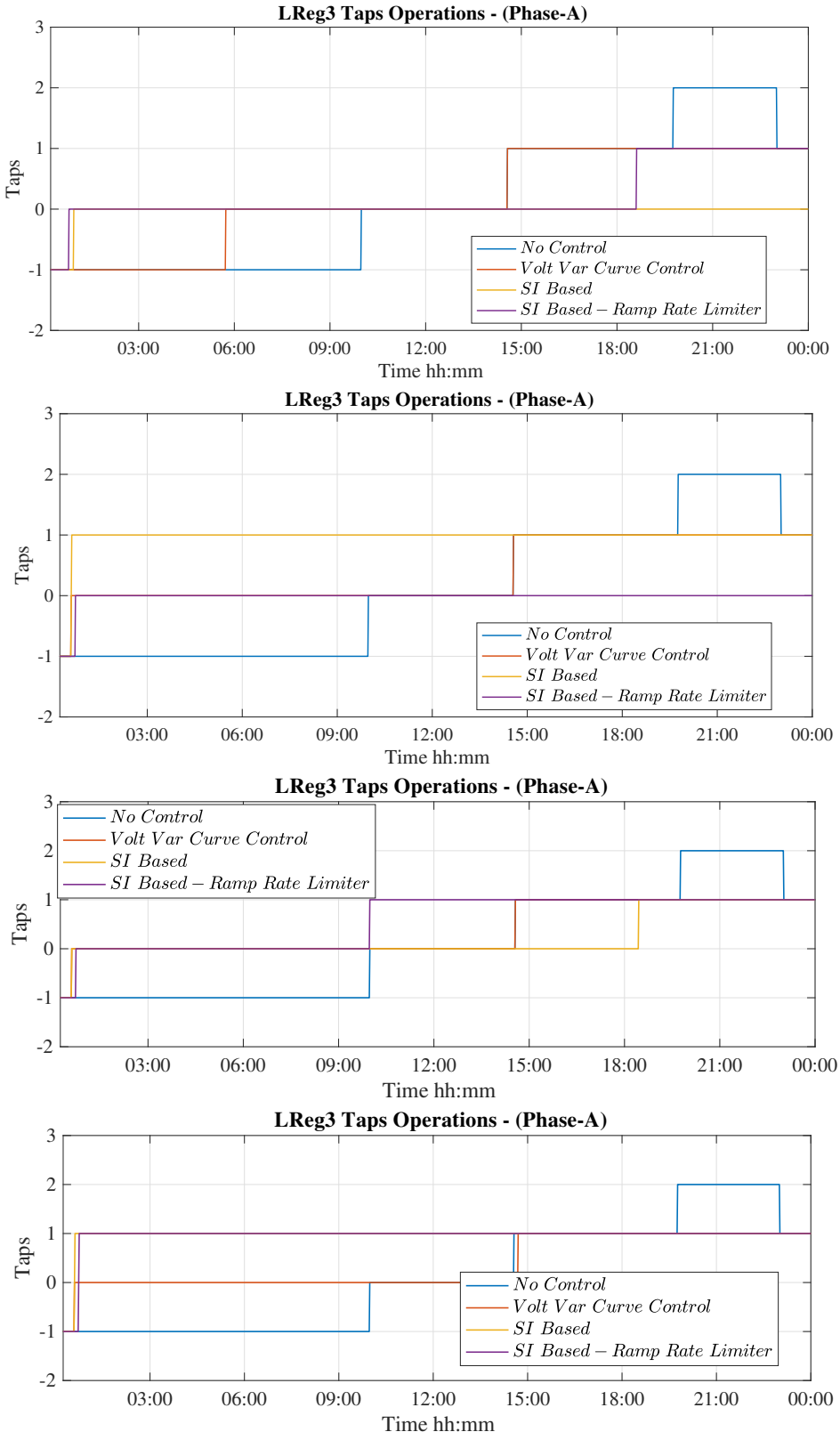

Fig. 6.15. LReg3 taps operations for four cases - Phase (C); base case, volt-var curve control based and sensitivity analysis based control without and with reference point ramp rate control.(a) Case-1; (b) Case-2; (c)Case-3. (d)Case-4

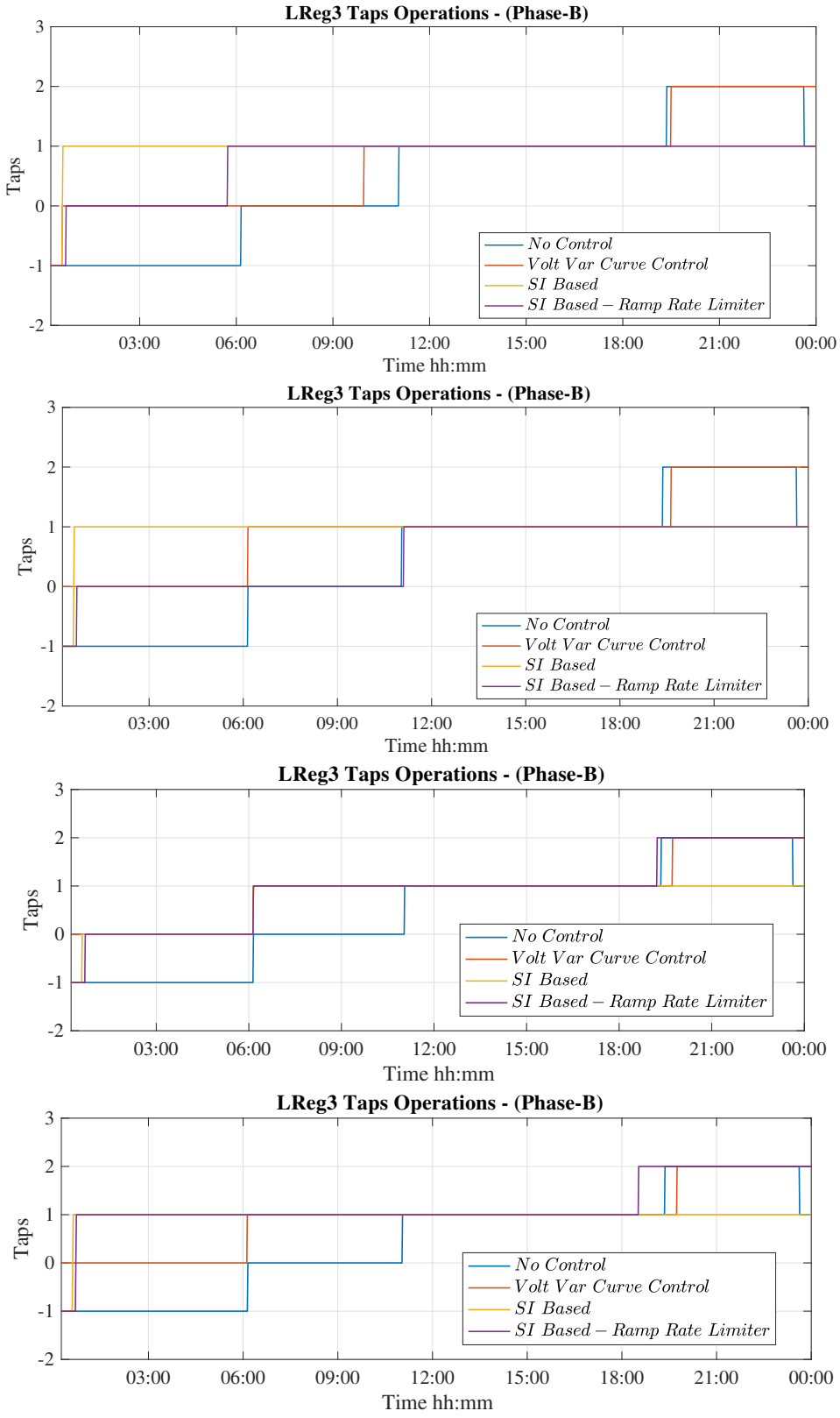

Fig. 6.16. LReg3 taps operations for four cases - Phase (C); base case, volt-var curve control based and sensitivity analysis based control without and with reference point ramp rate control.(a) Case-1; (b) Case-2; (c)Case-3. (d)Case-4

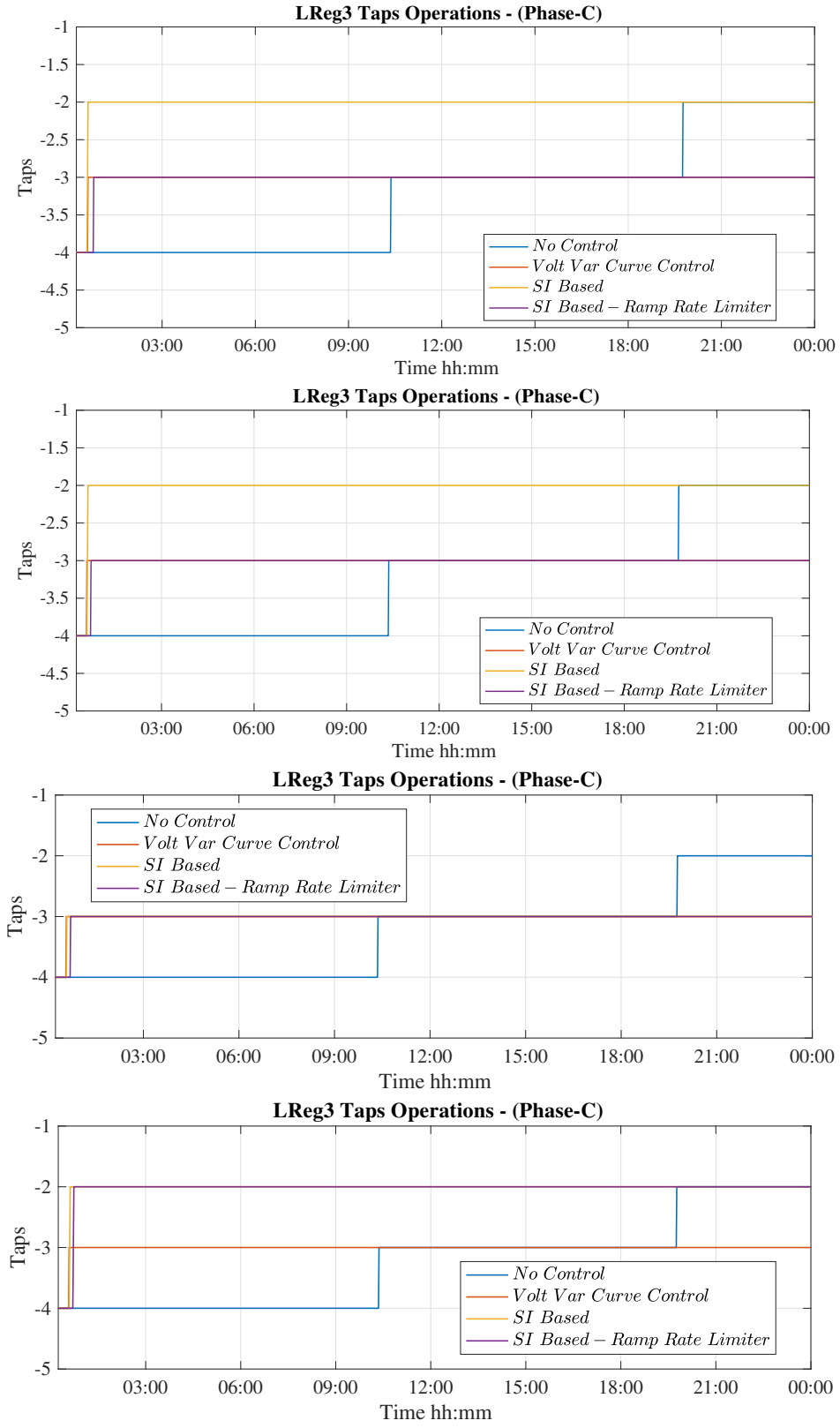

Fig. 6.17. LReg3 taps operations for four cases - Phase (C); base case, volt-var curve control based and sensitivity analysis based control without and with reference point ramp rate control. (a) Case-1; (b) Case-2; (c) Case-3. (d) Case-4

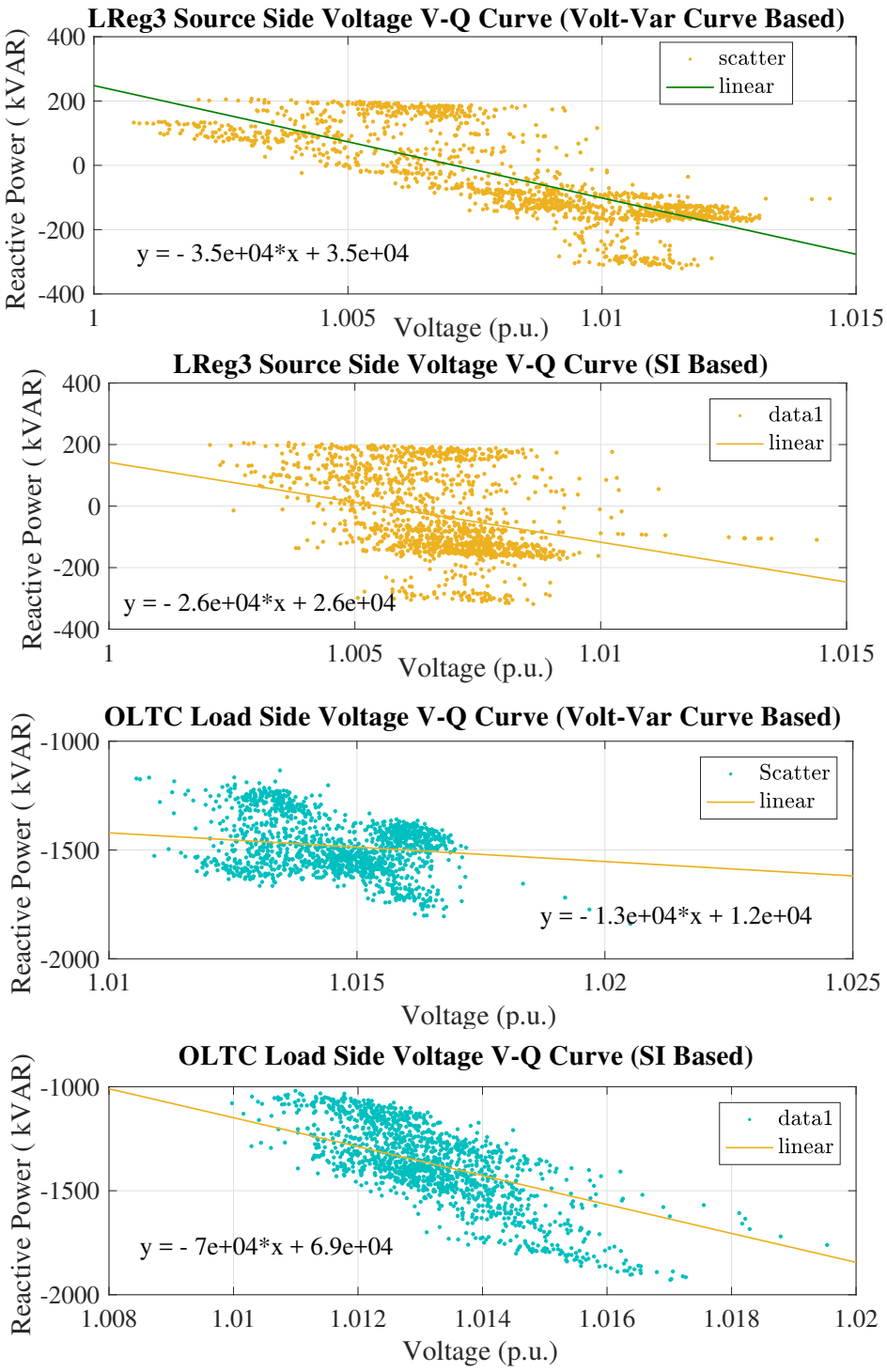

Fig. 6.18. V-Q Scatter for both source side voltage of line regulator-3 and load side voltage of OLTC. (a) LReg3 source side V-Q (Volt-Var Curve Based); (b) LReg3 source side V-Q (Sensitivity Analysis Based); (c) OLTC load side (Volt-Var Curve Based). (d) OLTC load side V-Q (Sensitivity Analysis Based)

CHAPTER 7: COORDINATED VOLT-VAR-WATT CONTROL (VVWC) APPROACH FOR ACTIVE POWER DISTRIBUTION SYSTEM CONSIDERING FEEDER LEVEL PEAK LOAD

Active and reactive power management became essential parts of each power distribution networks with high PV penetration level. Depending upon each network's scale and voltage level, R/X ratio tends to be changeable between different types of feeders. So, either Volt-Var Control (VVC) or Volt-Watt Control (VWC) is in a position of supremacy in some networks, or both would have an equal contribution in voltage regulation application in other networks. Nevertheless, active power management is imperative ancillary service due to the severe and fast fluctuations in PV output power. This chapter presents multi-objective optimization Volt-Var-Watt Control (VVWC). The main goal is to evaluate the contribution of each individual control methodology, as well as the outcome of incorporating both controls.

7.1 Introduction

Authors in [101], and [85] proposed performance assessment for the smart inverter volt-var and volt-watt function in power distribution network. The main goal is to avoid PV active power curtailment as a solution to mitigate the over-voltage due to high PV penetration levels. Results show that volt-var is more efficient in regulating the voltage limits when X/R is high, however in cases with lower X/R ration. Also, this research uses volt-watt control as a function of PV inverter in the form of active

power curtailment. Also, [25] presents an instability study between volt-watt and volt-var for PV inverters when volt-var is sought to interfere to reduce voltage profile due to high penetration level. Recently, authors in [52] used established active power linear voltage sensitivities to curtail for PV inverter for power curtailment to mitigate over-voltage. Nevertheless, in regards to volt-var-watt control, power curtailment is mainly used to mitigate over-voltage due to high PV penetration level. Also, reference [24] presented voltage stability for grid-connected inverter using volt-var and volt-watt control. It was concluded that more vulnerability is added to the system by having both volt-var and volt-watt functions in operations and volt-watt is taking precedence over volt-var. Nevertheless, over-voltage mitigation is not addressed in the literature by active and reactive power management of energy storage units located at local net-load locations of power distribution networks. This chapter presents a multi-objective optimization approach to evaluate utilizing both sensitivity analysis based volt-var control as well as error minimization based local net-load control. The contribution of this chapter is it controls the system's duck curve at high PV penetration level while in the meantime it mitigates over-voltage. The main purpose of incorporating sensitivity analysis based VVC is not only to regulate the voltage profiles at certain targeted values but also prevent the risk of over-generation and steep ramp rate on conventional generation units. This chapter is organized as follows: Section 7.2. explains the details of the proposed methodology. Section 7.3. discusses test feeder used in the performed case study. Section 7.4. discusses the simulation results for five potential scenarios which elaborate in methodology evaluation, and section 7.5. summarizes the results and conclusions.

7.2 The Proposed Methodology

This section discusses the both active and reactive power management parts of the proposed methodology and the impacts on reactive power management due to PQ-Curves limitations of voltage source converters.

7.2.1 Net-Load Active Power Management

This section presents the details of the active power management part in the proposed methodology. First, Fast Fourier Transform (FFT) is applied to historical net-load profiles at certain PV penetration level. Then, these frequency components are multiplied by active power and energy-related parameters 7.2-7.8.

$$P_{NLHist.} = average(P_{NL1}, P_{NL2}, P_{NL3}, ..., P_{NL7}) \tag{7.1}$$

$$FFT(f(k)) = F(\omega) = \int_{-\infty}^{\infty} f(t)e^{j\omega}dx \tag{7.2}$$

$$\alpha = (P_{NL\ pk-pk} - P_{ESS})/(P_{NLpk-pk}) \tag{7.3}$$

$$e_2 = (E_2 - E_{ESS}) \tag{7.4}$$

$$\beta = e_2 * T_2 \tag{7.5}$$

$$P_{NL.Ref}(\omega) = \alpha * P_{NL}(\omega) \tag{7.6}$$

$$IFFT(F(\omega)) = \frac{1}{N} conj(FFT(conj(F(\omega)))) \tag{7.7}$$

$$P'_{NLRef.}(k) = IFFT[P_{NL.Ref}(\omega)] \tag{7.8}$$

$$P_{NLRef.}(k) = P'_{NLRef.}(k) - \beta \tag{7.9}$$

Then, an inverse fast Fourier transform (IFFT) is applied to these frequency components to generate net-load reference curve 7.8-7.9. Given the starting (SoC) and net-load reference curve, least squares minimization based objective function is developed as shown in 7.10 and it aims to calculate the optimal active power set-point for the energy storage unit that maintain both ramp rate as well as SoC within certain limits through set of equality and inequality constraints 7.13-7.16.

$$min\ U = \sum_{k=t}^{t-10}(1/2) * (P_{NL}(k) - m * P_{NLRef.}(k))^2 \tag{7.10}$$

$$P_{NLset-point}(k) = m(k) * P_{NLRef.}(k) \tag{7.11}$$

$$P_{ESSset-point}(k) = P_{NL}(k-1) - P_{NLset-point}(k) \tag{7.12}$$

$$P_{ESSMax.} \geq P_{ESS}(k) \geq P_{ESSmin} \tag{7.13}$$

$$P_{ESS}(k) = P_L(k) - m(k) * P_{NLRef.}(k) - P_{PV}(k) \tag{7.14}$$

$$m(k) \leq \frac{P_{ESSmin} + P_{PV}(k) - P_L(k)}{P_{NLRef.}(k)} \tag{7.15}$$

$$m(k) \geq \frac{P_{ESSmax} + P_{PV}(k) - P_L(k)}{P_{NLRef.}(k)} \tag{7.16}$$

such that Eq. (7.13) is the algebraic inequality constraint for the energy storage system active power capability, and Eq. (7.14)-(7.16) are the inequality constraints for the multiplication factor $m(k)$ that achieves that algebraic constraint through the optimization formulation. The proposed methodology incorporates energy time shift (ETS) application where energy storage unit aims to dispatch the maximum active power capability during the predicted peak load time. Equations (7.17)-(7.18) show integral control for ramp rate threshold value based on the optimal SoC at certain time.

$$e_{SoC}(k) = SoC(k) - SoC_{Target}(k) \tag{7.17}$$

$$\zeta_{SoC} = K_i \int_{k}^{k+t} e_{SoC}\, dk \tag{7.18}$$

7.2.2 Sensitivity Analysis Based Reactive Power Management

This section presents the details of the reactive power management part of the proposed methodology (VVC). The main purpose is to regulate the voltage profile throughout a given distribution network using available measurements. Therefore, source side voltage for line regulators is selected to be locations of interest for the proposed methodology. The main concept of the proposed reactive power management is utilizing reactive power capability of distributed energy storage systems' VSCs to regulate voltage profile based on sensitivity analysis and targeted values rather than volt-var curve settings. Equations (7.19)-(7.20).

$$\Delta Q = (K_{Q_j})^{-1}(\Delta V_j - K_{n_j}\Delta n) \tag{7.19}$$

such that K_{Q_j} is the online sensitivity index between reactive power of VSC and voltage of location of interest, ΔV_j is the step change in voltage at that location, K_{n_j} is the sensitivity index of voltage change due to taps operations changes, and Δn is the number of changed taps per time step.

$$Q^1_{ref}(t) = Q^1_{ref}(t_0) + a * k * \Delta t \tag{7.20}$$

$$Q^2_{ref}(t) = Q^2_{ref}(t_0) + a * k1 * \Delta t \tag{7.21}$$

From ((7.20)) and ((7.21)) the output reactive power from VSCs can be calculated as follows:

$$Q_{BESS}(t) = Q^1_{ref}(t) + Q^2_{ref}(t) \tag{7.22}$$

The main purpose for each VSC is to maintain the source side voltage of the nearest line regulator at 1 p.u. such that the voltage violations are prevented as well as taps operations are avoided.

7.2.3 Active and Reactive Power Capability Limitations

Nevertheless, PQ curves, or capability curves [36] which represent the inverter's operating ranges, are the anticipated limitations to this methodology, especially with voltage source converters operated at high power factor (P.F. = 0.9). Also, since installing oversized VSCs is not the most economical choice, after calculating the active power set-point, maximum reactive power reference point is calculated based on the PQ curve and kVA ratings of the converter system. For example, an inverter with 100 kVA ratings operating at unity power factor (100 kW) has no reactive power

capability at this operating point. However, using an oversized inverter (110kVAR) allows using 45% of reactive power with 100% of active power capacity as discussed in [68]. Therefore, by assuming that active power management is taking precedence

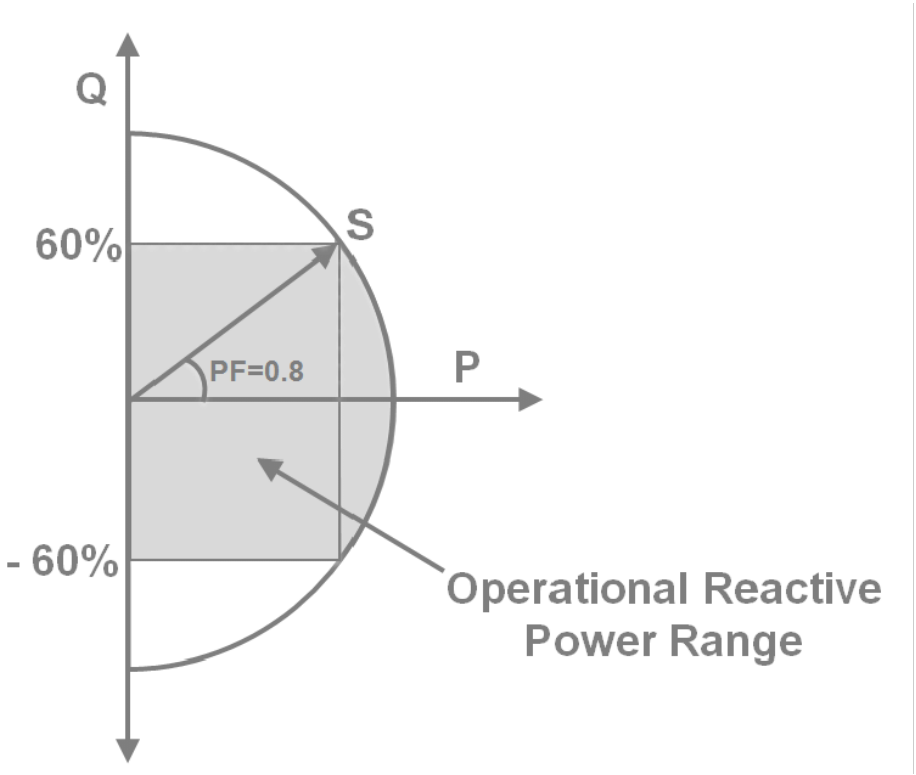

Fig. 7.1. Inverter capacity with reactive power capability range [36].

over reactive power management, reactive power constraints are calculated based on the power triangle of the kVA ratings of the VSC as shown in equations (7.23), (7.24)

$$Q_{max}^2 \leq \sqrt{S^2 - P_{Set}^2} \tag{7.23}$$

$$-Q_{max} \leq Q_{Set} \leq Q_{max} \tag{7.24}$$

such that Q_{max}^2 is the maximum allowed reactive power dispatch from VSC, S is the kVA ratings of the VSC, P_{Set} is the active power set-point from active power control (VWC), and finally Finally, Figure 7.2 shows flowchart of the proposed methodology,

where Q_{Set} is the reactive power set-point for reactive power management (VVC).

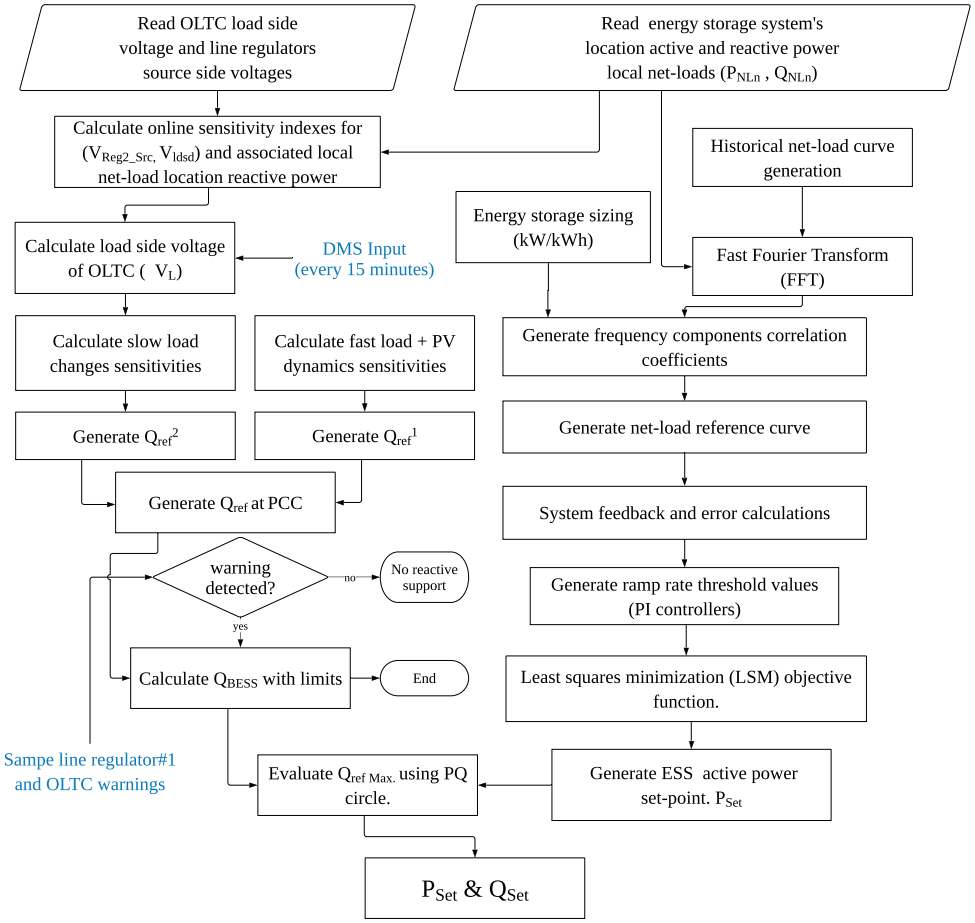

Fig. 7.2. Multi-objective optimization Volt-Var-Watt Control (VVWC) methodology flowchart.

7.3 Test Feeder Model (IEEE 8500-Node)

The test network used for this study is IEEE 8500-node test feeder. This feeder is selected as a more realistic feeder for testing the scalability and showing the methodology contribution to the existing methodologies in the literature. The model is developed in CYME including one online load tap changer (OLTC), three line voltage regulators, nine single phase and one three-phase capacitor. There are three PV units installed throughout the feeder in the downstream part of the three local net-

load locations; NL#1, NL#2, NL#3 where three energy storage units are installed to perform both active and reactive power management. Test network details are shown in Fig.7.3.

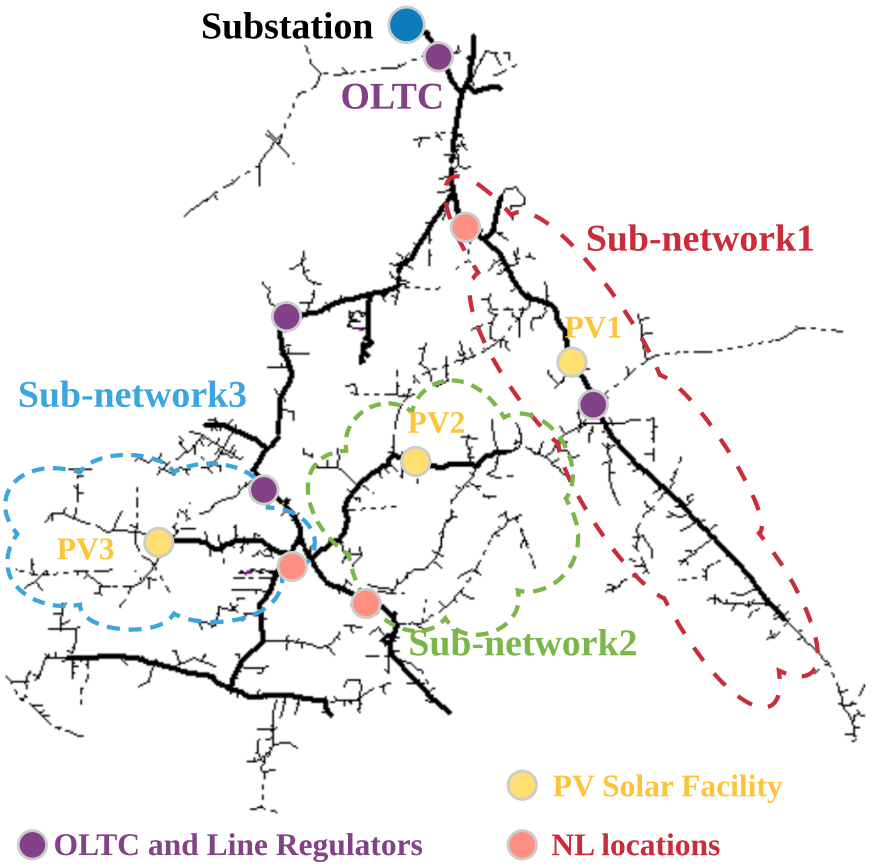

Fig. 7.3. IEEE 8500-Node test feeder

7.4 Simulation Results

This section evaluates the proposed Volt-Var-Watt-Control (VVWC) methodology and the substantial benefits from using either VVC, VWC or VVWC. Evaluation metrics are set as follows: Voltage deviation improvement (VDI): It is defined as percentage maximum voltage deviation of the mean value of the any given voltage

profile as shown in equation (7.27). Net-load ramp rate improvement (RRI): Ramp rate improvement (RRI) is the ratio of each local net-load ramp rate with volt-watt VW control on and without VW control on as shown in equation (7.25). Power losses index (ILP): Power losses index is the ratio between system losses with and without the control is applied as shown in equation (7.26). Besides, system's number of taps operations for OLTC and three voltage regulators are also compared to find out which control architecture contributes more to actions savings Finally, system's over-voltage is analyzed separately to evaluate levels of PV Penetration this given system could operate with.

$$RRI = \frac{RR_{controlled}}{RR_{basecase}} \tag{7.25}$$

$$ILP = \frac{P_{loss}^{controlled}}{P_{loss}^{basecase}} \tag{7.26}$$

$$VDI = \frac{V_{max} - V_{min}}{V_{mean}} \tag{7.27}$$

In this chapter case studies are performed using CYME and sorted into 5 cases:

- Scenario-1: CYME Long-Term Dynamics (LTD) Simulation of the given feeder load without solar PV units or control added.
- Scenario-2: CYME Long-Term Dynamics (LTD) Simulation of the given feeder load with three installed PV units, whereas no is control added.
- Scenario-3: CYME Long-Term Dynamics (LTD) Simulation of the given feeder load with all installed PV units and volt-var (VVC) is applied. In this case,

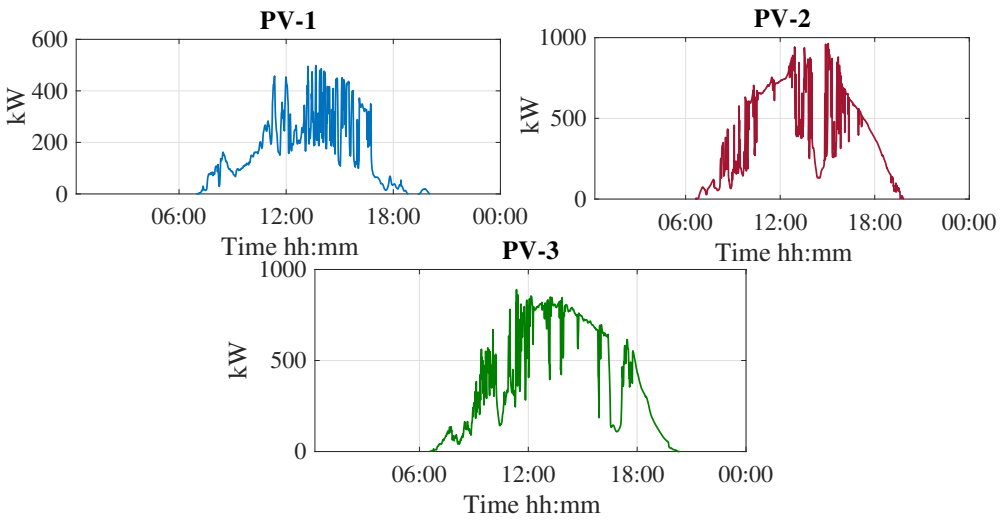

Fig. 7.4. Solar PV profiles for installed three PV facilities in test feeder

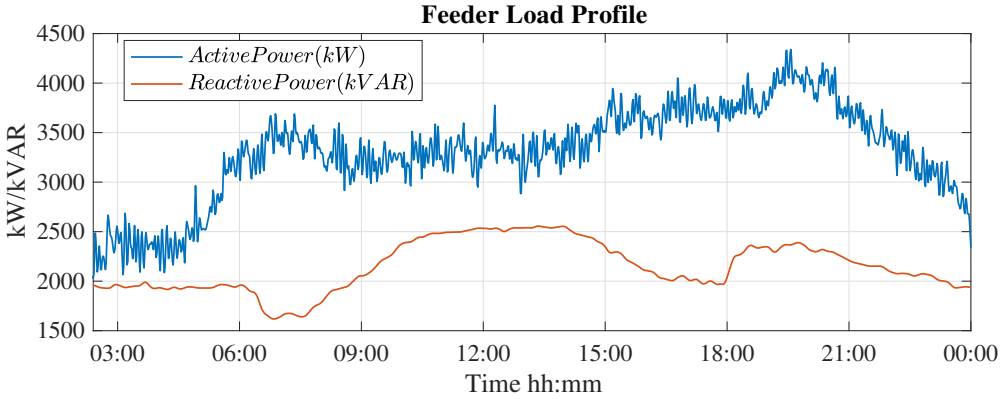

Fig. 7.5. Active and reactive power profiles for feeder load.

each voltage converter system (VCS) at each net-load location aims to regulate source side voltage of the nearest line regulator as well as considering load slow changes at OLTC load side voltage.

- Scenario-4: CYME Long-Term Dynamics (LTD) Simulation of the given feeder load with all installed PV units and volt-watt (VW) control is applied such that each energy storage system aims to smooth and ramp down the steep ramp rate at each local net-load locations.

- Scenario-5: CYME Long-Term Dynamics (LTD) Simulation of the given feeder load with all installed PV units and both VW and VVC are applied. This control scheme is defined as VVWC such that each energy storage system aims to optimally manage both active and reactive power so that all PV penetration effects are mitigated.

7.4.1 Feeder Load and Net-Load Active and Reactive Power Profiles

This section presents feeder load and PV active power profiles used in this case study. It also discusses active power management results for all net-load locations. Figure 7.5 shows active and reactive power profiles for the system's feeder load, whereas Figure 7.4 shows the active power profiles for three PV units used in this study. Also, Figure 7.6 depicts net-load active power profiles with and without active power control. PV penetration is 60% is 3 MW of the total load which is split between NL1, NL2 and NL3 as 1000 kW, 1000 kW and 1000 kW respectively. Similarly, energy storage systems sizing is selected 30% of PV ratings, hence ESS1/ESS2/ESS3 capacities are to be 300 kW/300 kW/300 kW respectively. It is clear in Figure 7.6 that net-loads ramp rate considerably decreased such that RRR_{NL1} is 37.06%, whereas RRR_{NL3} is 34.53%.

7.4.2 OLTC and Line Regulators Source Side Voltages

This section presents voltage analysis for all targeted voltage profiles throughout the feeder under all 5 cases. Figure. 7.9 present source side voltage profile for both line regulator#2 and line regulator#3. There is a significant over-voltage at both locations after adding three solar PV units as well as considerable fast fluctuations

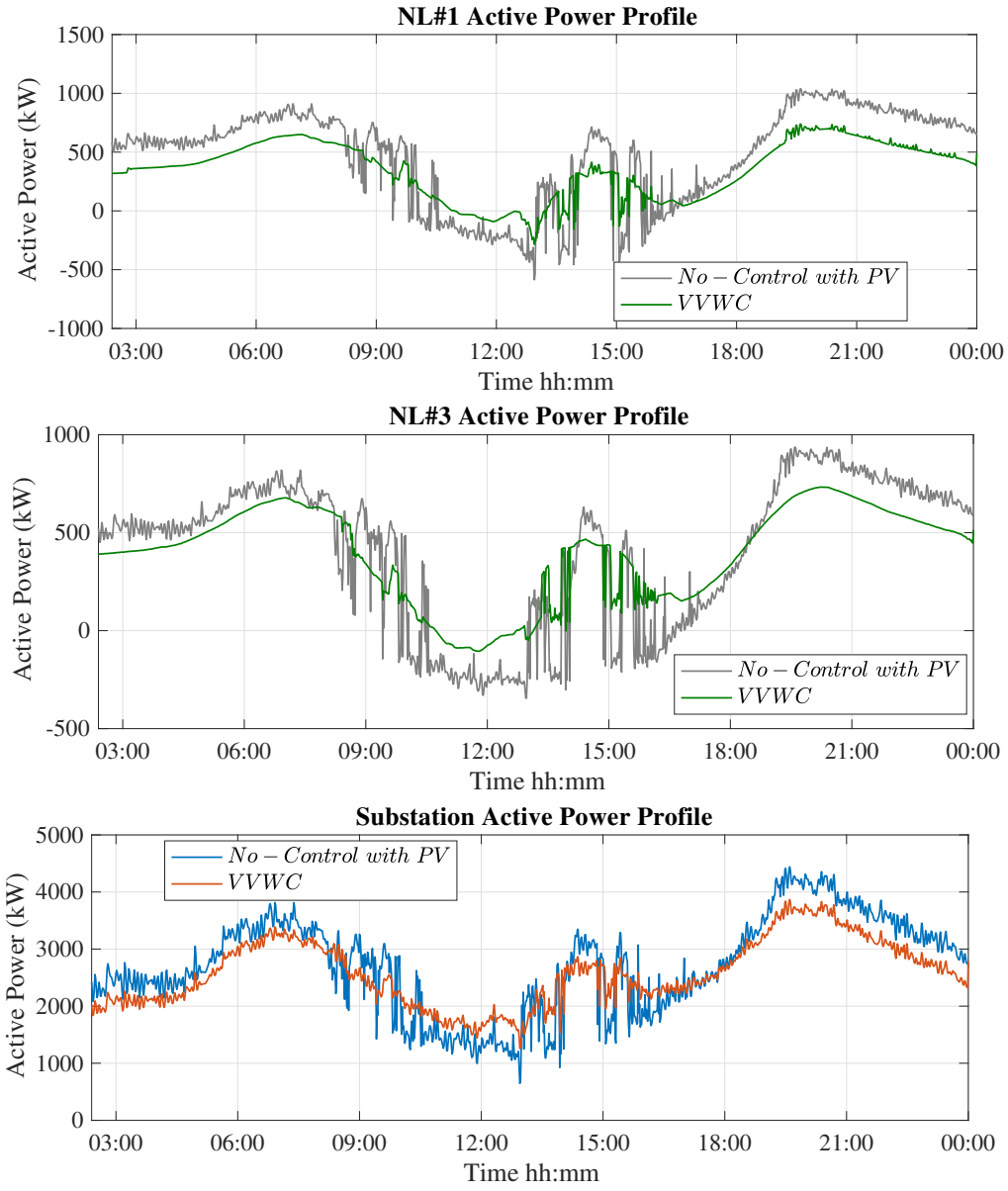

Fig. 7.6. Net-load#1 and Net-load#3 active power profile with and without net-load active powr control;(a) NL1. ; (b) NL3.; (c) Substation

in voltage profile due to active power intermittent of PV output power. Separately, VVC, VWC, and VVWC are used to tackle all above-mentioned active and reactive power issues for the given network due to the high penetration level of PV. Greatly, VVWC is mitigating voltage fluctuations by 45% ($VDI_5 = 0.4567$) of original voltage profile's fluctuations. Even though VWC is able to reduce voltage fast changes,

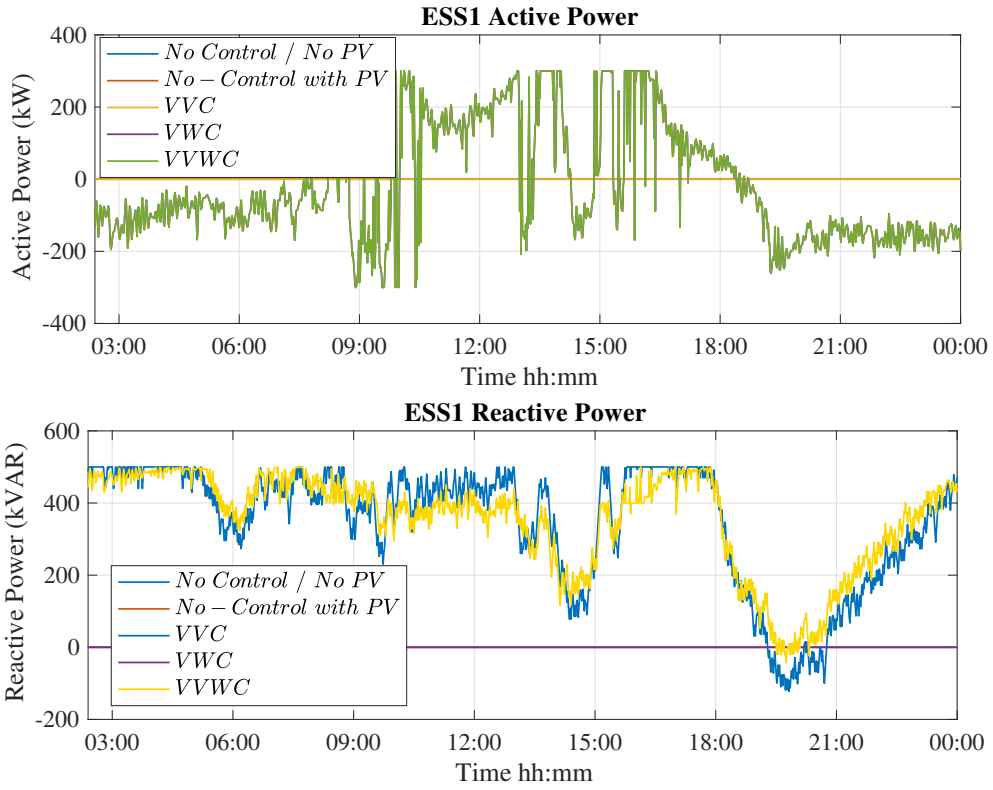

Fig. 7.7. Active and reactive power for energy storage system #1.

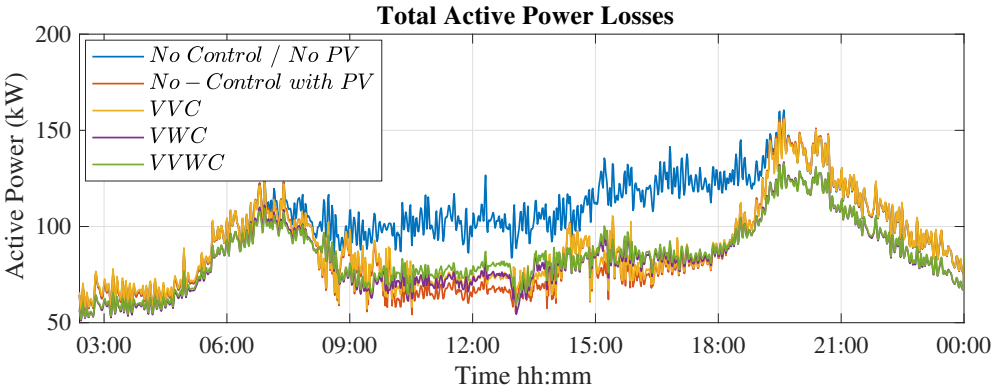

Fig. 7.8. Active power losses.

VVWC presents better regulation for voltage profiles due to reactive power dispatch to limit each location at targeted average value. Also, Figure. 7.11 shows voltage profiles for both net-load#1 and net-load#3 locations. Both locations' are successfully maintained at 1 p.u. to mitigate voltage span of 0.03 p.u. pk-pk. Table. 7.1

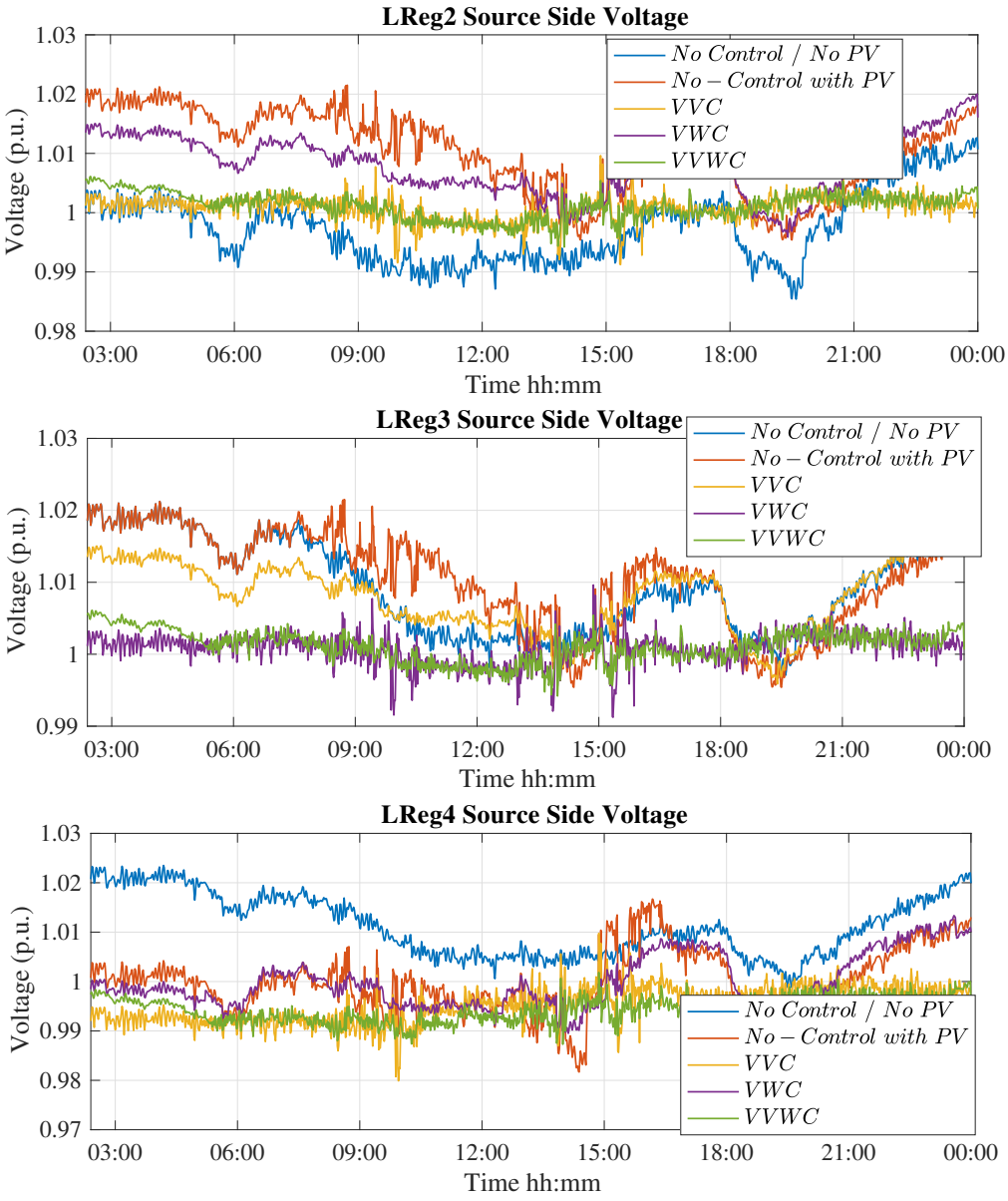

Fig. 7.9. Line regulators source side voltage profiles comparison for all cases;(a) LReg2-Source side voltage ; (b) LReg3-Source side voltage; (c) LReg4-Source side voltage

summarizes all voltage deviation index (VDI) for all cases.

7.4.3 OLTC and Line Regulators Taps Operations

Table 7.2 summarizes number of taps operations for all regulators in the system throughout the 5 scenarios. It could be seen that total number of taps operations

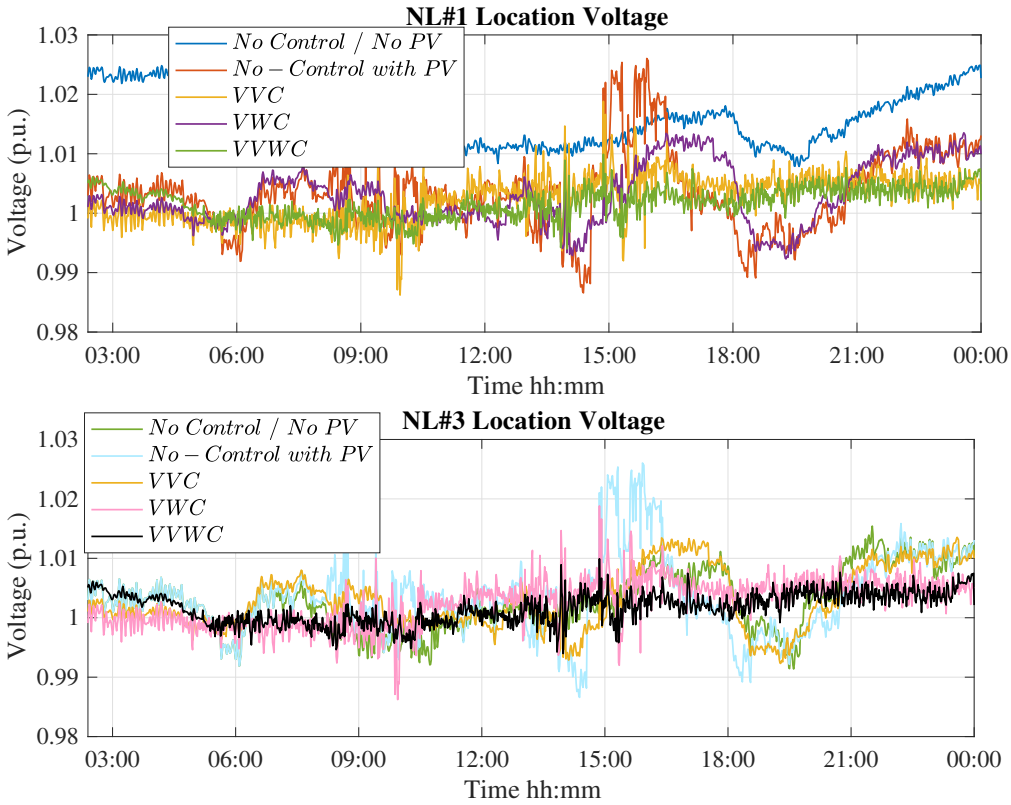

Fig. 7.10. Net-Load locations voltage profiles comparison for all cases;(a) NL1 voltage profile. ; (b) NL3 voltage profile.

Table 7.1
Voltage deviation index for net-load locations and source side locations of line regulators.

VDI (index is considering scenario2 as base case)			
	LReg2_Src	OLTC_Load	NL#1
Scenario3*(VVC)	0.7042	0.9729	0.8264
Scenario4*(VWC)	0.9868	0.6568	0.5381
Scenario5*($VVWC$)	0.4567	0.4202	0.4041

increased from 33 to 49 after adding three PV units. The increase in number of taps operations are due to intermittency and ramp rate of system net-load. However, scenario #4 (VWC) successfully brought these extra actions down to 37. Finally, (VVWC) provided the least number of taps operations for the network where active and reactive power management are bot provided by all storage systems at local net-load locations.

Table 7.2
OLTC and line regulators taps operations.

Taps Operations					
	OLTC	LReg2	LReg3	LReg4	Total
Scenario1	2	9	11	11	33
Scenario2	6	19	16	8	49
Scenario3 (VVC)	0	2	10	8	20
Scenario4 (VWC)	6	5	14	12	37
Scenario5 (VVWC)	0	2	9	8	19

7.4.4 Ramp Rate Improvement (RRI) and Power Losses Improvement (ILP)

Reference [3], [75] discussed the characteristics of conventional generation step response. As it is concluded, gas turbines based generation units have the fastest time response. Even though gas turbines seem to be the most available solutions to compensate for fast ramp rate changes due to duck curve ramp rate, it inversely impacts the efficiency of the generation unit to run at less than it's full potential output. As shown in Fig. 7.6, local net-load locations encountered noticeable improvement in both ramp rate decrease as well as fast changes smoothing. Also, Table. 7.3 shows ramp rate improvement for the following; NL#1, NL#3 and network substation (network's net-load profile). Total ramp rate at the substation location is decreased by 44%. Quantitatively, under the given assumptions of PV/energy storage units sizing, net-load ramp rate is successfully brought down from 52.5 kW/minute to 16.1 kW/minute. On larger scaled power distribution networks, this ramp rate improvement relieves gas-fired generation units from running less efficiently while energy storage units are best managed to cover ramp rate changes. On the other hand, the proposed methodology provided significant saving in active and reactive power losses.

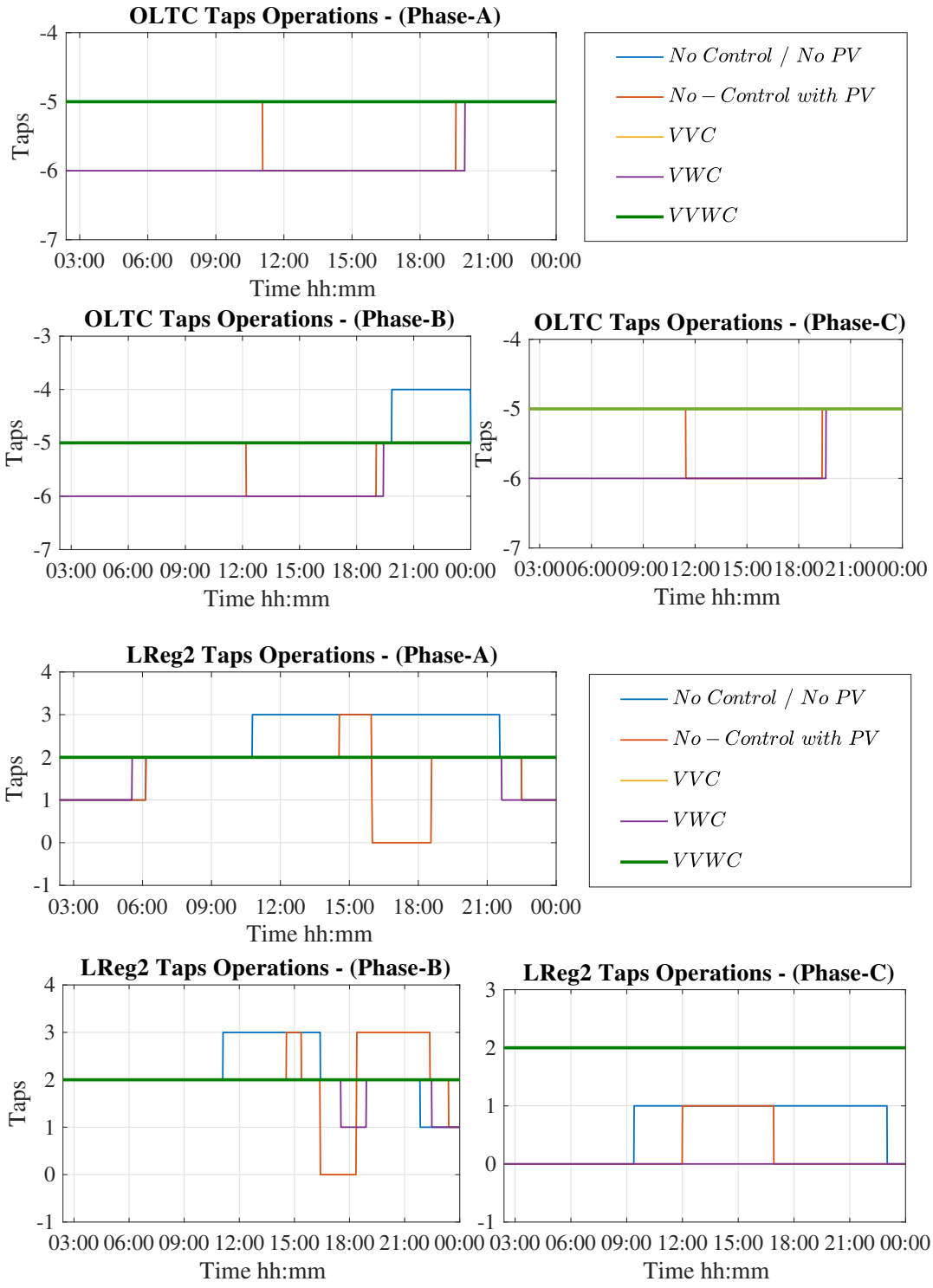

Fig. 7.11. OLTC and line regulator#2 taps operations for all scenarios.; (a) OLTC.; (b) LReg2.

Table 7.3
OLTC and line regulators taps operations.

NL Location	Ramp Rate Improvement (RRI)
NL1	42.2%
NL1	52%
Substation	44%

Table. 7.4 presented the percentage of saved system losses for each control case compared with scenario-2 (No control with PV profile). Energy losses are greatly reduced by (4.5%) for scenario-4, whereas it is reduced the most by (3%) for scenario-5.

Table 7.4
Power losses improvement (ILP) for control scenarios compared with scenario-2.

Scenario	Power losses improvement (ILP)
scenario 3	101.89%
scenario 4	95.46%
scenario 5	97.01%

7.5 Summary

This chapter presented a novel active and reactive power management (Volt-Var-Watt control) methodology. The methodology utilizes voltage source converters (VSC) at local net-load locations in power distribution networks to generate active and reactive power set-points to manage system net-load ramp rate, over-voltage and risk of overgeneration at high PV penetration level. The volt-var control calculates online sensitivity indexes to aid maintaining the nearest source side voltage of each line regulator at a tentative constant value (1 p.u.) not only to minimize line regulator's taps actions but also to mitigate over-voltage risk due to PV penetration level. The active power management part of the proposed methodology incorporates FFT based local net-load reference curves to meet with energy storage system active power

capability. Further, it develops least squares minimization based objective function to control fast swings as well as local net-loads ramp rate through a set of equality and inequality constraints. The optimization problems constraints are state of charge driven constraints when both state of charge and ramp rate are co-dependent. Results showed a high level of voltage regulation throughout the tested feeder where the voltage was kept within 1 p.u. and over-voltage due to installing PV farms were mitigated. Also, the total number of taps operations were best minimized by considering both active and reactive power management. Finally, the total system's net-load ramp rate was successfully decreased by 50% which allows energy storage units to pitch in "Duck Curve" solutions instead of having gas-fired generation units as a first solution to this phenomenon.

CHAPTER 8: CONCLUSIONS AND FUTURE WORK

8.1 Concluding Remarks

In this dissertation, new approaches to active power and reactive power management were presented. The proposed algorithms addressed properly locating energy storage units not only to control renewable energy active power swings but also to control large-scale power distribution network net-load profile and thus the so called "Duck Curve." Further, the proposed approaches utilized historical dataset and time series transformation techniques (FFT) to generate reference curves for each local net-load location. All control objectives and constraints were developed using the least squares error minimization technique. The effectiveness of the methodology was verified using large-system IEEE 8500-Node system. The proposed active power management approaches were developed in Python and tested through Long-Term Dynamic (LTD) simulation on the CYME platform.

Moreover, this dissertation presented integrated feeder peak load management based on active load prediction using weather forecasting. The proposed load prediction approach incorporated feeder load decomposition such that all load components and different behaviors were predicted separately. Also, the proposed load prediction methodology was tested and temporarily implemented on an existing energy storage controller at distribution feeder. The methodology was developed using JAVA pro-

gramming. The proposed prediction methodology was deployed to aid energy time shift (ETS) application where the energy storage system was expected to dispatch the full capacity of discharge to cover the peak load period. Both implementation and simulation results showed a high level of accuracy for both mean absolute percentage error (MAPE) as well as peak time instants prediction.

Furthermore, coordinated voltage control was presented in this dissertation which aimed to optimize the coordination between available voltage source converters (VSC) in any given system and the legacy voltage regulation equipment such as online load tap changer (OLTC), line regulators and capacitor banks. The approach was developed to fulfill the need for volt-var control (VVC) algorithms that are independent of the system topology by considering locations of interests as source side voltage of line regulators. The proposed volt-var methodology is further improved to take online sensitivity analysis into considerations where sensitivity indexes were calculated online based on the reactive power dispatch at VSC location and voltage profile at locations of interests. The proposed methodology proved effective in maintaining any chosen location at a given distribution feeder at a constant average voltage per unit value.

Also, both active and reactive power management control was developed (VVWC) by energy storage units installed at the tentative local net-load locations for any given feeder. The proposed methodology aimed to regulate voltage profiles as well as controlling system's net-load ramp rate. The method addressed the active and reactive power capability of the inverters and the consequences of operating with any of the controllers taking precedence over the other. The proposed methodology utilized dis-

tributed energy storage units to regulate the voltage at each line regulator in IEEE 8500-Node test model. VVWC was also developed in Python/CYME interface.

8.2 Future Work

Active and reactive power management approaches research could be further extended. Some of the potential future work are listed below:

- The selection of local net-load locations at large-scale power distribution networks could be addressed through certain criterion so that much distributed behind the meter (BTM) PV farms and utility-scale PV farms are considered.

- The impacts of PQ-curves capability of VSC could be further considered and determined based on characteristics and medium voltage levels of distribution networks. Distribution feeder R/X ratio could be an important aspect in determining the precedence of either VVC or VWC for better control effectiveness and system stability.

- The proposed VVWC approach could further incorporate feeder level active power prediction methodology to coordinate between different ancillary services provided by energy storage units such as energy time shift.

REFERENCES

[1] Ashrae-organization-chart. *American Society of Heating, Refrigerating and Air-Conditioning Engineers*.

[2] Grid energy storage. *U.S. Department of Energy, December 2013.*

[3] Maintaining reliability in the modern power system. *U.S. Department of Energy*.

[4] Flexible resources help renewables: Fastfacts. In *CAISO*, 2016.

[5] Fast rampings: Without it, the grid's sitting a duck. In *Embala, Power Networks*, 2017.

[6] S. Abdelrazek and S. Kamalasadan. Integrated control of battery energy storage management system considering pv capacity firming and energy time shift applications. In *2014 IEEE Industry Application Society Annual Meeting*, pages 1–7, Oct 2014.

[7] S. Abdelrazek and S. Kamalasadan. A novel integrated optimal battery energy management control architecture considering multiple storage functions. In *2014 North American Power Symposium (NAPS)*, pages 1–6, Sept 2014.

[8] S. Abdelrazek and S. Kamalasadan. A novel integrated optimal battery energy management control architecture considering multiple storage functions. In *2014 North American Power Symposium (NAPS)*, pages 1–6, Sept 2014.

[9] S. Abdelrazek and S. Kamalasadan. A weather-based optimal storage management algorithm for pv capacity firming. *IEEE Transactions on Industry Applications*, 52(6):5175–5184, Nov 2016.

[10] S. Abdelrazek, S. Kamalasadan, J. Enslin, and T. Fenimore. Integrated optimal control of battery energy storage management system for energy management and pv capacity firming. In *2015 IEEE Energy Conversion Congress and Exposition (ECCE)*, pages 62–69, Sept 2015.

[11] S. A. Abdelrazek and S. Kamalasadan. Integrated pv capacity firming and energy time shift battery energy storage management using energy-oriented optimization. *IEEE Transactions on Industry Applications*, 52(3):2607–2617, May 2016.

[12] S. A. Abdelrazek and S. Kamalasadan. Integrated pv capacity firming and energy time shift battery energy storage management using energy-oriented optimization. *IEEE Transactions on Industry Applications*, 52(3):2607–2617, May 2016.

[13] I. Afandi, P. Ciufo, A. Agalgaonkar, and S. Perera. Universal volt/var control strategy for different distribution networks in australia. In *2018 18th International Conference on Harmonics and Quality of Power (ICHQP)*, pages 1–6, May 2018.

[14] R. Aghatehrani and A. Golnas. Reactive power control of photovoltaic systems based on the voltage sensitivity analysis. In *2012 IEEE Power and Energy Society General Meeting*, pages 1–5, July 2012.

[15] M. Ahmed, R. Bhattarai, S. J. Hossain, S. Abdelrazek, and S. Kamalasadan. Coordinated voltage control strategy for voltage regulators and voltage source converters integrated distribution system. In *Industry Applications Society Annual Meeting, 2017 IEEE*, pages 1–8. IEEE, 2017.

[16] M. Ahmed and S. Kamalasadan. Energy storage pv capacity firming with forecasted power reference and optimal error minimization. In *2015 North American Power Symposium (NAPS)*, pages 1–6, Oct 2015.

[17] M. J. E. Alam, K. M. Muttaqi, and D. Sutanto. A novel approach for ramp-rate control of solar pv using energy storage to mitigate output fluctuations caused by cloud passing. *IEEE Transactions on Energy Conversion*, 29(2):507–518, June 2014.

[18] A. Alanazi, M. Alanazi, and A. Khodaei. Managing the microgrid net load variability. In *2016 IEEE/PES Transmission and Distribution Conference and Exposition (T D)*, pages 1–5, May 2016.

[19] E. Almeshaiei and H. Soltan. A methodology for electric power load forecasting. *Alexandria Engineering Journal*, 50(2):137 – 144, 2011.

[20] L. F. Amaral, R. C. Souza, and M. Stevenson. A smooth transition periodic autoregressive (stpar) model for short-term load forecasting. *International Journal of Forecasting*, 24(4):603 – 615, 2008. Energy Forecasting.

[21] R. F. Arritt and R. C. Dugan. The ieee 8500-node test feeder. In *IEEE PES T D 2010*, pages 1–6, April 2010.

[22] K. Balasubramaniam and S. Abhyankar. A combined transmission and distribution system co-simulation framework for assessing the impact of volt/var control on transmission system. In *2017 IEEE Power Energy Society General Meeting*, pages 1–5, July 2017.

[23] A. Bokhari, A. Raza, M. Diaz-Aguil, F. de Len, D. Czarkowski, R. E. Uosef, and D. Wang. Combined effect of cvr and dg penetration in the voltage profile of low-voltage secondary distribution networks. *IEEE Transactions on Power Delivery*, 31(1):286–293, Feb 2016.

[24] J. H. Braslavsky, L. D. Collins, and J. K. Ward. Voltage stability in a grid-connected inverter with automatic volt-watt and volt-var functions. *IEEE Transactions on Smart Grid*, pages 1–1, 2018.

[25] J. H. Braslavsky, J. K. Ward, and L. Collins. A stability vulnerability in the interaction between volt-var and volt-watt response functions for smart inverters. In *2015 IEEE Conference on Control Applications (CCA)*, pages 733–738, Sept 2015.

[26] M. Chamana, B. H. Chowdhury, and F. Jahanbakhsh. Distributed control of voltage regulating devices in the presence of high pv penetration to mitigate ramp-rate issues. *IEEE Transactions on Smart Grid*, 9(2):1086–1095, March 2018.

[27] C.-A. Chang, T.-C. Lo, W. Yuan-Kang, and B. K. Chen. Simplified frequency estimation for unit scheduling criteria with high wind penetration. In *2016 IEEE Industry Applications Society Annual Meeting*, pages 1–8, Oct 2016.

[28] H. Chen, C. A. Canizares, and A. Singh. Ann-based short-term load forecasting in electricity markets. In *2001 IEEE Power Engineering Society Winter Meeting. Conference Proceedings (Cat. No.01CH37194)*, volume 2, pages 411–415 vol.2, 2001.

[29] X. Chen, Y. Du, and H. Wen. Forecasting based power ramp-rate control for pv systems without energy storage. In *2017 IEEE 3rd International Future Energy Electronics Conference and ECCE Asia (IFEEC 2017 - ECCE Asia)*, pages 733–738, June 2017.

[30] M. Dai, Z. Yu, R. Zeng, C. Zhuang, J. Hu, T. Li, J. Liu, and W. Zhu. A neural network short-term load forecasting considering human comfort index and its accumulative effect. In *2013 Ninth International Conference on Natural Computation (ICNC)*, pages 262–266, July 2013.

[31] A. P. C. de Mello, D. P. Bernardon, L. L. Pfitscher, and W. S. Hokama. Volt/var control integration in smart distribution grids. In *2018 Simposio Brasileiro de Sistemas Eletricos (SBSE)*, pages 1–6, May 2018.

[32] P. Denholm, M. OConnell, G. Brinkman, and J. Jorgenson. Overgeneration from solar energy in california: A field guide to the duck chart. *National Renewable Energy Laboratory 2015*.

[33] P. Denholm, M. OConnell, G. Brinkman, and J. Jorgenson. Overgeneration from solar energy in california: A field guide to the duck chart. In *NREL*, 2015.

[34] A. Ellis, D. Schoenwald, J. Hawkins, S. Willard, and B. Arellano. Pv output smoothing with energy storage. In *2012 38th IEEE Photovoltaic Specialists Conference*, pages 001523–001528, June 2012.

[35] J. Eyer. Energy storage for the electricity grid: Benefits and market potential assessment guide,. Feb., 2010.

[36] S. C. Fei Ding, Adarsh Nagarajan and M. Baggu. Photovoltaic impact assessment of smart inverter volt-var control on distribution system conservation voltage reduction and power quality. *National Renewable Energy Laboratory*.

[37] D. Feldman, J. Hoskins, and R. Margolis. Q4 2017/q1 2018 solar industry update. *National Renewable Energy Laboratory*.

[38] C. L. Floch, F. Belletti, S. Saxena, A. M. Bayen, and S. Moura. Distributed optimal charging of electric vehicles for demand response and load shaping. In *2015 54th IEEE Conference on Decision and Control (CDC)*, pages 6570–6576, Dec 2015.

[39] C. L. Floch, F. Belletti, S. Saxena, A. M. Bayen, and S. Moura. Distributed optimal charging of electric vehicles for demand response and load shaping. In *2015 54th IEEE Conference on Decision and Control (CDC)*, pages 6570–6576, Dec 2015.

[40] L. Ghelardoni, A. Ghio, and D. Anguita. Energy load forecasting using empirical mode decomposition and support vector regression. *IEEE Transactions on Smart Grid*, 4(1):549–556, March 2013.

[41] N. M. Hesham Alfares. Electric load forecasting: Literature survey and classification of methods. *International Journal of Systems Science, 2002*.

[42] A. M. Howlader, S. Sadoyama, L. R. Roose, and S. Sepasi. Distributed voltage control method using volt-var control curve of photovoltaic inverter for a smart power grid system. In *2017 IEEE 12th International Conference on Power Electronics and Drive Systems (PEDS)*, pages 630–634, Dec 2017.

[43] H. O. R. Howlader, M. M. Sediqi, A. M. Ibrahimi, and T. Senjyu. Optimal thermal unit commitment for solving duck curve problem by introducing csp, psh and demand response. *IEEE Access*, PP(99):1–1, 2018.

[44] C. hsien Kung, M. J. Devaney, C. min Huang, and C. ming Kung. An adaptive power system load forecasting scheme using a genetic algorithm embedded neural network. In *IMTC/98 Conference Proceedings. IEEE Instrumentation and Measurement Technology Conference. Where Instrumentation is Going (Cat. No.98CH36222)*, volume 1, pages 308–311 vol.1, May 1998.

[45] B. A. Hverstad, A. Tidemann, H. Langseth, and P. ztrk. Short-term load forecasting with seasonal decomposition using evolution for parameter tuning. *IEEE Transactions on Smart Grid*, 6(4):1904–1913, July 2015.

[46] M. M. Ibrahim and W. A. Omran. A decentralized coordination strategy for voltage regulation of active distribution networks. In *2016 IEEE PES Innovative*

Smart Grid Technologies Conference Europe (ISGT-Europe), pages 1–6, Oct 2016.

[47] R. A. Jabr and I. Dafi. Sensitivity-based discrete coordinate-descent for volt/var control in distribution networks. *IEEE Transactions on Power Systems*, 31(6):4670–4678, Nov 2016.

[48] A. Jamehbozorg, S. N. Keshmiri, and G. Radman. Pv output power smoothing using energy capacitor system. In *2011 Proceedings of IEEE Southeastcon*, pages 164–168, March 2011.

[49] J. Johnson, A. Ellis, A. Denda, K. Morino, T. Shinji, T. Ogata, and M. Tadokoro. Pv output smoothing using a battery and natural gas engine-generator. In *2013 IEEE 39th Photovoltaic Specialists Conference (PVSC)*, pages 1811–1816, June 2013.

[50] R. Johnson, L. Johnson, L. Nelson, C. Lenox, and J. Stein. Methods of integrating a high penetration photovoltaic power plant into a micro grid. In *2010 35th IEEE Photovoltaic Specialists Conference*, pages 000289–000294, June 2010.

[51] M. G. Kashani, Y. Cho, and S. Bhattacharya. Design consideration of volt-var controllers in distribution systems with multiple pv inverters. In *2016 IEEE Energy Conversion Congress and Exposition (ECCE)*, pages 1–7. IEEE, 2016.

[52] M. G. Kashani, M. Mobarrez, and S. Bhattacharya. Smart inverter volt-watt control design in high pv penetrated distribution systems. In *2017 IEEE Energy Conversion Congress and Exposition (ECCE)*, pages 4447–4452, Oct 2017.

[53] G. W. Kim and K. Y. Lee. Coordination control of ultc transformer and statcom based on an artificial neural network. *IEEE Transactions on Power Systems*, 20(2):580–586, May 2005.

[54] G. W. Kim and K. Y. Lee. Coordination control of ultc transformer and statcom based on an artificial neural network. *IEEE Transactions on Power Systems*, 20(2):580–586, May 2005.

[55] T. E. Kim and J. E. Kim. Voltage regulation coordination of distributed generation system in distribution system. In *2001 Power Engineering Society Summer Meeting. Conference Proceedings (Cat. No.01CH37262)*, volume 1, pages 480–484 vol.1, July 2001.

[56] D. S. Kumar, D. Srinivasan, and T. Reindl. A novel hybrid method for planning and allocation of dgs in medium voltage networks considering voltage regulation and relay coordination. In *2016 IEEE Congress on Evolutionary Computation (CEC)*, pages 3654–3661, July 2016.

[57] N. R. E. Laboratory. Renewable portfolio standards, 2015.

[58] R. K. Lam and H.-G. Yeh. Pv ramp limiting controls with adaptive smoothing filter through a battery energy storage system. In *2014 IEEE Green Energy and Systems Conference (IGESC)*, pages 55–60, Nov 2014.

[59] A. D. T. Le, S. Member, K. M. Muttaqi, S. Member, M. Negnevitsky, G. Ledwich, and S. Member. 1 response coordination of distributed generation and tap changers for voltage support.

[60] A. D. T. Le, K. M. Muttaqi, M. Negnevitsky, and G. Ledwich. Applying protection principles for controlling distributed generation. *Australian Journal of Electrical and Electronics Engineering*, 4(3):249–258, 2008.

[61] A. D. T. Le, K. M. Muttaqi, M. Negnevitsky, and G. Ledwich. Applying protection principles for controlling distributed generation. *Australian Journal of Electrical and Electronics Engineering*, 4(3):249–258, 2008.

[62] D. Lew and N. Miller. Reaching new solar heights: integrating high penetrations of pv into the power system. *IET Renewable Power Generation*, 11(1):20–26, 2017.

[63] D. Li and D. L. Lubkeman. Simulation of integrated volt/var control for pv penetration studies. In *2017 IEEE Power Energy Society General Meeting*, pages 1–5, July 2017.

[64] D. Li and D. L. Lubkeman. Simulation of integrated volt/var control for pv penetration studies. In *2017 IEEE Power Energy Society General Meeting*, pages 1–5, July 2017.

[65] X. Li, D. Hui, and X. Lai. Battery energy storage station (bess)-based smoothing control of photovoltaic (pv) and wind power generation fluctuations. *IEEE Transactions on Sustainable Energy*, 4(2):464–473, April 2013.

[66] X. Li, Y. Li, X. Han, and D. Hui. Application of fuzzy wavelet transform to smooth wind/pv hybrid power system output with battery energy storage system. *Energy Procedia*, 12:994 – 1001, 2011.

[67] Z. Linsuo and L. Yanling. A method for power system short-term load forecasting based on radial basis function neural network. In *2013 Fourth International Conference on Intelligent Systems Design and Engineering Applications*, pages 12–14, Nov 2013.

[68] Y. Liu, J. Bebic, B. Kroposki, J. de Bedout, and W. Ren. Distribution system voltage performance analysis for high-penetration pv. In *2008 IEEE Energy 2030 Conference*, pages 1–8, Nov 2008.

[69] X. Luo, S. Xia, K. W. Chan, and X. Lu. A hierarchical scheme for utilizing plug-in electric vehicle power to hedge against wind-induced unit ramp cycling operations. *IEEE Transactions on Power Systems*, PP(99):1–1, 2017.

[70] A. Majzoobi and A. Khodaei. Application of microgrids in addressing distribution network net-load ramping. In *2016 IEEE Power Energy Society Innovative Smart Grid Technologies Conference (ISGT)*, pages 1–5, Sept 2016.

[71] A. Majzoobi and A. Khodaei. Application of microgrids in supporting distribution grid flexibility. *IEEE Transactions on Power Systems*, PP(99):1–1, 2016.

[72] J. K. Mandal and A. K. Sinha. Artificial neural network based hourly load forecasting for decentralized load management. In *Proceedings 1995 International Conference on Energy Management and Power Delivery EMPD '95*, volume 1, pages 61–66 vol.1, Nov 1995.

[73] G. Mokhtari, G. Nourbakhsh, G. Ledwich, and A. Ghosh. Overvoltage and overloading prevention using coordinated pv inverters in distribution network. In *IECON 2014 - 40th Annual Conference of the IEEE Industrial Electronics Society*, pages 5571–5574, Oct 2014.

[74] N. Navid and G. Rosenwald. Market solutions for managing ramp flexibility with high penetration of renewable resource. *IEEE Transactions on Sustainable Energy*, 3(4):784–790, Oct 2012.

[75] S. P. Nicholas W. Miller and K. Clark. Concentrating solar power impact on grid reliability. *National Renewable Energy Laboratory*.

[76] Y. Ning, Y. Liu, H. Zhang, and Q. Ji. Comparison of different bp neural network models for short-term load forecasting. In *2010 IEEE International Conference on Intelligent Computing and Intelligent Systems*, volume 3, pages 435–438, Oct 2010.

[77] T. Onoda. Next day peak load forecasting using an artificial neural network with modified backpropagation learning algorithm. In *Proceedings of 1994 IEEE International Conference on Neural Networks (ICNN'94)*, volume 6, pages 3766–3769 vol.6, June 1994.

[78] H. V. Padullaparti, Q. Nguyen, and S. Santoso. Advances in volt-var control approaches in utility distribution systems. In *2016 IEEE Power and Energy Society General Meeting (PESGM)*, pages 1–5, July 2016.

[79] H. V. Padullaparti, Q. Nguyen, and S. Santoso. Advances in volt-var control approaches in utility distribution systems. In *2016 IEEE Power and Energy Society General Meeting (PESGM)*, pages 1–5, July 2016.

[80] X. Pan, B. Lee, and C. Zhang. A comparison of neural network backpropagation algorithms for electricity load forecasting. In *2013 IEEE International Workshop on Inteligent Energy Systems (IWIES)*, pages 22–27, Nov 2013.

[81] Y. W. S. D. . J. Z. Q. A. Pengwei Su, Xue Tian and Y. Wang. Recent trends in load forecasting technology for the operation optimization of distributed energy system. *energies 2017*.

[82] A. Puri. Optimally smoothing output of pv farms. In *2014 IEEE PES General Meeting — Conference Exposition*, pages 1–5, July 2014.

[83] R. D. Quint. Time step simulation tool for studying the impact of solar photovoltaic penetration. In *2015 IEEE Power Energy Society General Meeting*, pages 1–5, July 2015.

[84] D. Ranamuka, A. P. Agalgaonkar, and K. M. Muttaqi. Dynamic adjustment of oltc parameters using voltage sensitivity while utilizing dg for volt/var support. In *2014 IEEE PES General Meeting — Conference Exposition*, pages 1–5, July 2014.

[85] L. C. Ribeiro, J. P. O. S. Minami, B. D. Bonatto, P. F. Ribeiro, and A. C. Z. de Souza. Voltage control simulations in distribution systems with high penetration of pvs using the opendss. In *2018 Simposio Brasileiro de Sistemas Eletricos (SBSE)*, pages 1–6, May 2018.

[86] J. B. Rosenkranz, C. B. Martinez-Anido, and B. M. Hodge. Analyzing the impact of solar power on multi-hourly thermal generator ramping. In *2016 IEEE Green Technologies Conference (GreenTech)*, pages 153–158, April 2016.

[87] V. Salehi and B. Radibratovic. Ramp rate control of photovoltaic power plant output using energy storage devices. In *2014 IEEE PES General Meeting — Conference Exposition*, pages 1–5, July 2014.

[88] A. Sangwongwanich, Y. Yang, and F. Blaabjerg. A cost-effective power ramp-rate control strategy for single-phase two-stage grid-connected photovoltaic systems. In *2016 IEEE Energy Conversion Congress and Exposition (ECCE)*, pages 1–7, Sept 2016.

[89] R. Schiopu, C. Barbulescu, S. Kilyeni, A. Deacu, and A. Vernica. Ann back-propagation power consumption forecasting. In *IEEE EUROCON 2015 - International Conference on Computer as a Tool (EUROCON)*, pages 1–6, Sept 2015.

[90] D. Shah and M. L. Crow. Online volt-var control for distribution systems with solid-state transformers. *IEEE Transactions on Power Delivery*, 31(1):343–350, Feb 2016.

[91] S. Shajari and R. K. Pour. Reduction of energy storage system for smoothing hybrid wind-pv power fluctuation. In *2012 11th International Conference on Environment and Electrical Engineering*, pages 115–117, May 2012.

[92] Z. Shen and M. E. Baran. Gradient based centralized optimal volt/var control strategy for smart distribution system. In *2013 IEEE PES Innovative Smart Grid Technologies Conference (ISGT)*, pages 1–6, Feb 2013.

[93] N. Sinha, L. L. Lai, P. K. Ghosh, and Y. Ma. Wavelet-ga-ann based hybrid model for accurate prediction of short-term load forecast. In *2007 International Conference on Intelligent Systems Applications to Power Systems*, pages 1–8, Nov 2007.

[94] J. Smith. Stochastic analysis to determine feeder hosting capacity for distributed solar pv. *Electric Power Research Institute, 2012*.

[95] J. W. Taylor and R. Buizza. Neural network load forecasting with weather ensemble predictions. *IEEE Transactions on Power Systems*, 17(3):626–632, Aug 2002.

[96] H. K. Temraz, M. M. A. Salama, and V. H. Quintana. Application of the decomposition technique for forecasting the load of a large electric power network. *IEE Proceedings - Generation, Transmission and Distribution*, 143(1):13–18, Jan 1996.

[97] K. Turitsyn, P. ulc, S. Backhaus, and M. Chertkov. Distributed control of reactive power flow in a radial distribution circuit with high photovoltaic penetration. In *IEEE PES General Meeting*, pages 1–6, July 2010.

[98] G. Wang, M. Ciobotaru, and V. G. Agelidis. Power smoothing of large solar pv plant using hybrid energy storage. *IEEE Transactions on Sustainable Energy*, 5(3):834–842, July 2014.

[99] Z. Wang and J. Wang. Review on implementation and assessment of conservation voltage reduction. *IEEE Transactions on Power Systems*, 29(3):1306–1315, May 2014.

[100] T. M. Wanzeler, J. P. A. Vieira, P. Radatz, V. C. Souza, and D. C. Pinheiro. Assessing the performance of smart inverter volt-watt and volt-var functions in distribution systems with high pv penetration. In *2018 Simposio Brasileiro de Sistemas Eletricos (SBSE)*, pages 1–6, May 2018.

[101] T. M. Wanzeler, J. P. A. Vieira, P. Radatz, V. C. Souza, and D. C. Pinheiro. Assessing the performance of smart inverter volt-watt and volt-var functions in distribution systems with high pv penetration. In *2018 Simposio Brasileiro de Sistemas Eletricos (SBSE)*, pages 1–6, May 2018.

[102] J. Wilson. Signal processing and control technology for conservation voltage reduction. In *2014 Saudi Arabia Smart Grid Conference (SASG)*, pages 1–7, Dec 2014.

[103] T. L. Wilson. Measurement and verification of distribution voltage optimization results for the ieee power amp; energy society. In *IEEE PES General Meeting*, pages 1–9, July 2010.

[104] D. Xin-hui, T. Feng, and T. Shao-qiong. Study of power system short-term load forecast based on artificial neural network and genetic algorithm. In *2010 International Conference on Computational Aspects of Social Networks*, pages 725–728, Sept 2010.

[105] F. Yang and Z. Li. Improve distribution system energy efficiency with coordinated reactive power control. *IEEE Transactions on Power Systems*, 31(4):2518–2525, July 2016.

[106] K. H. Youssef. A new method for online sensitivity-based distributed voltage control and short circuit analysis of unbalanced distribution feeders. *IEEE Transactions on Smart Grid*, 6(3):1253–1260, 2015.

[107] R. Zafar, J. Ravishankar, and H. R. Pota. Centralized control of step voltage regulators and energy storage system under high photovoltaic penetration. In *2016 IEEE Innovative Smart Grid Technologies - Asia (ISGT-Asia)*, pages 511–516, Nov 2016.

[108] Q. Zhao, L. Xian, S. Roy, X. Kong, and A. M. Khambadkone. Optimal control of pv ramp rate using multiple energy storage system. In *2017 IEEE 3rd International Future Energy Electronics Conference and ECCE Asia (IFEEC 2017 - ECCE Asia)*, pages 928–931, June 2017.